



Cite this: *Lab Chip*, 2025, **25**, 3879

## Autonomous wearable sensing enabled by capillary microfluidics: a review

Kiran Kuruvinashetti,<sup>ab</sup> Amin Komeili<sup>\*ab</sup> and Amir Sanati Nezhad <sup>\*ab</sup>

Capillary microfluidic wearables have emerged as a versatile class of autonomous biosensing platforms for continuous, non-invasive monitoring of biofluids such as sweat, saliva, tears, and interstitial fluid. This review critically examines recent advances in skin-conformal device architectures that enable passive, power-free fluid sampling and integration with biochemical sensing modalities. Systems are classified by fluid handling strategy chrono-sampling *versus* continuous flow and sensing mode on-body *versus* off-body analysis. Key design principles including the use of burst valves, evaporative reservoirs, multilayer channel networks, and hydrogel-assisted interfaces are discussed in the context of minimizing evaporation, backflow, and biofouling. Advances in electrochemical and optical biosensing for real-time quantification of physiologically relevant analytes such as cortisol, glucose, lactate, pH, and electrolytes are evaluated alongside emerging trends in multiplexing and closed-loop therapeutic integration. Finally, the review highlights translational challenges in clinical validation, biocompatibility, and manufacturing scalability, outlining a roadmap for future development of lab-on-skin diagnostics and personalized health monitoring.

Received 31st May 2025,  
Accepted 9th July 2025

DOI: 10.1039/d5lc00536a

rsc.li/loc

### 1. Introduction

Wearable sensors have transformed personal health monitoring by enabling continuous, real-time, and non-invasive tracking of physiological and biochemical markers.<sup>1–7</sup> These platforms address limitations of centralized diagnostic systems by offering decentralized, user-centric solutions for health assessment at home or the point of care.<sup>1</sup> Advances in material science, wireless electronics, and rapid prototyping have supported the development of lightweight, skin-interfaced devices with integrated sensing, fluidics, and data transmission capabilities.<sup>8–11</sup>

First-generation wearable devices were primarily designed to monitor physical signals such as body motion, heart rate, respiration rate, blood pressure, temperature, sweat rate, and conductivity<sup>1,11,12</sup> (Fig. 1a). As technology advanced, second-generation wearables emerged with multifunctional capabilities for biochemical sensing, enabling analysis of electrolytes, glucose, metabolites, hormones, pH, and other molecular markers present in sweat, saliva, interstitial fluid (ISF), and tears.<sup>1–3</sup> This evolution has brought new diagnostic potential but also introduced challenges in power-free sample

handling, miniaturized integration, and consistent bio signal extraction (Fig. 1b).

Capillary microfluidics addresses many of these limitations by enabling autonomous, self-powered transport of biofluids through engineered wettability and channel design.<sup>13–18</sup> Typically composed of layered hydrophilic or hydrophobic materials, these systems guide fluid through defined paths without external pumps, often using skin-contacting inlets or wicking textiles<sup>9,11,19</sup> (Fig. 1c). Collected biofluids are routed to sensing reservoirs sequentially, ensuring signal fidelity and preventing backflow or cross-contamination.<sup>14,20</sup> While flow saturation can impair prolonged operation, optimized geometries and evaporative disposal strategies mitigate these effects and support continuous sensing.<sup>15</sup>

Wearable biosensors primarily rely on optical or electrochemical transduction mechanisms.<sup>6,11,21,22</sup> Optical systems often integrate colorimetric or fluorescence reagents into microfluidic channels, while electrochemical systems incorporate working electrodes between the skin and fluidic reservoirs. Electrochemical detection operates *via* direct redox activity or indirect signal amplification using redox mediators.<sup>23,24</sup> For long-term monitoring, reversible binding elements such as aptamers<sup>25</sup> or electrode regeneration protocols<sup>26</sup> are essential. Clinical examples such as the Eversense E3 glucose monitor demonstrate successful multi-month deployment.<sup>27</sup> Molecularly imprinted polymers (MIPs) have become attractive transduction elements due to their

<sup>a</sup>Department of Biomedical Engineering, University of Calgary, Calgary, Alberta T2N 1N4, Canada. E-mail: amin.komeili@ucalgary.ca, amir.sanatinezhad@ucalgary.ca

<sup>b</sup>Department of Mechanical and Manufacturing Engineering, University of Calgary, Calgary, Alberta T2N 1N4, Canada



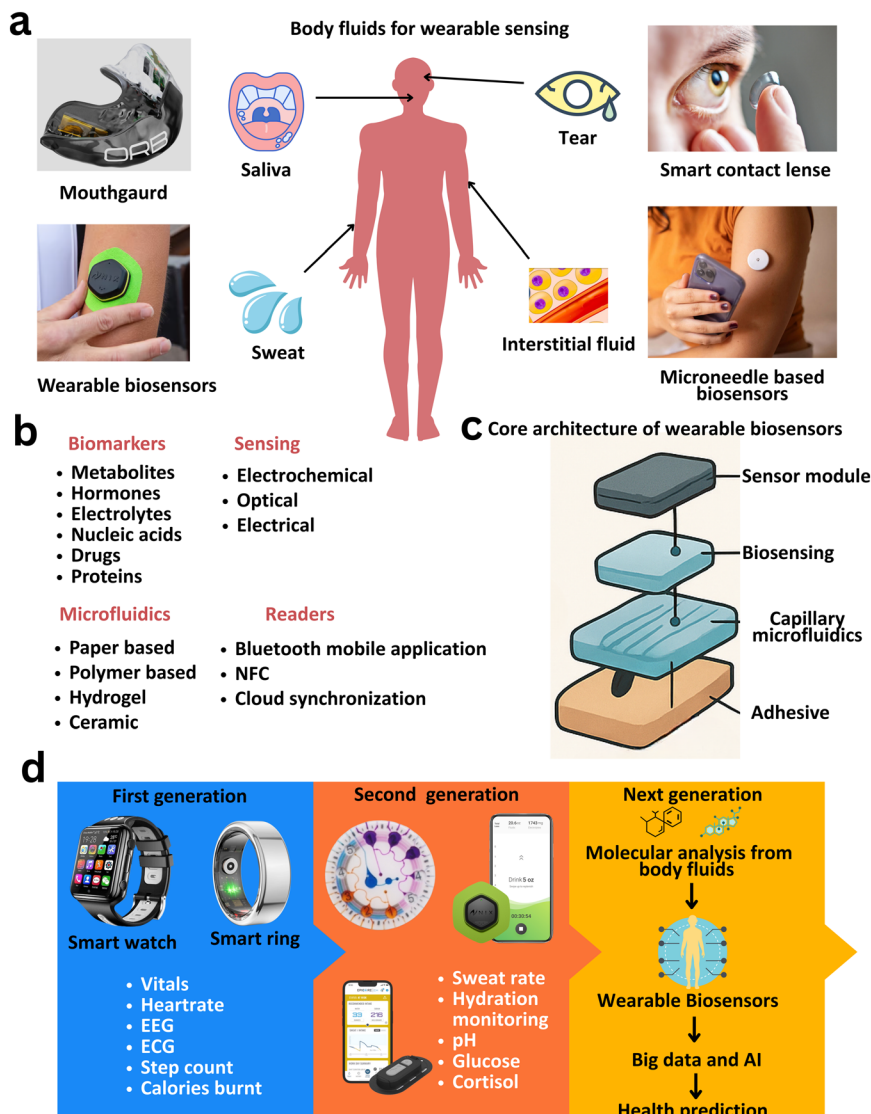


**Fig. 1** Overview of wearable biosensors integrating capillary microfluidics for non-invasive biofluid analysis. (a) Sweat, saliva, tears, and interstitial fluid are key targets for molecular monitoring using platforms such as smart rings, contact lenses, microneedle patches, and mouthguard sensors. (b) Wearable systems include components for biomarker detection (e.g., metabolites, nucleic acids), fluidics (e.g., paper, polymers, hydrogels), sensing (electrochemical, optical), and wireless data transmission (Bluetooth, near field communication (NFC), cloud). (c) Core architecture features stacked layers of adhesive backing, capillary microfluidics, biosensing interface, and signal readout modules. (d) Generational evolution highlights a transition from vital sign tracking to real-time molecular sensing and next-generation AI-enabled predictive diagnostics.

specificity, chemical stability, and facile fabrication.<sup>28–30</sup> These synthetic receptors mimic natural binding sites using template molecules, offering sensitive and selective detection across a range of analytes while requiring minimal power and offering excellent shelf-life.<sup>31–33</sup>

Despite significant advances in wearable biosensing, many recent reviews have focused narrowly on sensor materials, microneedle integration, AI-driven data analytics, or adaptive bioelectronics, with limited emphasis on the fluidic subsystems essential for power-free operation, reliability, and device longevity.<sup>2,34–36</sup> These works offer valuable insights into emerging sensing modalities and system-level designs, but they often address capillary microfluidics only peripherally—if at all.<sup>37–39</sup>

In contrast, this review provides a systematic and cross-cutting assessment of capillary microfluidics as the core fluid-handling strategy for wearable biosensors. We uniquely focus on autonomous, power-free sample acquisition and routing, highlighting design distinctions between chrono-sampling *versus* continuous flow and on-body *versus* off-body sensing—dimensions often overlooked in prior literature. Importantly, we cover all major non-invasive biofluids (sweat, saliva, tears, ISF), and evaluate their distinct properties in the context of fluid handling and sensor integration. This review also integrates recent advances in electrochemical, optical, and biomolecular biosensing—including aptamers, immunosensors, and MIPs—to demonstrate how capillary systems support robust, multimodal sensing. By bridging



sensing and fluidic domains within a unified capillary microfluidic framework, we address a critical gap left by earlier reviews and advance the design of next-generation wearable diagnostics that are truly autonomous, miniaturized, and clinically relevant. Fig. 1d summarizes the architectural integration of capillary elements with sensing and data modules, underscoring their importance in ensuring robust fluid delivery and sensor functionality across diverse health applications.

## 2. Biofluid composition, advantages, and limitations

While blood is a gold standard for clinical diagnostics, its invasive collection, need for trained personnel, and risk of clotting limit its use in wearable applications.<sup>40,41</sup> In contrast, alternative biofluids such as sweat, saliva, tears, and ISF are more suitable for continuous and minimally invasive monitoring.<sup>2,42</sup>

### 2.1 Sweat as a bodily fluid

Sweat, secreted by eccrine glands, comprises 99% water and 1% solutes, including electrolytes (sodium  $\text{Na}^+$ , chloride  $\text{Cl}^-$ , and potassium  $\text{K}^+$ ), metabolites (lactate, glucose, urea), proteins (cytokines, peptides), and trace elements (zinc, copper, iron).<sup>43–45</sup> Hormones like cortisol and disease biomarkers such as elevated chloride (cystic fibrosis) are also detectable.<sup>7,46</sup> Its diagnostic versatility has led to widespread integration of sweat into wearable platforms for analytes such as cortisol, chloride, and lactate.<sup>19</sup> However, individual variability, surface contamination, low biomarker concentrations, and limited correlation to blood levels present analytical challenges.<sup>3,9</sup> The emerging field of “iSudorology” emphasizes sweat’s potential for real-time digital diagnostics.<sup>47</sup>

### 2.2 Saliva as a bodily fluid

Saliva, composed of 99% water, contains a diverse biomolecular profile, including electrolytes ( $\text{Na}^+$ ,  $\text{K}^+$ ,  $\text{Cl}^-$ ), enzymes (amylase, lysozyme), immunoglobulins, mucins, hormones (cortisol, melatonin), metabolites (glucose, urea), nucleic acids, and microbial content.<sup>48–50</sup> Its continuous secretion, non-invasive collection, and good correlation with serum levels make it promising for wearable monitoring.<sup>51</sup> Saliva-based sensing has shown utility in monitoring oral, systemic, and neurological diseases, stress, and hormonal changes.<sup>50,52</sup> Nevertheless, intra- and inter-individual variability, along with sensor stability in the oral environment, remain barriers to deployment.<sup>53</sup>

### 2.3 Tears as a bodily fluid

Tears are a continuously secreted, minimally invasive biofluid with growing potential in wearable sensing. Many tear biomarkers correlate well with blood concentrations, making them suitable for real-time health monitoring.<sup>43</sup> Smart

contact lenses, for example, have been developed for glucose monitoring in diabetes.<sup>54,55</sup> Proteomic and inflammatory markers in tears have also been utilized for diagnosing dry eye disease,<sup>5</sup> while neurodegenerative biomarkers for Alzheimer’s and Parkinson’s have shown promise for early detection.<sup>56</sup> Tear analysis supports intraocular pressure monitoring and systemic disease detection, including cancer and multiple sclerosis.<sup>57</sup> However, low analyte concentrations demand highly sensitive detection platforms,<sup>56</sup> and long-term sensor stability within the ocular environment remains a key challenge.<sup>57</sup> Establishing standardized tear biomarker reference ranges is also essential for clinical utility.<sup>55</sup>

### 2.4 ISF as a bodily fluid

ISF, occupying ~45% of human skin volume, serves as an intermediary between blood and tissues and is an abundant source of biomarkers.<sup>58,59</sup> Its composition includes metabolites, proteins, nucleic acids, exosomes, drugs, and cytokines.<sup>60–62</sup> While many ISF biomarkers mirror those in plasma, diffusion barriers and electrostatic exclusion mechanisms influence analyte concentrations based on size and charge.<sup>58</sup> ISF contains over 92% of RNA species found in blood and is especially enriched in exosomes, making it a rich matrix for molecular diagnostics.<sup>58</sup> ISF offers several advantages for continuous biosensing: it is non-clotting, reflects local tissue states, and enables real-time monitoring using minimally invasive tools like microneedles.<sup>59,61,62</sup> However, dynamic dilution effects, cellular uptake, and biological variability can complicate analyte interpretation.<sup>58,62</sup> Affinity-based sensors, though promising, require improvements in longevity and fouling resistance for extended use.<sup>62</sup> ISF, like sweat and saliva, reinforces the importance of advanced microfluidic integration. Achieving real-time, autonomous biosensing depends on engineering capillary microfluidic systems that allow continuous, pump-free fluid handling. These platforms will be central to the next generation of personalized, real-time healthcare diagnostics.

A comparative analysis of metabolites, hormones, and electrolytes across sweat, saliva, ISF, and blood reveals distinct concentration profiles shaped by molecular weight, membrane permeability, and transport mechanisms. Among these fluids, metabolite concentrations are consistently highest in blood and ISF, reflecting their direct roles in systemic homeostasis. In contrast, sweat and saliva typically present more diluted analyte levels due to glandular filtration and extracellular exchange processes. Table 1 summarizes representative biomarker concentrations across these major biofluids, while Table 2 provides physiological and pathological relevance for each analyte. These values are critical for the rational design of wearable biosensors, where high selectivity and sensitivity are essential for accurate detection in low-concentration matrices.

In support of these insights, a wireless smart contact lens was recently developed for continuous, high-resolution



**Table 1** Concentration ranges of representative biomarkers across biofluids are commonly targeted in wearable sensing

Biomolecule	Sweat (μM)	Saliva (μM)	ISF (μM)	Blood (μM)	Ref.
Cortisol	22.08–386.37	0.331–82.79	0.276–27.6	11.04–1104	63–67
Glucose	10–1000	30–80	3900–6900	3900–6900	68–70
Lactate	3700–50 000	0–3500	500–2000	1600–12 100	71–74
Sodium	$10\text{--}90 \times 10^3$	$2\text{--}21 \times 10^3$	$135\text{--}145 \times 10^3$	$135\text{--}145 \times 10^3$	75–79
Potassium	$4\text{--}16 \times 10^3$	$1\text{--}36 \times 10^3$	$3.5\text{--}5 \times 10^3$	$3.5\text{--}5 \times 10^3$	80–83
Chloride	$10\text{--}70 \times 10^3$	$10\text{--}50 \times 10^3$	$98\text{--}107 \times 10^3$	$98\text{--}107 \times 10^3$	84–88
Uric acid	$2\text{--}10 \times 10^3$	$0.1\text{--}0.3 \times 10^3$	$0.2\text{--}0.4 \times 10^3$	$0.2\text{--}0.4 \times 10^3$	89–92
Immunoglobulin A	0.0000625–0.00625	0.0167–4.0	0.0000667–0.00667	0.0107–0.6667	93–96
α-Amylase	$714 \times 10^{-5}\text{--}714 \times 10^{-3}$	$143 \times 10^{-3}\text{--}0.0286$	$714 \times 10^{-5}\text{--}714 \times 10^{-3}$	$2.86 \times 10^{-6}\text{--}1.0 \times 10^{-5}$	97–100
Chromogranin A	0.00204–0.2044	0.00204–0.2044	0.00204–0.2044	0.511–2.862	101–105
Brain-derived neurotrophic factor	0.000370–0.0370	0.00248–0.1015	0.000370–0.0370	0.00222–0.5926	106–109
Albumin	1.50–75.19	1.50–7.52	300.75–451.13	526.32–751.88	110–114
Creatinine	50–200	4–30	60–100	60–100	60, 115–117
Zinc	0.4–1.2	1–10	10–18	10–18	118–120
Copper	0.3–1	0.1–1.5	11–22	11–22	119, 121–125
Iron	0.1–1	1–10	10–30	10–30	126–128
Bicarbonate	$1\text{--}40 \times 10^3$	$5\text{--}40 \times 10^3$	$22\text{--}29 \times 10^3$	$22\text{--}29 \times 10^3$	43, 44, 129, 130
Phosphate	$0.1\text{--}1 \times 10^3$	$2\text{--}10 \times 10^3$	$0.8\text{--}1.4 \times 10^3$	$0.8\text{--}1.4 \times 10^3$	131–133
Amino acids (total)	$1\text{--}10 \times 10^3$	$1\text{--}5 \times 10^3$	$2\text{--}5 \times 10^3$	$2\text{--}5 \times 10^3$	134–137
Urea	$2\text{--}10 \times 10^3$	$2\text{--}10 \times 10^3$	$2.5\text{--}7.1 \times 10^3$	$2.5\text{--}7.1 \times 10^3$	138–140
Cholesterol	$0.01\text{--}0.1 \times 10^3$	$0.01\text{--}0.1 \times 10^3$	$3.9\text{--}5.2 \times 10^3$	$3.9\text{--}5.2 \times 10^3$	141–143
Triglycerides	$0.01\text{--}0.1 \times 10^3$	$0.01\text{--}0.1 \times 10^3$	$0.4\text{--}1.8 \times 10^3$	$0.4\text{--}1.8 \times 10^3$	144–146
Testosterone	0.0347–3.47	0.0347–0.6935	10.4–34.68	10.4–34.68	147–150
Estradiol	$3.67 \times 10^{-6}\text{--}3.67 \times 10^{-4}$	$1.84 \times 10^{-6}\text{--}1.84 \times 10^{-5}$	$3.67 \times 10^{-5}\text{--}1.84 \times 10^{-4}$	$3.67 \times 10^{-5}\text{--}1.84 \times 10^{-4}$	151–154
Progesterone	0.318–3.18	0.159–1.59	0.636–63.6	0.636–63.6	155–158
C-reactive protein	0.00087–0.0870	0.00043–0.0435	0.00087–0.0870	0.00087–0.0870	159–161
Interleukin-6	$4.76 \times 10^{-9}\text{--}4.76 \times 10^{-7}$	$4.76 \times 10^{-9}\text{--}2.38 \times 10^{-7}$	$0.4\text{--}4.76 \times 10^{-7}$	$0\text{--}4.76 \times 10^{-7}$	162–165
Tumor necrosis factor-α	$5.88 \times 10^{-9}\text{--}5.88 \times 10^{-7}$	$5.88 \times 10^{-9}\text{--}2.94 \times 10^{-7}$	$0\text{--}1.18 \times 10^{-6}$	$0\text{--}1.18 \times 10^{-6}$	166–169
Leptin	0.00625–0.625	0.00625–0.3125	0.0625–6.25	0.0625–6.25	170–173
Adiponectin	0.00333–0.333	0.00333–0.1667	0.0667–1.0	0.0667–1.0	171, 174–176
Ghrelin	$3.03 \times 10^{-6}\text{--}3.03 \times 10^{-5}$	$3.03 \times 10^{-6}\text{--}1.52 \times 10^{-5}$	$3.03 \times 10^{-5}\text{--}3.03 \times 10^{-4}$	$3.03 \times 10^{-5}\text{--}3.03 \times 10^{-4}$	171, 177–179
Melatonin	$4.30 \times 10^{-6}\text{--}4.30 \times 10^{-5}$	$4.30 \times 10^{-6}\text{--}2.15 \times 10^{-5}$	$4.30 \times 10^{-5}\text{--}2.15 \times 10^{-4}$	$4.30 \times 10^{-5}\text{--}2.15 \times 10^{-4}$	155, 180–182
Serotonin	0.568–5.68	0.568–2.84	283.7–1134.9	283.7–1134.9	183–186
Dopamine	0.653–6.53	0.653–3.27	$6.53 \times 10^{-5}\text{--}6.53 \times 10^{-4}$	$6.53 \times 10^{-5}\text{--}6.53 \times 10^{-4}$	187–191
Epinephrine	0.0546–0.546	0.0546–0.273	$5.46 \times 10^{-5}\text{--}5.46 \times 10^{-4}$	$5.46 \times 10^{-5}\text{--}5.46 \times 10^{-4}$	192–197
Vitamin C	5.68–56.78	5.68–28.39	22.71–113.54	22.71–113.54	198–203
Folate	2.27–22.66	2.27–11.33	4.53–45.33	4.53–45.33	204–206
Thyroid-stimulating hormone	$3.57 \times 10^{-4}\text{--}3.57 \times 10^{-3}$	$3.57 \times 10^{-4}\text{--}1.79 \times 10^{-3}$	0.0143–0.143	0.0143–0.143	207–209

monitoring of basal tear glucose.<sup>55</sup> The device showed a strong correlation between tear and blood glucose levels in both human and animal studies, particularly when subject-specific lag times—typically 5 to 15 min—were appropriately calibrated. Despite significantly lower glucose concentrations in tears (approximately 0.1–0.6 mM) compared to blood (0.5–3 mM), consistent glycemic patterns emerged once the effects of diffusion delays and reflex tearing were addressed. Real-time electrochemical sensing with sub-minute resolution confirmed that tear glucose levels reliably mirrored blood glucose dynamics, underscoring the feasibility of tear-based biosensing as a non-invasive and practical approach for glycemic monitoring.

### 3. Capillary microfluidics: material selection and fabrication strategies

Capillary microfluidics enable self-driven fluid manipulation *via* surface tension and wettability, making

them ideally suited for wearable biosensors where compact, power-free operation is critical.<sup>13,16,17</sup> The selection of materials and fabrication methods must account for the target biofluid, device geometry, and intended use (disposable *versus* long-term monitoring), as these parameters influence extraction efficiency, flow dynamics, and signal reliability. For example, capillary channel dimensions must match the active sensing area to ensure uniform biofluid distribution and minimal sample loss. Material stability under mechanical stress and environmental exposure is also essential, particularly for skin-interfacing devices.

Materials with tailored hydrophilic/hydrophobic properties, electrostatic behavior, and biocompatibility are key to optimizing capillary action and ensuring consistent fluid transport.<sup>13,14</sup> Paper, polymer films, hydrogels, and hybrid composites have been used extensively, each offering specific advantages in wettability, flexibility, and integration with sensors.



**Table 2** Representative biomolecules and their relevance to physiological functions and disease states for wearable biosensing applications

Biomolecule	Physiological conditions	Pathological conditions
Cortisol	Stress response, immune modulation, maintaining homeostasis. Regulation of blood pressure, metabolism, and inflammatory responses	Cushing's syndrome, characterized by excessive cortisol levels; Addison's disease, caused by insufficient cortisol production. Mental health disorders like depression and anxiety
Glucose	Glycolysis, glycogen storage, and glucose homeostasis, regulated by hormones like insulin and glucagon. Essential for ATP production, oxidative stress management, and neurotransmitter synthesis <sup>210</sup>	Diabetes mellitus (type 1 and type 2), hyperglycemia, hypoglycemia, diabetic ketoacidosis <sup>211</sup>
Lactate	An energy source for the myocardium, regulates smooth vascular muscle cells (VSMCs), promotes angiogenesis, and modulates immune cell functions <sup>212</sup>	Lactic acidosis, cardiovascular diseases like heart failure and pulmonary hypertension, cancer progression, and inflammatory conditions. It is also associated with metabolic disorders and mitochondrial dysfunction <sup>213</sup>
Sodium	Maintaining fluid balance, nerve conduction, muscle contraction, and blood pressure regulation. It is essential for the functioning of the nervous system and muscle activity, as well as for maintaining cellular osmotic pressure and blood volume	Hyponatremia (low sodium levels), hypernatremia (high sodium levels), heart failure, kidney diseases, and hypertension <sup>214</sup>
Potassium	Maintaining normal levels of fluid inside cells, muscle contraction, nerve function, and blood pressure regulation	Hypokalemia (low potassium levels) and hyperkalemia (high potassium levels) are associated with muscle weakness, cardiac arrhythmias, and other health issues <sup>215</sup>
Chloride	Maintaining ionic homeostasis, osmotic pressure, acid-base balance, and electrical excitability. It is involved in cell volume regulation, transepithelial transport, and the regulation of membrane potential in various tissues <sup>216</sup>	Cystic fibrosis, myotonia congenita, Bartter's syndrome, hyperchloremia, and hypochloremia <sup>216</sup>
Uric acid	A major antioxidant in human plasma, scavenging reactive oxygen species and protecting against oxidative stress. It also plays a role in immune responses and tissue healing <sup>217</sup>	Elevated uric acid levels are associated with gout, kidney stones, cardiovascular diseases, and metabolic syndrome. Low levels are linked to neurological disorders such as multiple sclerosis and Parkinson's disease <sup>217</sup>
Immunoglobulin A (IgA)	(IgA) is the most abundant antibody at mucosal surfaces, playing a key role in host-pathogen defense, immune exclusion, and maintaining homeostasis. It interacts with the intestinal microbiota to enhance diversity and provides protection against pathogens by immune exclusion. IgA also contributes to mucosal immunity by neutralizing toxins and viruses, blocking colonization and penetration of pathogenic bacteria, and promoting antigen sampling <sup>218</sup>	IgA nephropathy, IgA vasculitis, celiac disease, inflammatory bowel disease, dermatitis herpetiformis, and autoimmune diseases like rheumatoid arthritis and Sjögren's syndrome. Aberrant IgA immune complexes can lead to excessive immune cell activation, causing tissue damage in autoimmune diseases <sup>218</sup>
$\alpha$ -Amylase	$\alpha$ -Amylase plays a critical role in carbohydrate digestion by breaking down starch into simpler sugars. It is involved in glucose metabolism and has been studied as a stress biomarker due to its activity in response to adrenergic system activation	Acute and chronic pancreatitis, diabetes, Alzheimer's disease, and stress-related conditions. Elevated levels are often diagnostic markers for pancreatic disorders, while low levels are linked to metabolic syndromes and other chronic conditions
Chromogranin A	Chromogranin A (CgA) plays a role in endocrine, cardiovascular, metabolic, and immune system regulation. It is involved in the formation of dense core secretory vesicles in neuroendocrine cells and regulates calcium homeostasis, glucose metabolism, and vascular physiology. CgA-derived peptides such as vasostatin, catestatin, and pancreastatin contribute to these physiological roles <sup>219</sup>	Neuroendocrine tumors, cardiovascular diseases, inflammatory diseases (e.g., rheumatoid arthritis, systemic inflammatory response syndrome), and neuropsychiatric conditions. It is also linked to conditions like chronic atrophic gastritis, renal insufficiency, and prostate cancer <sup>220</sup>
Brain-derived neurotrophic factor (BDNF)	BDNF plays a critical role in neuronal survival, differentiation, synaptic plasticity, and memory formation. It is involved in the growth and maintenance of neurons, synaptic transmission, and neurogenesis, particularly in the hippocampus and cortex <sup>221</sup>	Several neurological and psychiatric disorders, including Alzheimer's disease, Parkinson's disease, depression, Huntington's disease, and multiple sclerosis. Abnormal BDNF signaling is associated with neurodegeneration, cognitive decline, and mood disorders <sup>222</sup>
Albumin	Maintaining oncotic pressure, preventing fluid leakage into extravascular spaces. It acts as a carrier for various endogenous and exogenous compounds, including fatty acids, hormones, and drugs <sup>223</sup>	Hypoalbuminemia, which can result from liver diseases (e.g., cirrhosis), kidney diseases (e.g., nephrotic syndrome), malnutrition, burns, sepsis, and critical illnesses. Hypoalbuminemia is linked to increased morbidity and mortality, as it affects vascular homeostasis and immune responses <sup>223</sup>
Creatinine	It is a byproduct of muscle metabolism, specifically from the breakdown of creatine phosphate, which is involved in energy production in muscles. It is excreted by the kidneys and serves as a marker for kidney function	Elevated levels are associated with kidney dysfunction, including chronic kidney disease, acute kidney injury, and conditions like diabetes, hypertension, and glomerulonephritis. Low creatinine levels may indicate reduced muscle mass or liver disease



Table 2 (continued)

Biomolecule	Physiological conditions	Pathological conditions
Calcium	Calcium plays a critical role in bone structure, muscle contraction, nerve function, enzymatic processes, and blood coagulation. It is also essential for cell signaling and maintaining the potential difference across excitable cell membranes	Pathological conditions associated with calcium include hypocalcemia, hypercalcemia, osteoporosis, kidney stones, and cardiovascular issues related to abnormal calcium levels <sup>224</sup>
Magnesium	Magnesium is essential for over 300 biochemical reactions in the body, including maintaining normal nerve and muscle function, supporting a healthy immune system, keeping the heartbeat steady, and aiding in bone health and energy production <sup>225</sup>	Magnesium deficiency is associated with cardiovascular diseases, type 2 diabetes, osteoporosis, migraines, depression, and neurological disorders. It can also lead to hypocalcemia, hypokalemia, and cardiac arrhythmias <sup>226</sup>
Zinc	Zinc is essential for enzymatic reactions, immune function, cell division, wound healing, and growth. It plays a role in the synthesis of DNA, RNA, and proteins, and is critical for the function of over 300 enzymes. Zinc also supports the senses of taste and smell, and is involved in hormonal regulation, including insulin and thyroid hormones <sup>227</sup>	Zinc deficiency is associated with conditions such as acrodermatitis enteropathica, immune dysfunction, delayed wound healing, growth retardation, and increased susceptibility to infections. Chronic diseases like diabetes, neurodegenerative disorders, and certain cancers are also linked to zinc imbalance <sup>228</sup>
Copper	Copper plays a critical role in oxidative metabolism, antioxidant defense, neurotransmitter synthesis, immune system functioning, angiogenesis, and regulation of gene expression. It is essential for the production of red blood cells, maintenance of nerve cells, and energy production <sup>229</sup>	Copper dysregulation is associated with Menkes disease, Wilson's disease, Alzheimer's disease, Parkinson's disease, amyotrophic lateral sclerosis, cardiovascular diseases, and certain cancers. It can lead to oxidative stress, neurodegeneration, and other systemic dysfunctions <sup>229</sup>
Iron	Iron plays a critical role in oxygen transport (as hemoglobin), muscle oxygenation (as myoglobin), DNA synthesis, cellular respiration (as cytochromes), immune function, and myelin sheath formation	Pathological conditions associated with iron include hemochromatosis (iron overload), anemia (iron deficiency), organ damage due to iron deposits in the liver, heart, and pancreas, and conditions like diabetes and cirrhosis
Bicarbonate	Bicarbonate plays a vital role in the physiological pH buffering system, maintaining acid-base homeostasis. It is involved in the regulation of pH in the stomach and small intestine, neutralizing acidic chyme, and is essential for metabolic functions such as carbon dioxide transport and excretion	Pathological conditions associated with bicarbonate include metabolic acidosis, systemic acidosis, kidney stones, hypertension, and brain dysfunction. It is also implicated in cancer progression and chronic kidney disease <sup>230</sup>
Phosphate	Phosphate is essential for bone and teeth formation, energy metabolism, cellular signaling, and pH buffering. It is also involved in the synthesis of DNA and RNA, and the regulation of protein phosphorylation <sup>231</sup>	Hypophosphatemia can lead to osteomalacia, rickets, and muscle weakness, while hyperphosphatemia is associated with chronic kidney disease, cardiovascular complications, and vascular calcification <sup>232</sup>
Amino acids (total)	Amino acids serve as building blocks of proteins, regulators of metabolic pathways, and precursors for hormones, neurotransmitters, and other biomolecules. They are essential for growth, repair, immune function, and maintaining homeostasis	Disorders in amino acid metabolism are associated with metabolic diseases, cardiovascular diseases, immune dysfunctions, and cancer. Specific conditions include phenylketonuria, maple syrup urine disease, and homocystinuria <sup>233</sup>
Urea	Urea plays a key role in osmoregulation, nitrogen excretion, and urine concentration. It is involved in the urea cycle, which detoxifies ammonia into urea for excretion. Urea transporters facilitate its movement across membranes, aiding in water balance and nutrient recycling	Pathological conditions associated with urea include chronic kidney disease (CKD), uremia, and cardiovascular diseases. High urea levels can lead to oxidative stress, endothelial dysfunction, and protein carbamylation, contributing to these diseases <sup>234</sup>
Cholesterol	Cholesterol is essential for cell membrane structure and fluidity, serves as a precursor for steroid hormones (e.g., cortisol, aldosterone, testosterone, estrogens), vitamin D, and bile acids, and facilitates the absorption of fat-soluble vitamins (A, D, E, K) <sup>235</sup>	High levels of LDL cholesterol are associated with atherosclerosis, coronary artery disease, stroke, and peripheral arterial disease. Other conditions include familial hypercholesterolemia and hypothyroidism <sup>235</sup>
Triglycerides	Triglycerides serve as the body's primary energy storage molecules, stored in adipose tissue and released during periods of energy demand. They are also involved in the transport of dietary fats via lipoproteins like VLDL and chylomicrons	High triglyceride levels (hypertriglyceridemia) are associated with cardiovascular diseases, pancreatitis, metabolic syndrome, and atherosclerosis. Extremely high levels can lead to acute pancreatitis



Table 2 (continued)

Biomolecule	Physiological conditions	Pathological conditions
Testosterone	Testosterone plays a key role in male reproductive development, including the formation of male reproductive tissues such as the testicles and prostate. It promotes secondary sexual characteristics like increased muscle and bone mass, body hair growth, and deepening of the voice. It also regulates libido, sperm production, and erythropoiesis (red blood cell production)	Pathological conditions associated with testosterone include hypogonadism, characterized by low testosterone levels leading to symptoms like reduced libido, erectile dysfunction, and decreased muscle mass. High testosterone levels can be linked to prostate cancer, cardiovascular risks, and metabolic syndrome. Other conditions include polycystic ovary syndrome (PCOS) in women and androgenic alopecia
Estradiol	Estradiol plays a critical role in the reproductive system, including the development and maintenance of female secondary sexual characteristics and the menstrual cycle. It also contributes to cardiovascular health by improving lipid profiles and promoting vasodilation, supports bone density by inhibiting bone resorption, and has neuroprotective effects, including anti-inflammatory actions and stimulation of neurogenesis <sup>236</sup>	Estradiol is implicated in pathological conditions such as breast cancer, cardiovascular diseases (e.g., stroke, deep vein thrombosis), and neurodegenerative disorders like Alzheimer's disease. It is also associated with conditions like endometriosis, uterine fibroids, and estrogen-induced cholestasis <sup>237</sup>
Progesterone	Progesterone plays a critical role in the menstrual cycle, pregnancy, and lactation. It prepares the endometrium for implantation, maintains pregnancy by suppressing uterine contractions, and supports mammary gland development. Additionally, it has neuroprotective effects, modulates immune responses, and regulates bone mass	Progesterone is implicated in pathological conditions such as endometriosis, breast cancer, endometrial hyperplasia, and progesterone resistance. It is also associated with neurodegenerative diseases and certain gynecological disorders <sup>238</sup>
C-reactive protein	C-reactive protein (CRP) is an acute-phase protein synthesized by the liver in response to inflammatory cytokines. It plays a role in the innate immune system by binding to damaged tissue, nuclear antigens, and certain pathogens. CRP activates the complement system, enhances phagocytosis, and promotes the clearance of cellular debris and pathogens. It also regulates platelet adhesion and chemotaxis during inflammation <sup>239</sup>	CRP is associated with various pathological conditions, including cardiovascular diseases (e.g., atherosclerosis, myocardial infarction), rheumatoid arthritis, systemic lupus erythematosus, type 2 diabetes, Alzheimer's disease, and Parkinson's disease. Elevated CRP levels are indicative of acute and chronic inflammation, and it is used as a biomarker for these conditions <sup>240</sup>
Interleukin-6	Interleukin-6 (IL-6) plays a role in immune responses, hematopoiesis, metabolism, and acts as both a pro-inflammatory cytokine and an anti-inflammatory myokine. It is involved in acute-phase responses, B and T lymphocyte activation, and metabolic regulation during exercise	IL-6 is implicated in autoimmune diseases such as rheumatoid arthritis, Castleman disease, and juvenile idiopathic arthritis. It is also associated with chronic inflammation, cytokine release syndrome, and conditions like Alzheimer's disease and multiple sclerosis <sup>241</sup>
Tumor necrosis factor- $\alpha$	Tumor necrosis factor- $\alpha$ (TNF- $\alpha$ ) plays roles in immunomodulation, fever, inflammatory response, inhibition of tumor formation, and inhibition of viral replication. It regulates survival, proliferation, and apoptosis of embryonic stem cells and progenitor cells, and is involved in neurogenesis, myelination, and synaptic plasticity in the central nervous system <sup>242</sup>	TNF- $\alpha$ is associated with autoimmune diseases such as rheumatoid arthritis, inflammatory bowel disease, and psoriasis. It is also linked to chronic inflammation, neuroinflammation, and diseases like multiple sclerosis, asthma, and chronic obstructive pulmonary disease <sup>243</sup>
Leptin	Leptin regulates energy homeostasis, neuroendocrine function, and metabolism. It signals the hypothalamus to suppress appetite, increase energy expenditure, and regulate body weight. It also plays roles in thermogenesis, glucose homeostasis, and reproductive function	Leptin is implicated in obesity, leptin resistance, hypothalamic amenorrhea, metabolic syndrome, and cardiovascular diseases. It is also associated with immune dysfunctions and certain infectious diseases due to its role in cytokine production <sup>244</sup>
Melatonin	Melatonin regulates sleep cycles, circadian rhythms, and acts as an antioxidant. It modulates immune function, reduces oxidative stress, and influences mitochondrial dynamics, including biogenesis, fission, fusion, and mitophagy <sup>245</sup>	Melatonin is associated with sleep disorders (e.g., insomnia, circadian rhythm sleep disorders), neurodegenerative diseases (e.g., Alzheimer's, Parkinson's), metabolic disorders (e.g., type 2 diabetes), and certain cancers <sup>245</sup>
Serotonin	Serotonin plays a role in mood regulation, gastrointestinal motility, cardiovascular function, sleep, appetite, and blood clotting. It acts as a neurotransmitter in the central nervous system and as a hormone in peripheral systems	Conditions associated with serotonin include serotonin syndrome, depression, anxiety disorders, schizophrenia, and gastrointestinal disorders like irritable bowel syndrome
Dopamine	Dopamine plays a role in motor control, reward and pleasure systems, mood regulation, attention, learning, memory, sleep, kidney function, and cardiovascular regulation	Dopamine is associated with Parkinson's disease, schizophrenia, ADHD, depression, addiction, and bipolar disorder <sup>246</sup>
Epinephrine	Epinephrine plays a key role in the fight-or-flight response, increasing cardiac output, raising glucose levels in the blood, and enhancing alertness. It also causes bronchodilation and vasodilation in skeletal muscles and the liver	Pathological conditions associated with epinephrine include pheochromocytoma, hypoglycemia, myocardial infarction, and cardiac arrhythmias



Advances in laser cutting and 3D printing have democratized the fabrication of capillary networks, supporting low-cost and rapid prototyping without cleanroom infrastructure.<sup>247</sup> Laser-cut films enable precise channel patterning, while 3D printing facilitates complex multilayered designs with embedded capillary elements. These techniques streamline development of capillary microfluidic components tailored for diverse wearable applications. The section below details material types and fabrication methods, comparing their functional benefits and limitations for wearable implementation.

### 3.1 Material selection

**3.1.1 Paper-based materials.** Paper-based substrates have gained considerable traction in capillary microfluidics due to their low cost, biocompatibility, and compatibility with simple, scalable fabrication methods such as wax printing, inkjet printing, and roll-to-roll processes.<sup>20,247–251</sup> Their porous structure supports passive fluid wicking, making them particularly attractive for wearable and point-of-care devices.<sup>248</sup> As shown in Fig. 2a, a representative platform uses paper microfluidics coupled with screen-printed

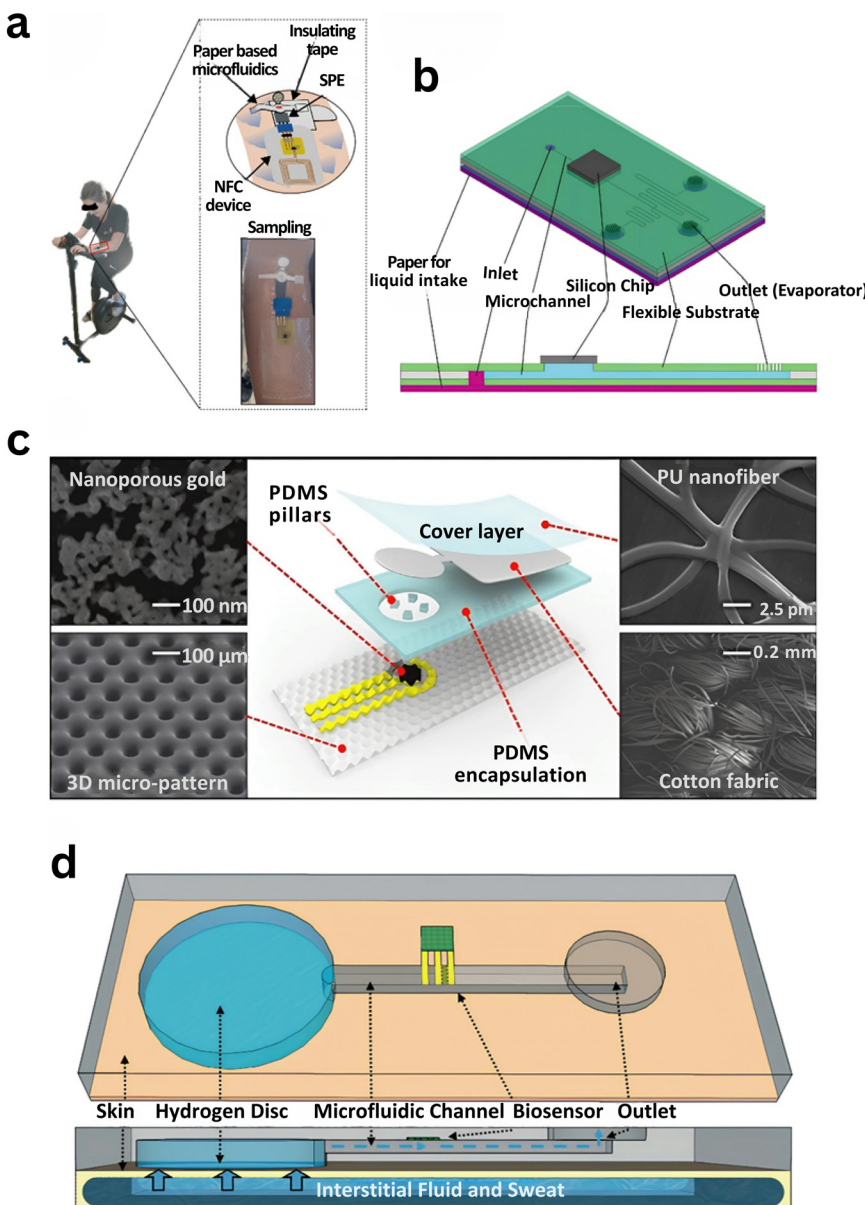


**Fig. 2** Representative materials used in wearable capillary microfluidic systems: (a) paper-based microfluidic patch with a screen-printed electrode for sweat cortisol sensing.<sup>247</sup> (b) Silicon-based microfluidic device for electrochemical sweat pH detection, integrating a paper inlet and laser-fabricated microchannels.<sup>276</sup> (c) Polymer-based stretchable patch for glucose monitoring using a nanoporous gold electrode and passive microfluidics.<sup>261</sup> (d) Hydrogel-disc-driven osmotic microfluidic system enabling fluid transport for biosensing through solute-induced flow.<sup>266</sup>



electrodes for cortisol detection in sweat. However, key limitations include inconsistent flow due to pore heterogeneity, poor reproducibility, and environmental sensitivity to humidity and temperature.<sup>17,20,248,250,252</sup> Recent efforts aim to enhance fluid control and durability through material modification and new patterning techniques to better suit wearable contexts.

**3.1.2 Silicon-based materials.** Silicon remains a widely used substrate in microfluidic systems, favored for its precision microfabrication, integration with electronics, and suitability for high-resolution channel architectures *via* photolithography and deep reactive ion etching.<sup>1,2,13,253</sup> Fig. 2b illustrates a hybrid silicon-paper device where paper facilitates sweat entry into structured silicon channels. These platforms offer high sensitivity and miniaturization, ideal for lab-on-chip and biosensing applications.<sup>254</sup> However, silicon's high fabrication cost, mechanical brittleness, and lack of flexibility limit its use in skin-conformal or disposable wearable formats.<sup>254–258</sup> Additionally, reliance on cleanroom-based processes presents further barriers for scalable, low-cost wearable deployment.

**3.1.3 Polymer-based materials.** Polymers such as polydimethylsiloxane, (PDMS), poly(methyl methacrylate) (PMMA), and polystyrene have gained widespread application in capillary microfluidics due to their flexibility, biocompatibility, optical transparency, and chemical resistance.<sup>29,254,256,259,260</sup> These properties make them particularly suitable for wearable and point-of-care applications. Fig. 2c illustrates a wearable PDMS-based capillary microfluidic platform incorporating a nanoporous gold electrode and PDMS pillar structure for sweat biomarker detection.<sup>261</sup> Various fabrication methods including soft lithography, injection molding, and hot embossing enable the creation of reproducible and complex microfluidic architectures.<sup>1,4,14,262,263</sup> However, polymeric materials face challenges such as analyte absorption into the matrix, which can compromise detection sensitivity and reproducibility.<sup>254</sup> Some polymers are also prone to temperature- and humidity-induced performance drift.<sup>251</sup> Potential leaching of monomers or additives raises concerns about contamination and assay interference. Finally, while these materials are common in research settings, their current fabrication processes are not yet optimized for scalable mass production, limiting commercial translation.

**3.1.4 Hydrogels.** Hydrogels are 3D polymer networks that absorb significant water, mimicking tissue softness and enhancing biocompatibility in wearable sensors and biosensors.<sup>15,259,264–267</sup> They can respond to external stimuli like temperature or pH and are useful in drug delivery and biosensing. Fig. 2(d) shows a hydrogel-based wearable patch integrating sensors for sweat and interstitial fluid.<sup>266</sup> Despite their utility, hydrogels may deform due to swelling, reducing structural integrity and sensing.<sup>259,265</sup> Their fabrication is complex, requiring tight control over polymerization and crosslinking, and degradation or leaching may limit long-term stability.<sup>264,266</sup>

**3.1.5 Composite materials.** Composite materials integrate two or more components like polymers, metals, or ceramics—to combine favorable mechanical and chemical traits for wearable microfluidics.<sup>268–271</sup> They support robust, multifunctional designs for sensing and diagnostics. However, issues like material compatibility, fabrication complexity, and higher production costs can limit their scalability.<sup>270–273</sup> Careful matching of thermal, chemical, and mechanical properties is essential to ensure device stability and long-term functionality. Material choice is central to designing wearable capillary microfluidics, requiring balanced consideration of performance, cost, fabrication ease, and biocompatibility.<sup>1,2,13,15–17,274,275</sup>

### 3.2 Key design principles for capillary microfluidics in wearable and point-of-care applications

A critical aspect of capillary microfluidic design is selecting materials suited to the target biofluid and application. Materials such as paper and fabric enable passive fluid movement by capillary action without requiring external pumps.<sup>15,20</sup> Their inherent porosity and hydrophilicity facilitate efficient wicking of small fluid volumes, making them well-suited for wearable sampling of sweat, saliva, tears, and interstitial fluid.<sup>277</sup> Fabrics, in particular, offer capillary channels formed by fiber gaps that allow liquid wicking along threads, which is advantageous for on-body applications due to their comfort and flexibility.<sup>278,279</sup> Biocompatible materials like PDMS, acrylics, and hydrogels are also widely used in wearable systems.<sup>13</sup> These materials are soft, stretchable, and conformable to skin, which helps maintain device integrity during movement. Material selection must be guided by both the physicochemical properties of the interface—such as wettability, swelling behavior, and fouling resistance—and the geometric features of the fluidic network, such as channel width, depth, and orientation.<sup>13,16</sup> Fluid transport performance is also strongly influenced by the layout of the microfluidic system. Design considerations include the shape and size of the channels, the surface properties that govern fluid spreading (wettability),<sup>280</sup> and the ability to sustain passive flow without external power.<sup>13</sup> Key components such as inlets, reservoirs, burst valves, and retention zones must be optimized to enable regulated fluid distribution and efficient use of small sample volumes. Minimizing the need for external actuators not only enhances portability but also improves usability in decentralized or low-resource settings.<sup>13,16</sup> In addition, effective designs must reduce evaporation losses and resist clogging or contamination from biofouling.<sup>281</sup> Sensors should be seamlessly integrated for real-time biomarker monitoring, and their performance should remain stable across varying hydration states and environmental exposures.<sup>282</sup> For manufacturing and deployment, systems must be cost-effective and robust. In wearable applications, the device should also be soft, lightweight, breathable, and safe for prolonged skin contact.<sup>262</sup> Fig. 3 summarizes these



key design principles, outlining how materials, fluidic geometry, sensor integration, and human factors together determine the functionality and translational success of wearable capillary microfluidic platforms.

## 4. Fabrication of wearable capillary microfluidic devices

The fabrication of capillary microfluidic devices plays a central role in defining their precision, scalability, and compatibility with wearable systems. Key fabrication strategies include rapid prototyping methods such as laser cutting and 3D printing, as well as cleanroom-based microfabrication approaches like photolithography, soft lithography, and deep reactive ion etching.<sup>5,13,17,32,44–46</sup> Laser cutting and 3D printing offer fast, cost-effective solutions for prototyping and scale-up, as shown in Fig. 4a, where laser-cut channels and 3D-printed molds demonstrate their utility in creating fluid conduits with varying volumes.<sup>11,19,199,283</sup> These methods support quick iterations but may be limited by resolution and material choices.<sup>17,251,254</sup> In contrast, photolithography and deep etching provide high fidelity and fine features but require expensive cleanroom infrastructure and are less suited for flexible or wearable formats.<sup>13</sup> Soft lithography presents a compromise between precision and accessibility, supporting fabrication of flexible PDMS-based microfluidic systems (Fig. 4b), though it can still be time-

intensive and not ideal for high-throughput production. The integration of capillary elements including flow resistors, stop valves, trigger valves, and burst valves enables passive and self-regulated flow, eliminating the need for external pumps.<sup>13</sup> Notably, affordable stereolithography (SLA)-based 3D printing now enables the high-resolution, low-cost fabrication of microneedles, with sensor manufacturing costs reported as low as €0.10 per patch. This cost-effective approach facilitates scalable production of microneedle arrays for both biofluid extraction and continuous biochemical monitoring, significantly improving the accessibility and translational potential of MN-based sensors for wearable and point-of-care diagnostics.<sup>284,285</sup> Together, these fabrication strategies enable the realization of autonomous microfluidic circuits tailored for wearable sensing applications.

Capillary microfluidics leverages physical forces such as surface tension, viscosity, and pressure to drive fluid flow through passive means.<sup>13,16,274,275</sup> This flow behavior is modulated by integrated capillary elements including retention burst valves, retention valves, trigger valves, capillary pumps, and vents which control timing, directionality, and flow rates (Fig. 4c). While numerous other components exist, these elements represent core building blocks in self-powered systems. For a more detailed treatment of capillary elements and their mechanisms, refer to comprehensive sources in ref. 13 and 14.

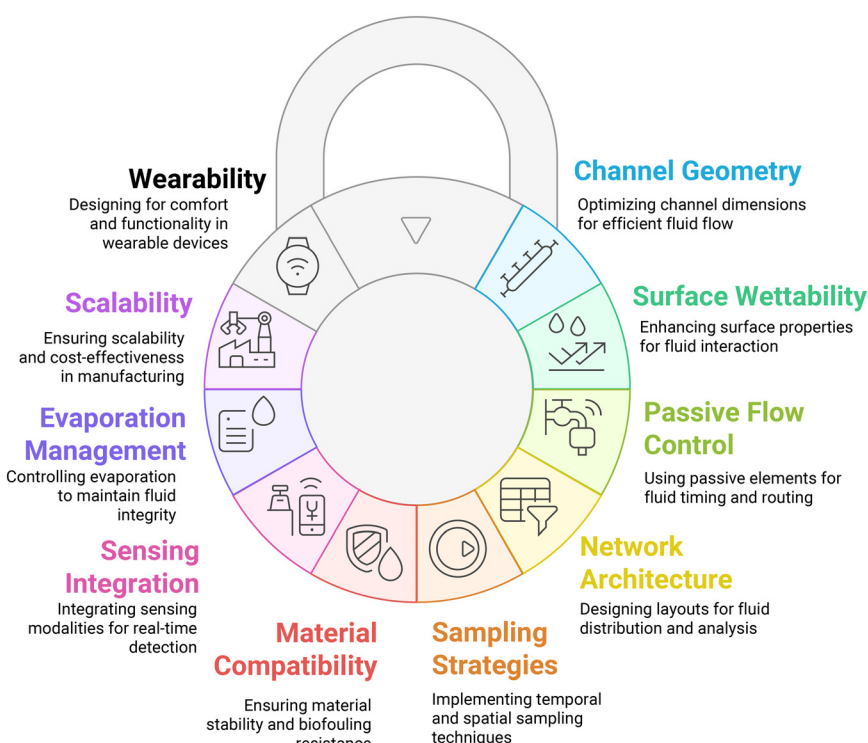


**Fig. 3** Key design principles for wearable capillary microfluidic systems ensuring efficient fluid handling, biochemical sensing, material compatibility, and user comfort. Integration of suitable materials, optimized channel layout, and sensor interfaces enables robust, autonomous operation for on-body and point-of-care applications.



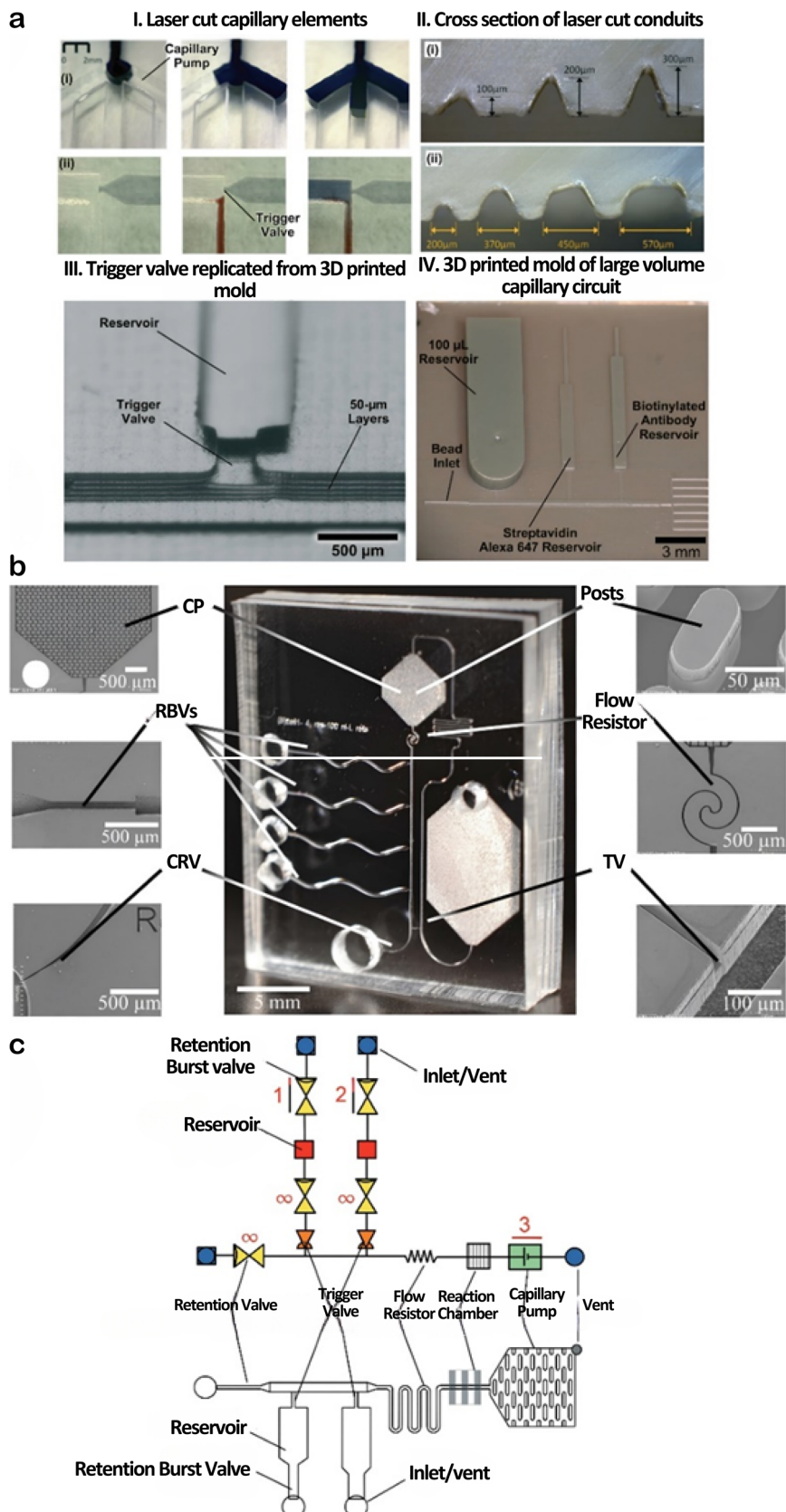


**Fig. 4** Fabrication approaches wearable capillary microfluidic devices. (a) Prototyping using carbon dioxide ( $\text{CO}_2$ ) laser cutting and 3D printing: (I) laser-cut capillary components,<sup>283</sup> (II) cross-sectional view of laser-cut conduits,<sup>283</sup> (III) trigger valve formed using a 3D-printed mold,<sup>286</sup> and (IV) mold for a large-volume capillary circuit.<sup>287</sup> (b) Optical image of a PDMS-based microfluidic circuit with side reservoirs, flow reversal, and venting via a PDMS cover.<sup>14</sup> (c) Schematic of integrated capillary elements (e.g., valves and resistors) for self-regulated fluid flow; see ref. 13 for detailed descriptions.

## 5. Capillary microfluidic-based wearable sensors and biosensors

Capillary microfluidic-enabled wearables can be systematically categorized by their sample acquisition

strategy chrono-sampling or continuous sampling and by the location of analysis on-body or off-body. This framework aids in mapping specific biosensing formats to corresponding cases in health monitoring and diagnostics.

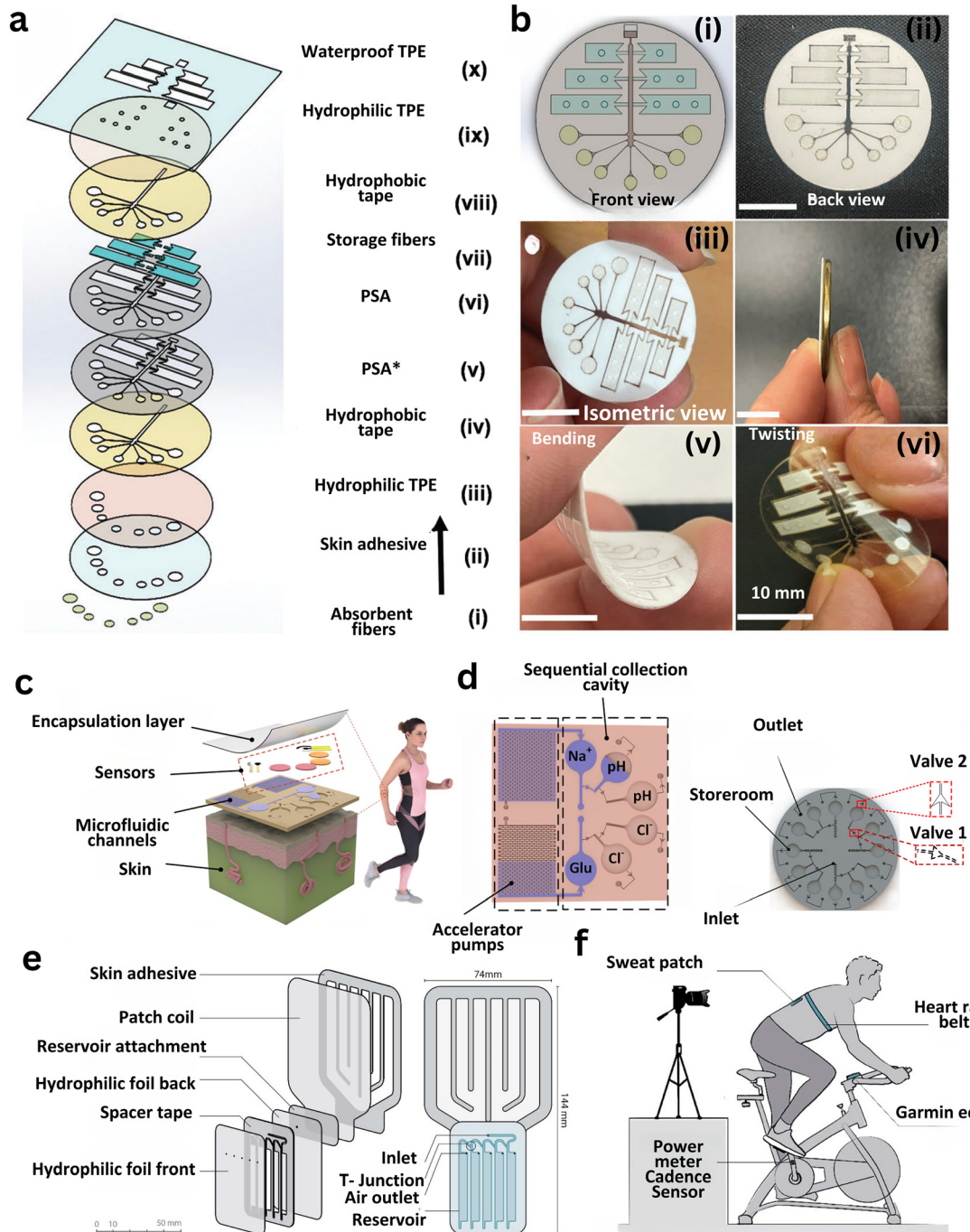


**Fig. 5** Representative designs of capillary microfluidic sweat patches developed for chrono-sampling and off-body analysis. (a) Schematic of the ten-layer MicroSweat patch designed for passive sweat collection, directional flow, and storage in fiber layers. (b) (i–vi) Images of the patch showing front, back, isometric, twisted, and bent configurations, demonstrating flexibility (scale bar: 10 mm).<sup>19</sup> (c) Integration of a capillary microfluidic patch on skin with layered encapsulation, sensors, and colorimetric chambers for offline biomarker analysis. (d) Layout of sequential sweat chambers with integrated capillary pumps for temporal glucose,  $\text{Na}^+$ , and pH sensing.<sup>288</sup> (e) Exploded and assembled views of a hydrophilic film-based microfluidic patch with funnel inlet, air vents, and channel architecture. (f) On-body validation during exercise with biometric monitoring setup.<sup>289</sup>



## 5.1 Chrono sampling and off-body analysis (CHOFF)

Chrono-sampling systems enable periodic fluid collection for downstream laboratory testing. They are particularly useful for applications that do not require continuous monitoring and benefit from simpler, disposable, and user-friendly platforms. By limiting contact time and minimizing on-device processing, CHOFF systems reduce contamination risk and are compatible with sweat, saliva, ISF, and tears.

**5.1.1 CHOFF in sweat.** Several CHOFF sweat patches utilize capillary microfluidics to autonomously collect sweat for offline analysis. The MicroSweat patch exemplifies this approach, combining passive capillary flow with integrated delay and trigger valves to capture sweat into fiber chambers (Fig. 5a and b).<sup>19</sup> The patch prevents evaporation and bubble formation, and collected samples are centrifuged and analyzed *via* Enzyme Linked Immunosorbent Assay (ELISA) for cortisol, with stress levels correlated through perceived stress scores. In a separate design, epidermal microfluidic patches incorporated capillary pumps and burst valves to achieve sequential sweat collection. Graded burst pressures allowed time-resolved sampling for multiplexed glucose, sodium, chloride, and pH analysis both *in vitro* and on-body (Fig. 5c and d).<sup>288</sup> Similarly, a disposable patch fabricated from hydrophilic film and 3M adhesive employed capillary action to guide sweat into five storage reservoirs ( $>100 \mu\text{L}$  each), which were later analyzed *via* ion chromatography (Fig. 5e and f).<sup>289</sup> The PharmChek™ patch, a commercially available system, uses a polyurethane adhesive layer and cellulose pad to collect sweat continuously over 24–168 hours. Post-wear, gas chromatography-mass spectroscopy (GC-MS) analysis of the patch detects drug metabolites like benzoylecgonine and egonine methyl ester, offering a non-invasive alternative for workplace testing and clinical drug monitoring.<sup>290,291</sup>

Capillary microfluidics have also been adapted with Tesla valves to promote unidirectional flow, reduce backflow, and spatially separate sweat samples. Filter paper-based chambers functionalized with colorimetric reagents enable glucose and pH detection, with PDMS microchannels and polyvinylpyrrolidone (PVP)-treated surfaces improving wettability.<sup>292</sup> Sweat patches for environmental exposure monitoring such as bisphenol A (BPA) have also been explored.<sup>293</sup> However, challenges like low sweat volume under typical conditions, variable patch placement, and matrix effects limit their sensitivity. Still, these studies highlight sweat's value as a non-invasive matrix for temporal exposure tracking. Programmable sweat capture has also been demonstrated using electrowetting valves. In one example, silver electrodes were inkjet-printed on hydrophilic polyethylene terephthalate (PET), with one surface rendered hydrophobic *via* a perfluorodecanethiol (PFDT) monolayer.<sup>294</sup> The valve held fluid for up to 9 h before actuated release, allowing selective time-point sampling for biomarker analysis. Finally, a low-cost wearable patch with integrated Ag/AgCl electrodes enabled both continuous conductivity

sensing and chronological sweat collection in passive capillary reservoirs. Fabricated with PET and adhesive layers, this system captured sweat into 5–10 chambers ( $\sim 50 \mu\text{L}$  each) and enabled ion chromatography-based  $\text{Na}^+/\text{Cl}^-$  analysis.<sup>295</sup> However, challenges like low secretion rates and contamination from skin residues remain and highlight the need for improved interface design.

**5.1.2 CHOFF in tears.** Tear fluid is an attractive biofluid for chrono-sampling due to its non-invasive collection and rich molecular content. Common collection methods include Schirmer strips (ScS) and capillary tubes (CT), each leveraging passive absorption or capillary action, respectively (Fig. 6a–c).<sup>296</sup> Comparative studies have shown similar total protein yields ( $\sim 4.6\text{--}4.8 \mu\text{g } \mu\text{L}^{-1}$ ), with ScS offering advantages in ease, speed, and minimal ocular manipulation.<sup>297</sup> ScS platforms also support multiplexed diagnostics, making them well-suited for periodic tear sampling. Recent innovations in capillary microfluidics have enabled tear collection directly from the ocular surface. For instance, scleral lenses integrated with capillary microchannels fabricated *via*  $\text{CO}_2$  laser micromilling enable continuous tear collection and multiplexed detection within embedded reaction chambers.<sup>298</sup> Capillary-based sampling systems have also incorporated ion-selective optode membranes for real-time  $\text{K}^+$ ,  $\text{Na}^+$ , and pH sensing,<sup>299</sup> although interference from tear additives remains a challenge. Mass spectrometry-based proteomics has expanded tear fluid diagnostics, revealing disease-specific protein signatures associated with conditions such as Sjögren's syndrome, keratoconus, and glaucoma.<sup>300</sup> Thread-based sampling using phenol red threads (PRTs) coupled with capillary electrophoresis has allowed detection of small molecules at nanoliter volumes, highlighting potential for metabolomics and pharmacological monitoring.<sup>301</sup> Colorimetric Schirmer strips integrating glucose oxidase have also demonstrated effective glucose detection *via* enzymatic dye formation,<sup>302</sup> with future adaptability toward inflammatory and drug-response biomarkers. Finally, detection of oligoclonal IgG bands in tear samples of patients with multiple sclerosis suggests that tear analysis could complement cerebrospinal fluid diagnostics in neurological assessments.<sup>303</sup> These advancements underscore the utility of CHOFF strategies in leveraging tear fluid for accessible and minimally invasive health monitoring.

**5.1.3 CHOFF in ISF.** Minimally invasive ISF sampling strategies have enabled chrono-sampling and off-body analysis of clinically relevant biomarkers. These platforms frequently integrate microneedle (MN) arrays with capillary microfluidics to autonomously draw small ISF volumes without pumps, preserving analyte integrity for delayed analysis (Fig. 6d). In one design, silicon MN arrays fabricated *via* deep reactive ion etching accessed epidermal ISF and routed it through capillary microchannels into backside reservoirs for colorimetric glucose detection ( $80\text{--}120 \text{ mg dL}^{-1}$ ).<sup>304</sup> A separate system employed crosslinked



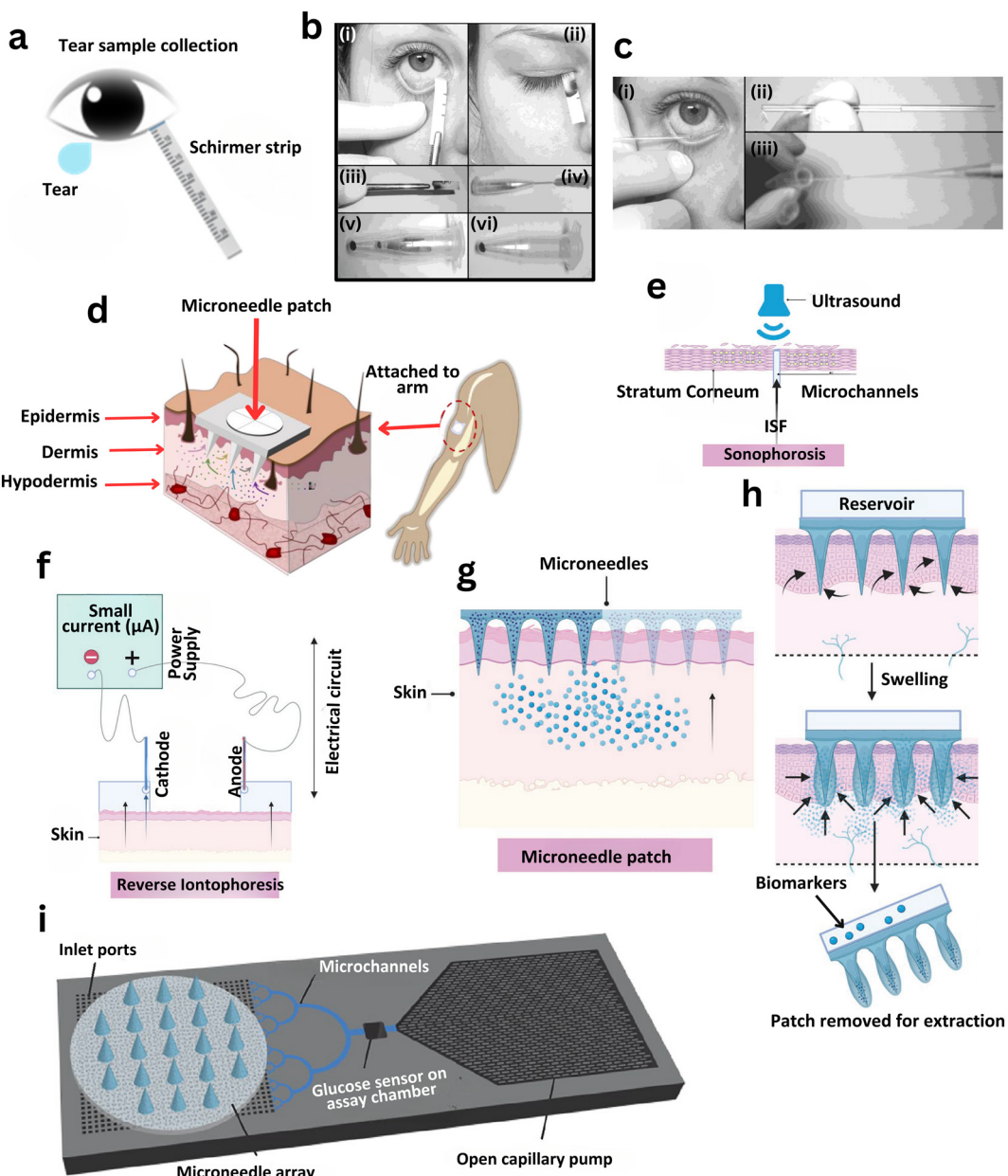


**Fig. 6** Capillary microfluidics enable minimally invasive chrono-sampling of tears and ISF using diverse techniques integrated with wearable platforms. (a) Schematic of tear fluid absorption via Schirmer strip, a passive method for chrono-sampling.<sup>312</sup> (b) Stepwise Schirmer strip application and removal: (i and ii) placement at lower eyelid, (iii and iv) capillary absorption, (v and vi) retrieval for downstream analysis. (c) (i-iii) Tear sampling with a capillary tube positioned at the canthus for passive fluid uptake.<sup>297</sup> (d) Microneedle patch penetrating skin layers to access ISF.<sup>305</sup> (e) Sonophoresis approach using low-frequency ultrasound to create transient microchannels for ISF extraction. (f) Reverse iontophoresis mechanism enabling migration of charged ISF constituents across the skin via mild electrical current. (g) Standard microneedle-based ISF sampling through skin-generated microchannels. (h) Hydrogel-based microneedle patch: (top) insertion and swelling, (middle) biomarker diffusion, (bottom) patch removal for analysis.<sup>306</sup> (i) Continuous ISF flow enabled by porous microneedles coupled with a glucose biosensor and open capillary pump for real-time analysis.<sup>308</sup>

methacrylated hyaluronic acid (MeHA) MNs, which swelled upon skin insertion to extract ISF for on-patch detection of glucose, lactate, cholesterol, and pH via wax-patterned test papers.<sup>305</sup> Beyond MNs, other minimally invasive techniques have emerged. Ultrasound (sonophoresis), reverse iontophoresis (Fig. 6e and f), and reservoir-based swelling patches (Fig. 6h) were used to disrupt the stratum corneum

and extract ISF for later lab-based analysis.<sup>306</sup> Additionally, thermal ablation using gold microheaters embedded in flexible substrates enabled ISF exudation into PDMS-*b*-PEO-modified hydrophilic microchannels, where biomarkers like 6-monoacetylmorphine were analyzed via voltammetry and liquid chromatography (LC) LC-MS.<sup>307</sup> Hybrid platforms combining porous MNs with silicon microfluidics have

demonstrated continuous ISF flow ( $0.08 \mu\text{L min}^{-1}$ ) using capillary pumps composed of micropillar arrays (Fig. 6i).<sup>308</sup> Although not sensor-integrated, this system supports future

real-time diagnostics. Another application fused hollow MNs with lateral flow immunoassays to detect malaria antigen (PfHRP2) within 20 min *via* capillary-fed gold nanoparticle

**Table 3** Summary of chrono-sampling and off-body (CHOFF) capillary microfluidic systems for non-invasive biomarker detection

S. no.	Analyte	Target biomarker	Sample volume	Concentration range	Sensing method	Number of participants	Ref.
1	Sweat	Glucose	70 $\mu\text{L}$	0 to 610 $\mu\text{M}$	Colorimetric analysis	1	292
2	Sweat	pH	70 $\mu\text{L}$	5	Colorimetric analysis	1	292
3	Sweat	Cocaine-d5, benzoylecgonine-d5, ecgonine methyl ester-d5	—	2 ng per patch	Gas chromatographic-mass spectrometric (GC-MS) assay	12	290
4	Sweat	Cortisol	120 $\mu\text{L}$	25 to 125 ng $\text{mL}^{-1}$ 100–1000 ng $\text{mL}^{-1}$ (armpit)	ELISA	11	19
5	Sweat	$\text{Na}^+$	5.9 $\mu\text{L}$	20–200 mM	Electrochemical	6	288
6	Sweat	$\text{Cl}^-$	5.9 $\mu\text{L}$	20–200 mM	Colorimetric analysis	6	288
7	Sweat	Glucose	5.9 $\mu\text{L}$	50–200 $\mu\text{M}$	Potentiostatic	6	288
8	Sweat	pH	5.9 $\mu\text{L}$	—	Colorimetric analysis	6	288
9	Sweat	Na	>100 $\mu\text{L}$	—	Ion chromatography	6	289
10	Sweat	Cl	>100 $\mu\text{L}$	—	Ion chromatography	6	289
11	Sweat	K	>100 $\mu\text{L}$	—	Ion chromatography	6	289
12	Sweat	Bisphenol-A (BPA)	—	195 ng $\text{mL}^{-1}$	Liquid chromatography-tandem mass spectrometry	50	293
13	Sweat	$\text{Na}^+$	14 $\mu\text{L}$	15–60 mM	Electrical impedance (ion chromatography)	5	313
14	Artificial sweat	—	50 $\mu\text{L}$	—	Electrowetting	<i>In vitro</i>	294
15	Sweat	$\text{Na}^+$ , $\text{Cl}^-$	70 $\mu\text{L}$	10–150 mM	Ion chromatography	6	295
16	Tear film	Proteins, nucleic acids, cytokines	5–10 $\mu\text{L}$	—	BCA assay – protein Proteomics – mass spectroscopy Western blot – protein IL-17 A – MSD immunoassay RT-qPCR-gene expression	10	312
17	Tears	Protein (surfactant protein)	—	—	Bradford assay Western blot – detection of surfactant protein	9	297
18	Tears	$\text{K}^+$	—	0.010–0.050 M	Ionophores and chromoionophores	1	299
19	Tears	$\text{Na}^+$	—	0.120–0.160 M	Ionophores and chromoionophores	1	299
20	Tears	pH	—	6.8–7.5	Bromophenol blue-doped sol-gel film	1	299
21	Tears	Glucose	—	—	Amperometry	1	298
22	Mice tears	Arginine, histamine, alanine, taurine, glutamate, and aspartate	$70 \pm 25 \text{ nL}$	—	Capillary electrophoresis with light-emitting diode-induced fluorescence detection (CE-LEDIF)	1	301
23	Tears	Glucose	6 $\mu\text{L}$	0.1–2 mM	Colorimetric	—	302
24	Tears	Total protein, immunoglobulin G (IgG)	10 $\mu\text{L}$	—	Total protein – Bradford assay	15	303
25	ISF	Glucose	—	80–120 mg $\text{dL}^{-1}$	ELISA – IgG Commercial blood glucose test	1	304
26	ISF	Glucose	16.22 $\mu\text{L}$	0–16 mM	Colorimetric	1	305
27	ISF	Lactate	16.22 $\mu\text{L}$	0–3.2 mM	Colorimetric	1	305
28	ISF	Cholesterol	16.22 $\mu\text{L}$	0–12 mM	Colorimetric	1	305
29	ISF	pH	16.22 $\mu\text{L}$	5–8	Colorimetric	1	305
30	ISF	6-Monoacetylmorphine	1 $\mu\text{L}$	—	Liquid chromatography-mass spectrometry	3	307
31	ISF	Glucose	—	50–400 mg $\text{dL}^{-1}$	Colorimetric	Rat models, rat skin	314
32	ISF	miRNA-21, miRNA-141, miRNA-155 (biomarkers for psoriasis)	21.34 $\mu\text{L}$ in 30 min	—	Fluorescence	Mouse	315
33	ISF	Cytokines (IL-6)	—	—	Ultrasensitive fluorescent immunoassay	Mice	301
34	ISF	Matricellular protein periostin	—	—	Plasmonic fluor-enhanced microneedles	Mice	301



strips.<sup>309</sup> Needle-free capillary microfluidic systems using magnetohydrodynamic (MHD) flow have also shown promise. These platforms apply orthogonal electric and magnetic fields to induce Lorentz-force-driven ISF transport for enzymatic glucose assays, yielding mean absolute relative difference values on par with commercial continuous glucose monitoring.<sup>310</sup> Expanding beyond skin, a capillary-integrated nanofluidic probe with peristaltic pumping enabled membrane-free sampling of brain ISF for neurochemical biomarker detection *via* LC-MS/MS.<sup>311</sup> highlighting the versatility of capillary microfluidics across biofluids and tissue types for chrono-sampling diagnostics. Summary of CHOFF capillary microfluidic systems for non-invasive biomarker detection is presented in Table 3.

## 5.2 Chrono sampling and on-body analysis (CHON)

Chrono sampling with on-body analysis integrates time-resolved biospecimen collection with real-time sensing, enabling dynamic health monitoring without requiring sample removal. These platforms utilize capillary microfluidics to autonomously route biofluid to integrated sensors for *in situ* biochemical detection.

**5.2.1 CHON in sweat.** To address delays in sweat ion detection due to fluid transport lag, a vision-sensor-assisted wearable patch was developed for point-by-point correction of  $\text{Na}^+$  concentration using sweating rate data, improving time-resolved diagnostic accuracy.<sup>316</sup> A multilayer microfluidic patch fabricated *via* laser cutting used passive flow to direct sweat into colorimetric assay wells for chloride sensing and sweat rate estimation (Fig. 7a and b).<sup>317</sup> Smartphone imaging quantified real-time analyte levels, which correlated well with standard absorbent patches. A 3D-printed integrated patch combined flexible ion-selective sensors and a microfluidic sweat handling unit on stretchable PDMS to simultaneously monitor  $\text{Na}^+$ ,  $\text{K}^+$ , and  $\text{Ca}^{2+}$  without external pumps (Fig. 7c).<sup>318</sup> SwEatch, another dual-channel platform, continuously measured  $\text{Na}^+$  and  $\text{K}^+$  during exercise, showing ranges of 0.03–2.97 mM and 0.13–7.25 mM, respectively, with minimal motion artifacts.<sup>319</sup> A nanofiber-integrated microfluidic sensor used an integrated microfluidic sensor sweat-extracting layer and a MIP-modified electrode for specific cortisol detection. On-body validation across five volunteers confirmed linear detection from 1.0 to 1000 nM (LOD: 0.35 nM) and correlation with ELISA.<sup>320</sup> Capillary burst valves and microfluidic pumps were employed for sequential sweat routing and analyte isolation. Burst valves with 125–150 Pa threshold ensured clean temporal separation, while microcolumn-based pumps enhanced passive flow (sweat volume ~5.9  $\mu\text{L}$  per chamber) for multiplex analysis of  $\text{Na}^+$ ,  $\text{Cl}^-$ , glucose, and pH.<sup>288</sup> Electrowetting valves further enabled chrono-controlled sweat capture and dynamic delivery of redox agents for real-time cortisol and glucose sensing.<sup>294</sup> In another MIP-based system, electrospun nanofiber microchannels enabled capillary-driven cortisol transport to electrochemical sensors

with built-in Prussian blue nanoparticles (PBnPs) for signal amplification.<sup>320</sup> A closed-loop platform integrated sweat diagnostics with transdermal nutrient delivery (Fig. 7d and e), using colorimetric detection and triggered reagent release for personalized feedback.<sup>321</sup>

Biodegradable microfluidics employing porous paper and capillary routing have emerged for eco-friendly hydration monitoring.<sup>322</sup> Waterproof epidermal patches now enable real-time biomarker detection even during aquatic activity. Spectroscopy-enabled 3D-printed devices with microcuvettes offer optical precision, while ketone-sensing patches expand metabolic tracking *via* colorimetric sensing.<sup>323,324</sup> To address sweat accumulation beneath sensors, a 3D paper-based electrochemical device (3D-PMED) was developed with layered microfluidics for vertical and lateral sweat flow, continuous refresh, and real-time glucose detection (Fig. 7f–h).<sup>21</sup> Iontophoresis-assisted systems stimulate sweat secretion for consistent sampling,<sup>325</sup> while soft microfluidic devices store sweat chronologically for retrospective analysis.<sup>7</sup> Further innovations include potentiometric ion sensors for electrolyte monitoring,<sup>326</sup> skin-mounted enzymatic sensors for alcohol and ammonia detection,<sup>327</sup> and multilayer patches for colorimetric analysis with embedded standard references (Fig. 7i and j). Printable microfluidics now support simultaneous cortisol and glucose detection,<sup>328</sup> and tattoo-based electrochemical biosensors enable discreet alcohol monitoring in real-time.<sup>329</sup>

**5.2.2 CHON in saliva.** Recent advancements have enabled real-time, on-body analysis of salivary biomarkers using wearable mouthguard-based biosensors. A lactate biosensor embedded in a mouthguard was developed, using a screen-printed electrode modified with lactate oxidase (LOX) for amperometric detection of hydrogen peroxide, a byproduct of lactate metabolism.<sup>330</sup> Building on this, a wearable biosensor for uric acid detection was introduced, featuring a uricase-modified electrode and wireless transmission *via* Bluetooth low energy (BLE), enabling seamless monitoring of salivary uric acid in real-time (Fig. 8a).<sup>331</sup> The lactate-sensing mechanism, illustrated in Fig. 8b, uses LOX to convert lactate to pyruvate and  $\text{H}_2\text{O}_2$ , which is then detected electrochemically using a Prussian blue-modified carbon electrode.<sup>330</sup> For diabetes management, a “Cavitas sensor” embedded with a platinum electrode coated in glucose oxidase enabled oral glucose monitoring through amperometry, with real-time readouts enabled by an integrated telemetry system.<sup>332</sup> Further innovations led to a fully assembled glucose-sensing mouthguard incorporating a BLE telemetry module and compact power source, with PDMS encapsulation and conductive springs ensuring mechanical stability and electrical interfacing (Fig. 8c).<sup>333</sup>

**5.2.3 CHON in tears.** Capillary microfluidics-based platforms have advanced tear-based chrono-sampling by enabling passive, real-time analyte tracking with minimal disruption. A microfluidic smart contact lens fabricated *via*  $\text{CO}_2$  laser ablation features ring-shaped microchannels for capillary-driven tear uptake and direct biomarker sensing



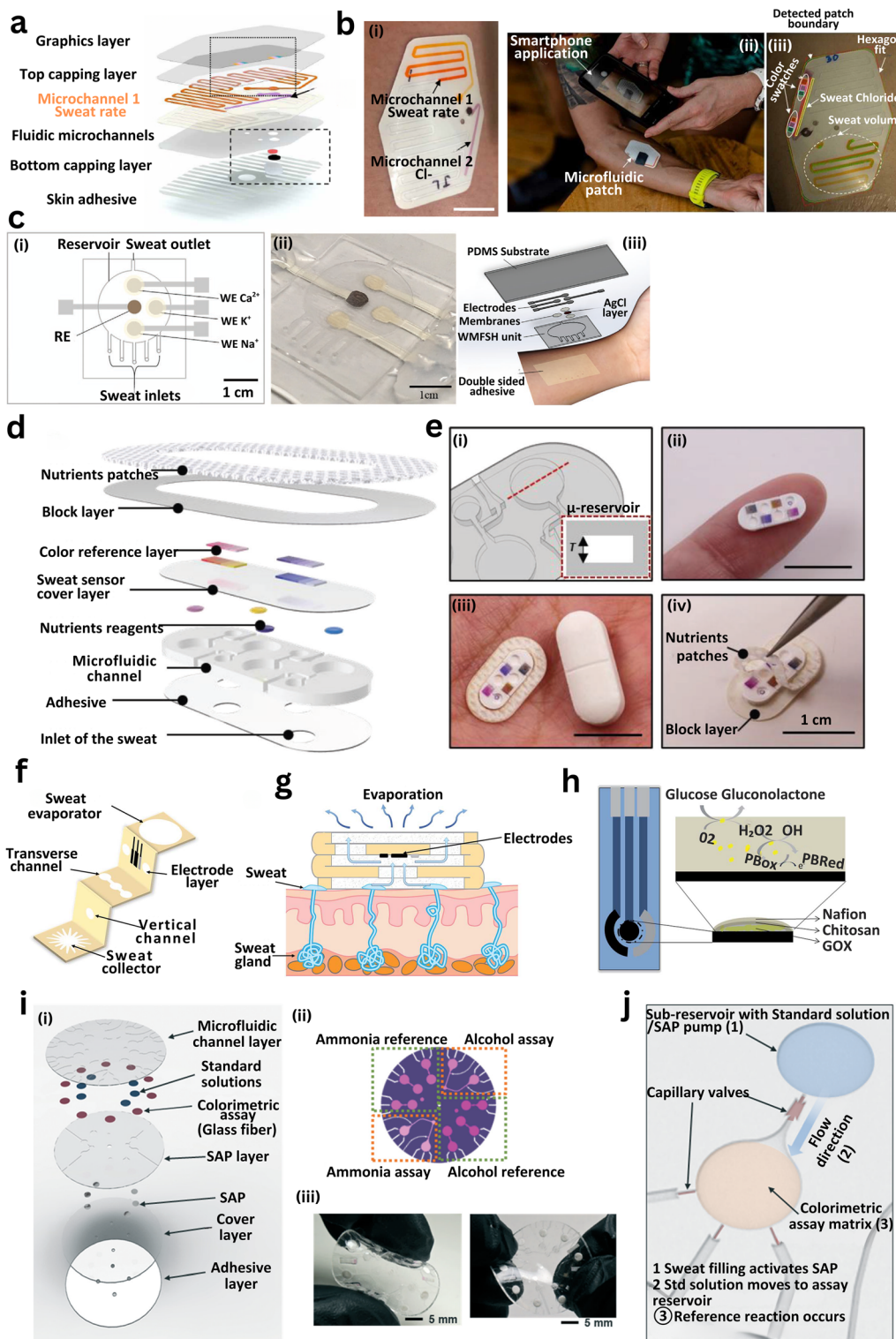


**Fig. 7** Wearable microfluidic platforms developed for chrono-sampling and on-body analysis of sweat biomarkers. (a) Schematic of a multilayered sweat patch comprising graphics, capping, microfluidic, and skin-adhesive layers. (b) (i) Microchannels for simultaneous sweat rate and chloride sensing; (ii) on-body application with smartphone readout; (iii) sensing regions and patch boundaries.<sup>317</sup> (c) (i) Layout for ion-selective sweat detection ( $\text{Ca}^{2+}$ ,  $\text{K}^+$ ,  $\text{Na}^+$ ); (ii) assembled patch; (iii) on-skin deployment with labeled cross-section.<sup>318</sup> (d) Exploded view showing nutrient sensing, colorimetric, blocking, adhesive, and channel layers. (e) (i) Embedded micro-reservoir design; (ii and iii) fingertip and pill-size comparison; (iv) annotated sensing locations.<sup>321</sup> (f) 3D paper-based evaporator with transverse/vertical fluidics, central collector, and electrode layer. (g) Operational diagram: sweat uptake, guided evaporation, and electrode-based sensing.<sup>21</sup> (h) Schematic of electrochemical glucose sensor using Nafion, chitosan, and GOx for enzymatic detection.<sup>21</sup> (i) (i) Exploded patch view with sweat transport, colorimetric assay (ammonia/alcohol), superabsorbent polymer retention, and adhesive layers; (ii) assay layout with reference zones; (iii) assembled patch image.<sup>327</sup> (j) Mechanism of reference channel operation: SAP activation, capillary flow of standard solution, and calibration reaction sequence.

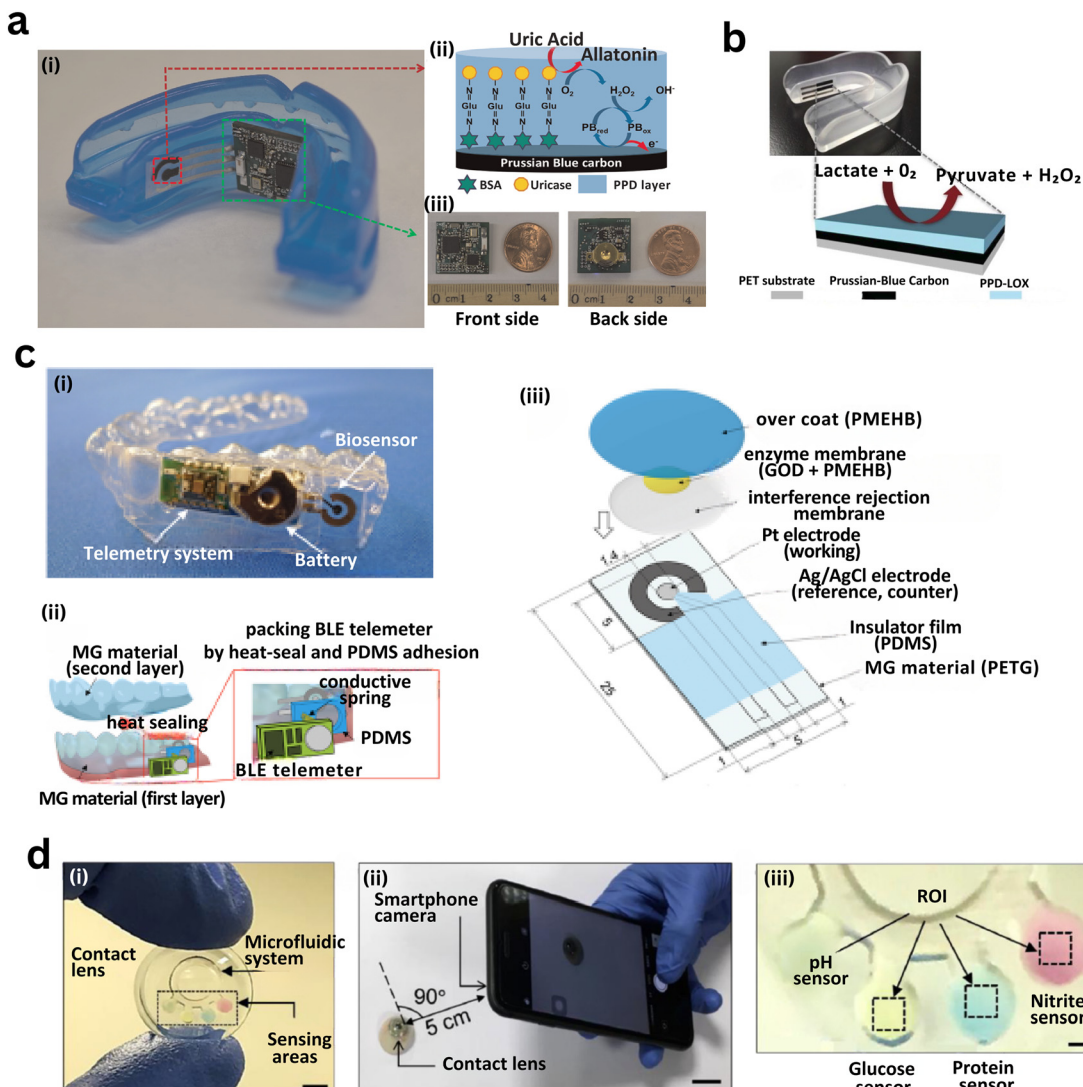


**Fig. 8** Capillary-integrated biosensing strategies have been implemented for real-time, on-body salivary and tear fluid analysis using wearable platforms such as mouthguards and smart contact lenses. (a) Wearable mouthguard biosensor for uric acid detection: (i) photograph of the mouthguard integrating a miniaturized electronic module for signal acquisition and wireless data transmission. (ii) Enzymatic detection mechanism: uricase catalyzes uric acid to allantoin, producing  $\text{H}_2\text{O}_2$  detected via a Prussian blue-modified carbon electrode. (iii) Front and rear views of the fabricated mouthguard with coin scale for size comparison.<sup>331</sup> (b) Schematic of lactate detection using a mouthguard biosensor: lactate oxidase (LOX) converts lactate to pyruvate and  $\text{H}_2\text{O}_2$ , which is quantified electrochemically via a Prussian blue-modified electrode.<sup>330</sup> (c) Fully integrated wireless glucose biosensor system: (i) photograph of the assembled device including glucose sensor, BLE telemetry, and battery. (ii) Assembly steps showing PDMS encapsulation and conductive spring contacts. (iii) Exploded view of multilayer biosensor components including enzyme membrane, interference rejection layer, electrode system, insulating film, and MG substrate.<sup>333</sup> (d) Smart contact lens with integrated microfluidic biosensors for multiplexed tear analysis: (i) lens with structured capillary microchannels and embedded biosensing zones. (ii) Illustration of smartphone-based optical readout positioned at 90° and 5 cm from the eye. (iii) Annotated sensing zones for detection of pH, glucose, protein, and nitrite biomarkers within tear fluid.<sup>334</sup>

(Fig. 8d(i)). The device uses reflection peak shifts for naked-eye detection of pH, glucose, protein, and nitrite levels within 15 s (Fig. 8d(ii and iii)).<sup>334</sup> To enhance selectivity and eliminate external power requirements, a Prussian blue-based lens was created, where PB electrodes catalyze  $\text{H}_2\text{O}_2$  from glucose oxidation, triggering a blue color shift visible to the eye and quantifiable via smartphone imaging, with a detection limit of 0.05 mM.<sup>335</sup> In another platform, a graphene-glucose oxidase biosensor modulates light emitting diode (LED) brightness in response to glucose concentration

changes, using metal nanofiber electrodes and a wireless RF-powered antenna system; *in vivo* tests on rabbits confirmed stable operation.<sup>336</sup> Beyond diagnostics, therapeutic lenses were developed using a three-electrode glucose sensor integrated with a flexible drug delivery system (f-DDS) for genistein release via electrical stimulation, targeting diabetic retinopathy. Animal studies validated both glucose sensing and drug delivery performance.<sup>337</sup> For stress hormone monitoring, a smart lens with NFC transmission and cortisol immunosensor was designed using a hybrid architecture of



rigid islands and flexible joints, allowing comfort and stability. This system wirelessly transmitted cortisol levels to a smartphone, with rabbit and human trials confirming its feasibility for continuous stress assessment.<sup>338</sup>

**5.2.4 CHON in ISF.** Capillary-integrated ISF biosensors enable minimally invasive chrono-sampling of dynamic biomarkers such as glucose, lactate, pH, drugs, DNA, and electrolytes. Reverse iontophoresis and microneedle-based systems are central to these advances. A wearable patch using reverse iontophoresis with a dual-layer hydrogel captured lactate from ISF for real-time electrochemical detection *via* lactate oxidase and Prussian blue-modified electrodes, providing continuous metabolic assessment without blood sampling (Fig. 9a).<sup>339</sup> A 3D-printed hollow microneedle array was employed for Parkinson's drug (apomorphine) monitoring using square wave voltammetry and chronoamperometry, achieving direct pharmacokinetic feedback, while polyaniline-coated polymeric microneedles enabled real-time pH monitoring for metabolic disorders (Fig. 9a(ii and iii)).<sup>340,341</sup> Dual-mode hydrogel microneedle patches extracted cell-free DNA (cfDNA) *via* passive absorption and electrical enhancement, with downstream recombinase polymerase amplification and electrochemical detection enabling Epstein–Barr virus diagnostics (Fig. 9b).<sup>342</sup> A flexible microneedle-based extended-gate field effect transistor (FET) (MN-EGFET) sensor enabled wireless sodium tracking in ISF for hydration monitoring.<sup>343</sup> Further, a dual-iontophoretic tattoo collected ISF and sweat simultaneously for glucose and alcohol sensing, incorporating PB- and alcohol oxidase-based biosensors and wireless circuitry for mobile data transmission (Fig. 9c(i-iii)).<sup>343</sup> A poly(ethylene glycol) diacrylate (PEGDA)-based 3D-printed hydrogel microneedle array optimized for swelling and skin penetration allowed bloodless ISF access; embedded colorimetric pH and glucose sensors enabled visual or RGB-based detection (Fig. 9d(i-iv)).<sup>344</sup> A CRISPR-graphene microneedle patch integrated with reverse iontophoresis facilitated long-term cfDNA monitoring for viral and transplant biomarkers, maintaining *in vivo* sensitivity for over 10 days (Fig. 9e(i-iii)).<sup>345</sup> A stretchable hybrid patch with integrated ultrasonic and electrochemical sensors captured metabolic (glucose, lactate, caffeine, alcohol) and hemodynamic (blood pressure) signals, validated during exercise and nutrient intake (Fig. 9f(i-iii)).<sup>346</sup> Finally, a wireless microneedle array system for glucose, lactate, and alcohol monitoring was deployed on volunteers, offering disposable sensor modules and smartphone readout, with its internal layout and electrode configuration shown in Fig. 9g-i (Table 4).<sup>347</sup>

### 5.3 Continuous sampling and off-body analysis (COFF)

COFF leverages the continuous fluid acquisition capabilities of wearable systems while relying on off-body instrumentation for high-accuracy biomarker analysis. This hybrid model enables long-duration monitoring and

facilitates personalized health tracking in both clinical and at-home contexts. Paper-based microfluidic systems are particularly advantageous for COFF applications due to their inherent ability to wick, store, and evaporate biofluids without pumps. Integrated with osmotic extraction, these systems can harvest and dispose of sweat over extended periods ( $\geq 10$  days), using linear paper strips for capillary transport and high-surface-area pads for evaporation. Sampling is passive and sustained, and collected analytes such as sweat lactate can be quantified offline *via* laboratory analysis.<sup>15,295</sup> To reduce labor and contamination risks associated with traditional absorbent patches, a simplified sweat collection system was introduced featuring an onboard conductivity sensor and multiple reservoirs with fill-level indicators. The system enabled both continuous conductivity tracking and off-body  $\text{Na}^+$  and  $\text{Cl}^-$  quantification *via* ion chromatography.<sup>295</sup> Despite advancements, conventional biosensors often require large sweat volumes due to limited sensitivity of bio-recognition components such as antibodies,<sup>364</sup> aptamers,<sup>365,366</sup> enzymes,<sup>367,368</sup> or molecularly imprinted polymers.<sup>28</sup> Reducing assay volumes not only accelerates response times by mitigating sweat evaporation delays but also facilitates rapid re-priming for subsequent tests. Hydrogel-paper hybrid patches have addressed this issue by coupling osmotic extraction through skin-integrated hydrogel membranes with paper-based capillary microchannels. The sweat extraction rate is tunable *via* osmolyte concentration and evaporation pad size, enabling controlled and sustained biomarker delivery to test zones. On-skin validation revealed successful lactate sampling at rest (11 mM in 2 h) and during exercise (20 mM in 1 h), demonstrating efficacy without inducing perspiration.<sup>369</sup>

To support dynamic profiling of biomarker fluctuations, a compact wearable integrating continuous fluid sampling with *in situ* chemical assays was developed for simultaneous glucose and lactate tracking.<sup>370</sup> The platform combines peristaltic nanoliter droplet generation, optical detection, and microfluidic flow control within a single patch. A screen-driven micropump circulates reagents and biofluid to an optical flow cell, enabling continuous, colorimetric readout. Clinical testing in five volunteers during an oral glucose tolerance test demonstrated strong correlation between dermal interstitial glucose and blood glucose levels, validating the system's utility for longitudinal, non-invasive diagnostics.

### 5.4 Continuous sampling and on-body analysis (CONN)

Continuous sampling combined with on-body analysis enables real-time monitoring of sweat biomarkers, eliminating reliance on bulky external systems and providing timely feedback for dynamic physiological and pathological conditions. This approach requires two key components: efficient and sustained sample acquisition and robust sensor integration for uninterrupted biomarker detection.



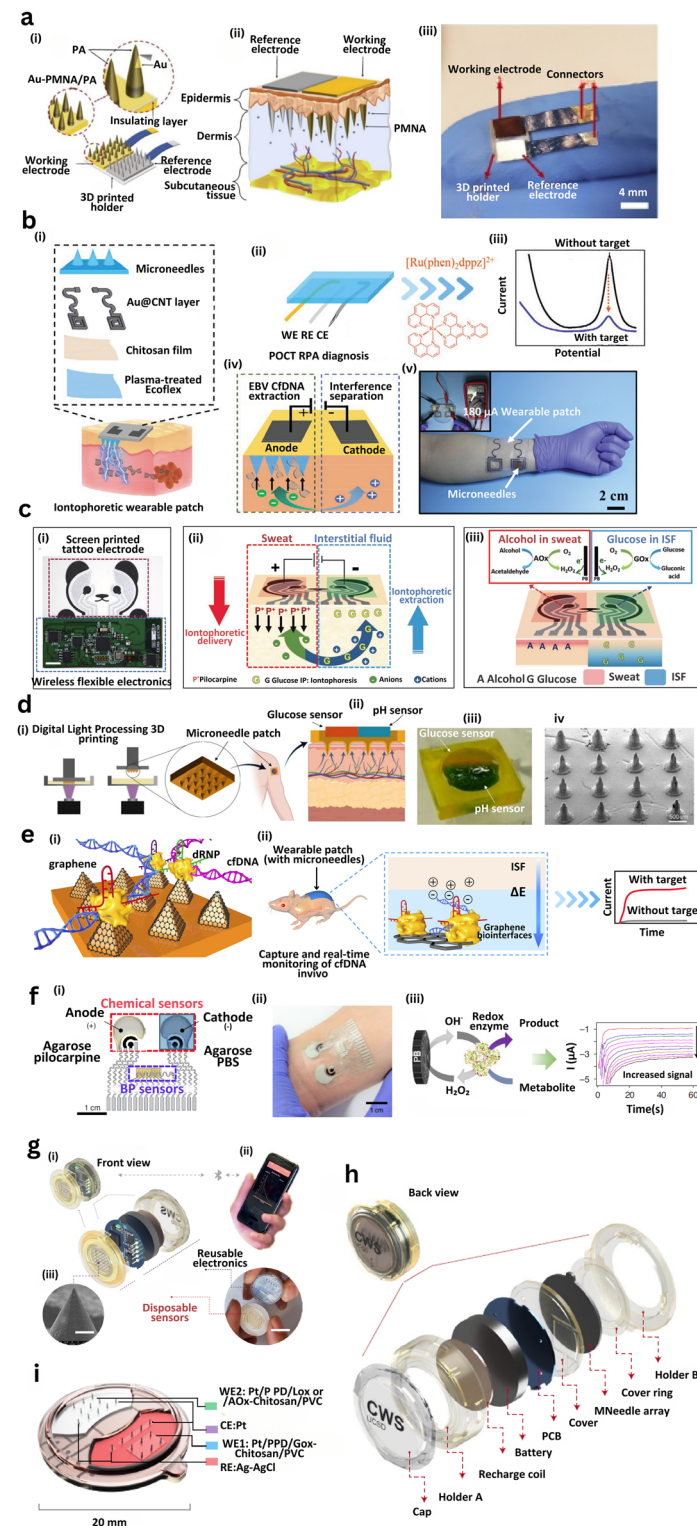
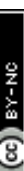


**Fig. 9** Wearable microneedle-based and iontophoretic platforms for chrono-sampling and on-body analysis of ISF biomarkers. (a) Microneedle biosensor: (i) schematic of Au-coated polyamide microneedles integrated with a 3D-printed holder; (ii) skin insertion showing electrode positioning; (iii) photo of fabricated biosensor.<sup>341</sup> (b) Dual-mode EBV cfDNA patch: (i) Au@CNT microneedles on Ecoflex; (ii) point of care testing mechanism using  $[\text{Ru}(\text{phen})_2\text{dppz}]^{2+}$ ; (iii)  $I-V$  curves with/without target; (iv) EBV cfDNA separation schematic; (v) patch on forearm.<sup>342</sup> (c) Tattoo-based dual-fluid biosensor: (i) screen-printed electrodes; (ii) iontophoretic extraction mechanism; (iii) alcohol and glucose sensing via enzymatic pathways.<sup>343</sup> (d) 3D-printed hydrogel microneedle array: (i) fabrication process; (ii) glucose/pH sensing in skin; (iii) device photo; (iv) microneedle microscopy.<sup>344</sup> (e) CRISPR microneedle patch: (i) graphene biointerfaces for cfDNA/dRNP capture; (ii) patch on mouse; (iii) current-time plots indicating target detection.<sup>345</sup> (f) Integrated BP/metabolite patch: (i) device layout with agarose electrodes; (ii) on-body application; (iii) metabolite sensing via redox current.<sup>346</sup> (g) Wireless microneedle sensor: (i) device front view; (ii) smartphone interface; (iii) microneedle array detail. (h) Exploded view of wearable system with labeled components.<sup>347</sup> (i) Electrode configuration and device dimensions.<sup>347</sup>

**Table 4** Summary of targeted biomarkers, corresponding analytes, sensing methods, sample volumes, participant details, and associated detection platforms used in chrono-sampling and on-body analysis systems

Analyte	Target biomarker	Sample volume	Concentration range	Sensing methods	On-body location	Number of participants	Ref.
Sweat	Cortisol	N/A	0.1–100 ng mL <sup>-1</sup>	Electrochemical	Portable	N/A	348
Sweat	Ethyl glucuronide (EtG)	N/A	0.003–0.3 ng mL <sup>-1</sup>	Electrochemical	Wrist	5	349
Sweat	Na <sup>+</sup>	N/A	10–200 mM	Potentiometric	Forearm	12	350
Sweat	Na <sup>+</sup>	20 μL	10–100 mM	Potentiometric	Forearm	10	319
Sweat	K <sup>+</sup>	20 μL	N/A	Potentiometric	Forearm	10	319
Sweat	Glucose	5 μL	0–1 mM	Colorimetric	Arm	5	351
Sweat	Lactate	1.6 μL	1–20 mM	Electrochemical	Forearm	7	325
Sweat	Glucose	N/A	0–1 mM	Amperometric	Arm	10	352
Sweat	Na <sup>+</sup>	N/A	10–100 mM	Colorimetric	“Glove fingers”	3	353
Sweat	K <sup>+</sup>	N/A	N/A	Colorimetric	“Glove fingers”	3	353
Sweat	pH	N/A	N/A	Colorimetric	“Glove fingers”	3	353
Sweat	Lactate	N/A	0–25 mM	Electrochemical	“Textile patch”	6	354
Sweat	Cl <sup>-</sup>	30 μL	10–100 mM	Colorimetric	Forearm	15	355
Sweat	Cortisol	1.5 μL	1–200 ng mL <sup>-1</sup>	Colorimetric	Forearm	10	328
Sweat	Glucose	1.5 μL	N/A	Colorimetric	Forearm	10	328
Sweat	Ketones	N/A	0–10 mM	Colorimetric	Forearm	5	324
Sweat	Cl <sup>-</sup>	25 μL	10–100 mM	Colorimetric	“Forearm, back”	12	317
Sweat	Sweat rate	1.0 μL	N/A	Colorimetric	Forearm	8	322
Sweat	Ammonia	N/A	0.05–1 mM	“Enzymatic assays”	Forearm	5	327
Sweat	Ethanol	N/A	0.05–1 mM	“Enzymatic assays”	Forearm	5	327
Sweat	Na <sup>+</sup>	N/A	10–100 mM	Potentiometric	Arm	5	356
Sweat	K <sup>+</sup>	N/A	N/A	Potentiometric	Arm	5	356
Sweat	pH	N/A	N/A	Potentiometric	Arm	5	356
Sweat	Glucose	0.5 μL	0–2 mM	Electrochemical	Arm	6	21
Sweat	Lactate	1.2 μL	1–20 mM	Microfluidic	Various	9	357
Sweat	Cortisol	N/A	“1 pg mL <sup>-1</sup> –1 μg mL <sup>-1</sup> ”	“Aptamer-FET”	Forearm	10	358
Sweat	Na <sup>+</sup>	N/A	1–100 mM	Potentiometric	Forearm	8	359
Sweat	K <sup>+</sup>	N/A	N/A	Potentiometric	Forearm	8	359
Sweat	Glucose	15 μL	0–0.5 mM	Electrochemical	Arm	12	360
Sweat	pH	15 μL	N/A	Electrochemical	Arm	12	360
Sweat	Cortisol	5 μL	0.01–1000 ng mL <sup>-1</sup>	Molecularly imprinted	Arm	7	320
Sweat	pH	N/A	4–8 pH units	Piezoelectric	Arm	5	361
Sweat	Na <sup>+</sup>	N/A	10–100 mM	Potentiometric	Arm	10	326
Sweat	Glucose	20 μL	0–1 mM	Amperometric	Forearm	8	362
Sweat	Glucose	20 μL	0–1 mM	Amperometric	Forearm	8	362
ISF	Glucose	—	0–20 mM	Colorimetric – enzymatic	Porcine skin <i>ex vivo</i> (mimicking human skin)	Pig skin	344
ISF	pH	—	5–8	Bromothymol blue dye – colorimetric	Porcine skin <i>ex vivo</i> (mimicking human skin)	Pig skin	344
ISF	Lactate	100 μL (for <i>in vitro</i> )	1–5 mM	Amperometry – enzymatic biosensor	Forearm	4	339
ISF	Apomorphine	100 mL (in <i>vitro</i> )	5–60 μM	Chronoamperometry	Mimicked on phantom gel model	—	340
ISF	pH	<i>Ex vivo</i>	4–8.6	Potentiometry	Mouse skin	—	341
ISF	Na <sup>+</sup>	<i>In vivo</i>	10–160 mM	Gate-field effect transistor	Arm or forearm	—	363
Tear	pH	<i>In situ</i>	6.5–7.6	Colorimetric	Eye	—	334
Tear	Glucose	<i>In situ</i>	0–5 mmol L <sup>-1</sup>	Colorimetric	Eye	—	334
Tear	Protein	<i>In situ</i>	3–7 μg mL <sup>-1</sup>	Colorimetric	Eye	—	334
Tear	Nitrite ion	<i>In situ</i>	120 μmol L <sup>-1</sup>	Colorimetric	Eye	—	334
Tear	Cortisol	<i>In situ</i>	1 to 40 ng mL <sup>-1</sup>	Graphene – FET	Eye	Human and animal (rabbit)	338

**5.4.1 CONN in sweat.** A notable advance in this field is a passive, enzyme-free wearable patch for monitoring cortisol, Mg<sup>2+</sup>, and pH without sweat stimulation.<sup>371</sup> The microfluidic platform leverages natural gland pressure for fluid intake into reservoirs housing polypyrrole-based MIP for cortisol, ion-selective membranes for Mg<sup>2+</sup>, and polyaniline sensors for pH. On-body validation confirmed the system's potential

for non-invasive stress monitoring (Fig. 10a(i–iv)). However, limitations remain in long-term durability and multiplexing capability. To track sweat rate continuously, a tape-free wearable system was developed featuring a soft, 3D-printed concave collector that forms a watertight seal with skin.<sup>372</sup> Sweat is directed into a spiral microchannel with face-to-face comb-like Ag electrodes, where admittance changes yield



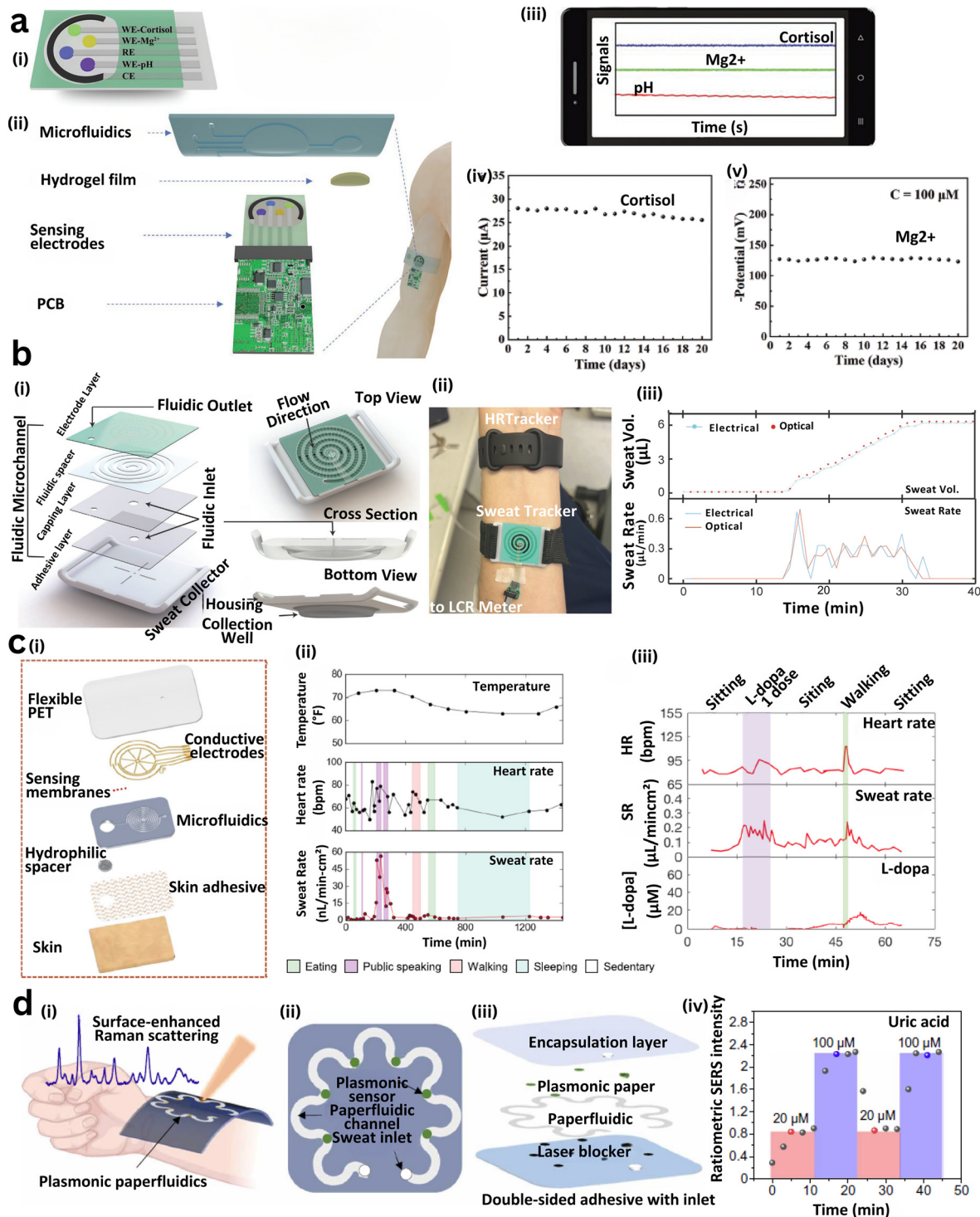


**Fig. 10** Capillary microfluidic systems integrated into wearable platforms enable continuous on-body sweat sampling and real-time multiplexed biochemical analysis. (a) Wearable microfluidic patch for simultaneous detection of cortisol, Mg<sup>2+</sup>, and pH. (i) Schematic of the skin-mounted patch showing sweat routing to sensing zones. (ii) Exploded view of layered construction, including microfluidic, sensing, and electronic components. (iii) Real-time mobile interface for monitoring biomarkers. (iv) Long-term performance of the cortisol sensor. (v) Mg<sup>2+</sup> sensor stability during prolonged operation.<sup>371</sup> (b) Spiral microfluidic collector system. (i) Structural views of a 3D-printed concave sweat collector guiding fluid through a spiral path. (ii) Device embedded in a digital band for sweat and heart rate tracking. (iii) Electrical and optical data showing time-resolved sweat rate and volume.<sup>375</sup> (c) Flexible epidermal patch for physiological monitoring. (i) Multilayer assembly with PET, electrodes, hydrogel, and adhesive. (ii) Tracking of temperature, HR, and sweat rate during exertion. (iii) Comparison of HR, sweat rate, and L-dopa concentration.<sup>376</sup> (d) Paper-based plasmonic SERS patch. (i) Schematic showing gold nanorod-enabled SERS detection of uric acid. (ii) Channel structure with sweat inlet and sensor region. (iii) Cross-section of patch architecture with PDMS encapsulation and laser protection layers. (iv) Quantified SERS signal response over time and analyte concentration.<sup>252</sup>



real-time sweat volume profiles. While effective for sweat quantification, the system lacks analyte sensing and long-term validation. Li *et al.*<sup>373</sup> introduced a microfluidic patch for non-enzymatic glucose detection using Pt/MXene nanocomposites. Their capillary-guided system prevents sweat accumulation by ensuring unidirectional flow from collection to sensing zones. Though capable of real-time glucose tracking, it does not address other biomarkers or include sweat stimulation elements. Another wearable sensor combined sweat rate and electrolyte monitoring using a microchannel with a hydrophobic outlet, electrodes, and an absorbent layer.<sup>374</sup> While functional, the specific electrolytes and methods were not disclosed, and on-body robustness remains untested. A smartwatch-compatible band for digital sweat rate tracking used a tape-free 3D-printed concave collector to eliminate adhesives and enable reuse.<sup>375</sup> Sweat advanced through a spiral channel, bridging comb-like electrodes and generating admittance profiles in real-time. Multisite validation confirmed the platform's robustness and potential for longitudinal hydration assessment (Fig. 10b(i-iii)). To enable monitoring at low sweat rates, a flexible patch was fabricated with PET substrates, interdigitated electrodes, selective membranes, and agarose-glycerol hydrogel to minimize lag time and evaporation.<sup>376</sup> The multilayer system tracked sweat dynamics during light activity, stress, hypoglycemia, and levodopa dosing, with sensors for pH, Cl<sup>-</sup>, and levodopa showing reliable performance (Fig. 10c(i-iii)). For label-free detection, a plasmonic microfluidic device with gold nanorods (AuNRs) and cellulose paper was developed for Surface Enhanced Raman Spectroscopy (SERS)-based uric acid sensing.<sup>252</sup> Sweat is guided through serpentine channels to SERS-active zones, with cetyltrimethylammonium bromide (CTAB) removal and PDMS encapsulation optimizing signal fidelity. The device showed robust detection (LOD: 1  $\mu$ M), mechanical stability under strain, and successful on-body operation (Fig. 10d(i-iv)). A ratiometric analysis strategy ensured quantification across different instruments.

Understanding thermoregulatory sweat behavior is critical for evaluating hydration status and metabolic function. A PDMS-based microfluidic patch incorporating a patterned SU-8 filler and a hydrogel uptake layer was developed for continuous sweat analysis in resting conditions.<sup>376</sup> The device integrates electrochemical sensors for pH, chloride, and levodopa, and uses an interdigitated wheel-shaped electrode array to monitor sweat flow dynamics. It enables 24-hour on-body monitoring across various body locations, capturing physiological changes in sweat composition. However, its reusability and multiplexing capacity for additional biomarkers require further investigation. To improve fluid control and storage, a three-layered microfluidic system using interconnected reservoirs and capillary burst valves was introduced.<sup>325</sup> The patch features electrochemical sensors targeting glucose, creatinine, lactate, chloride, and pH, and is designed for continuous monitoring under exercise-induced sweating. The system maintains strong skin adhesion and leak-proof performance, with

reservoir-stored samples remaining stable for up to 125 hours, facilitating delayed or *ex situ* biochemical analysis. Advancing multimodal sensing, a wearable patch was developed that couples biochemical and electrophysiological monitoring with microfluidic sweat handling.<sup>377</sup> The system integrates a reduced graphene oxide-based glucose biosensor with MXene-polyvinylidene fluoride (PVDF)-based carbon nanofiber dry electrodes for electrocardiogram (ECG) recording. Wireless communication enables real-time data transmission to a smartphone app, allowing simultaneous tracking of glucose, ECG, pH, and temperature. On-body exercise trials confirmed the sensor's ability to dynamically adjust readings based on sweat composition and skin temperature, improving measurement accuracy and contextual insight.

**5.4.2 CONN in saliva.** Wearable mouthguard biosensors have emerged as a promising platform for continuous, real-time salivary monitoring, offering a non-invasive alternative to blood-based diagnostics. Kim *et al.*<sup>331</sup> developed a screen-printed, uricase-modified biosensor integrated into a mouthguard, enabling continuous monitoring of salivary uric acid *via* natural saliva flow (1–2 mL min<sup>-1</sup>). The sensor employs a PB-modified electrode for low-potential amperometric detection of hydrogen peroxide, a byproduct of uricase-catalyzed uric acid oxidation. An electropolymerized protective layer enhances selectivity by minimizing interference from salivary electroactive species. Building on this, the group developed a similar mouthguard biosensor for lactate detection using lactate oxidase (LOX) immobilized on a PB-based transducer coated with poly-orthophenylenediamine (PPD).<sup>330</sup> The PPD layer improves stability by rejecting interferents and reducing biofouling. The device demonstrated consistent electrochemical performance in both buffer and undiluted saliva, maintaining signal integrity over a 2-hour window with 10-minute sampling intervals. While short-term reusability was confirmed, challenges remain in achieving long-term operation, particularly in calibration stability and biofilm mitigation. These mouthguard platforms, which eliminate the need for microfluidic handling by leveraging intrinsic salivary flow, show strong potential for integration into daily life. Their demonstrated capability for real-time uric acid and lactate monitoring highlights their utility in metabolic health tracking and personalized medicine. Future efforts should prioritize multiplexing, extending operational lifetime, and developing robust reusability protocols to fully realize their clinical and lifestyle potential.

**5.4.3 CONN in tears.** The emergence of microfluidic-integrated ocular biosensors marks a pivotal shift in real-time, continuous tear analysis for non-invasive health monitoring. Recent studies highlight contact lenses as platforms for sensing glucose, intraocular pressure (IOP), and other biomarkers, though full integration of microfluidic sampling remains limited. A study using silicone hydrogel lenses embedded with a glucose-sensitive fluorophore (Quin-C18) successfully demonstrated fluorescence-based glucose



detection;<sup>378</sup> however, it lacked microfluidic control, tear transport functionality, and on-body validation. Future designs must incorporate microfluidic channels to manage tear flow, prevent sensor fouling, and enable multiplexed detection of lactate, pH, and other metabolites. Clinical studies underscore the diagnostic potential of tear composition due to its correlation with plasma biomarkers,<sup>379</sup> but manual sampling methods like Schirmer strips remain incompatible with continuous analysis. Microfluidic-enabled lenses or periocular patches could automate tear extraction, filtration, and concentration for dynamic biochemical profiling. Integration with AI-powered analytics may support real-time decision-making, early disease prediction, and closed-loop feedback in personalized medicine. In glaucoma management, stretchable contact lenses with embedded inductive coils have shown promise for wireless, non-invasive IOP tracking. While effective, these devices do not incorporate tear sampling or biochemical sensing. Hybrid systems combining mechanical and

biochemical tear analysis could provide comprehensive ocular diagnostics. A notable advancement is the development of smart lenses using incompressible fluid-filled microchannels to detect corneal deformation from IOP fluctuations.<sup>380</sup> These devices dynamically alter electrical properties in response to pressure, achieving continuous 24-hour IOP monitoring. Their microfluidic design offers the potential for expansion into multiplexed biomarker detection, addressing systemic and neurodegenerative diseases. Ultimately, the convergence of microfluidics, biosensing, and wireless technology within ocular platforms can unlock real-time, on-eye diagnostics. These devices promise to transform both ophthalmic care and broader systemic health monitoring by enabling non-invasive, personalized, and continuous access to dynamic biomarker information.

**5.4.4 CONN in ISF.** Microneedle-based ISF biosensors present a compelling alternative to sweat-based platforms, overcoming challenges such as low secretion rates, sample dilution, and limited analyte stability. A graphene-integrated

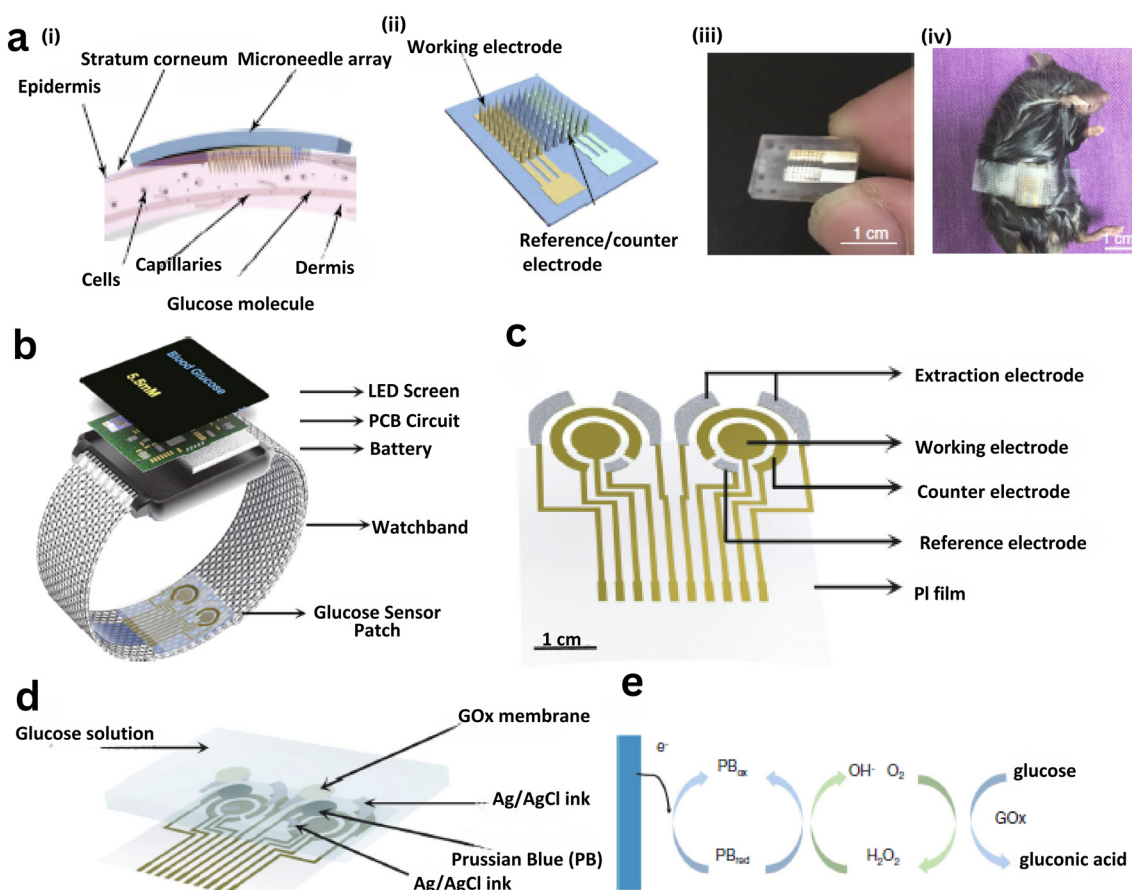


**Fig. 11** Overview of capillary microfluidic and microneedle-based systems for continuous glucose monitoring via ISF and their integration into wearable formats. (a) (i) Schematic representation of skin cross-section showing microneedle insertion into the dermis for direct ISF access. (ii) Microneedle-based sensor with integrated working, reference, and counter electrodes. (iii) Photograph of the assembled glucose-sensing patch. (iv) *In vivo* application of the patch on mouse skin demonstrating real-time monitoring.<sup>382</sup> (b) Wearable smartwatch system incorporating a glucose sensor patch with built-in LED display, printed circuit board (PCB), and battery within the strap for standalone operation.<sup>384</sup> (c) Electrode design on flexible polyimide substrate displaying glucose extraction, sensing, and reference components. (d) Structural composition of the sensor including glucose oxidase (GOx) membrane, Ag/AgCl reference layer, and Prussian Blue (PB) mediator. (e) Enzymatic glucose sensing mechanism: glucose is catalyzed to gluconic acid and  $H_2O_2$  by GOx, and the  $H_2O_2$  is electrochemically reduced at the PB electrode, generating a quantifiable signal.<sup>384</sup>



wearable patch was developed to monitor sweat glucose and deliver metformin *via* bioresorbable phase-change microneedles.<sup>381</sup> The system features a humidity-sensitive

PEDOT sensor and a Nafion-based sweat control layer for pH and glucose detection, triggering drug release through a thermally responsive Au mesh/graphene heater. However, it

**Table 5** Summary of targeted biomarkers monitored through continuous sampling and on-body analysis (CONN), including fluid source, sensing method, sample handling strategy, and device integration details

Analyte	Target biomarker	Sample volume	Concentration range	Detection methods	On-body location	Duration	Number of participants	Ref.
Sweat	Lactate, glucose, $\text{Cl}^-$ , pH	—	Lactate: 0–20 mM; $\text{Cl}^-$ : 10–100 mM	Colorimetric assays with smartphone image analysis	Skin (cycling)	Exercise duration	—	7
Sweat	pH, $\text{Cl}^-$ , levodopa	<5 $\mu\text{L}$	pH: 4–8; $\text{Cl}^-$ : 10–200 mM; levodopa: 1–50 $\mu\text{M}$	Electrochemical (pH, $\text{Cl}^-$ ), enzymatic (levodopa)	Shoulder, chest, wrist	Up to 24 h	—	376
Sweat	Glucose	—	0–25 mM	Electrochemical (enzyme-based)	Not specified	Not specified	—	68
Sweat	Electrolytes, metabolites	<10 $\mu\text{L}$	$\text{Na}^+$ : 10–100 mM; $\text{K}^+$ : 1–20 mM	Electrochemical (ion-selective electrodes)	Forearm	2 h	—	387
Sweat	Cortisol, IL-6	~20 $\mu\text{L}$	Cortisol: 1–100 ng $\text{mL}^{-1}$ ; IL-6: 0.1–100 pg $\text{mL}^{-1}$	Electrochemical immunosensors	Wrist	8 h	15	371
Sweat	Glucose	—	2–20 mM	Reverse iontophoresis + electrochemical	Wrist	Continuous	12	384
Sweat	Lactate, EEG signals	—	Lactate: 0–25 mM	Electrochemical (lactate), electrophysiological (EEG)	In-ear	6 h	20	388
Sweat	Glucose, lactate, $\text{Na}^+$ , $\text{K}^+$ , pH	1–3 $\mu\text{L}$	Glucose: 0–0.5 mM; lactate: 0–25 mM	Electrochemical (enzyme-based), impedance ( $\text{Na}^+/\text{K}^+$ ), potentiometric (pH)	Arm	6 h	10	377
Sweat	Skin hydration, sweat loss	—	Hydration: 0–100 a.u.; sweat loss: 0–500 mL	Optical reflectance/fluorescence	Wrist	8 h	25	389
Sweat	Ascorbate (vitamin C)	—	10–500 $\mu\text{M}$	Colorimetric (natural oxidase-mimicking copper-organic frameworks)	Not specified	Not specified	—	390
Sweat	Glucose	0.5–2 $\mu\text{L}$	0.01–1 mM	Non-enzymatic electrochemical (Pt/MXene)	Forearm	2 h	8	373
Sweat	Sweat rate, $\text{Na}^+$ , $\text{K}^+$	Not specified	$\text{Na}^+$ : 10–100 mM; $\text{K}^+$ : 1–20 mM	Microfluidic impedance sensing	Back	1 h	10	374
Sweat	$\text{Na}^+$ , $\text{K}^+$ , pH, glucose	~5 $\mu\text{L}$	$\text{Na}^+$ : 10–100 mM; glucose: 0–1 mM	Plasmonic colorimetry (paper-based microfluidics)	Forearm	3 h	12	252
ISF	Glucose	~500 nL	2–20 mM	Electrochemical (graphene microneedles with thermos-responsive drug release)	Skin (microneedle array)	72 h	5	381
Tear	Intraocular pressure (IOP)	NA	10–50 mmHg	Capacitive sensing (wireless LC resonance circuit)	Contact lens	24 h	12	391
ISF	Glucose, lactate	1–2 $\mu\text{L}$	Glucose: 2–20 mM; lactate: 0.5–25 mM	Electrochemical (hollow microneedles with microfluidic chip)	Forearm (wearable patch)	12 h	8	347
ISF	Anti-SARS-CoV-2 IgM/IgG	—	—	Paper-based lateral flow immunoassay (porous microneedles)	Skin (patch)	Single use	25	392
Tear	Corneal temperature	—	30–40 °C	Thermochromic liquid crystals (colorimetric analysis)	Contact lens	4 h	10	393
ISF	Glucose	0.5–1 $\mu\text{L}$	3–20 mM	Electrochemical (3D printed microneedle with GOx enzyme)	Arm	48 h	7	382
Tear	Glucose	—	0–2 mM	Fluorescence resonance energy transfer (FRET-based hydrogel lens)	Contact lens	6 h	—	378
Tear	Glucose	—	0.1–0.6 mM	Colorimetric (glucose oxidase/tetramethylbenzidine)	Contact lens	—	20	54
Tear	Glucose	—	0.05–1 mM	Reflectance spectroscopy (gold nanoparticle-embedded lens)	Contact lens	8 h	12	394
Tear	Glucose	—	0–2 mM	Fluorescent nanosensors (smartphone camera detection)	Contact lens	Continuous	—	395
Saliva	Uric acid	20–100 $\mu\text{L}$	50–1000 $\mu\text{M}$	Amperometric (screen-printed electrode with wireless BLE)	Mouthguard	Real-time	10	330
Tear	Glucose	—	0.1–1 mM	Electrochemical (wireless potentiostat with drug delivery)	Contact lens	Continuous	6	337



lacks active or capillary-driven ISF extraction and relies solely on passive diffusion, limiting its robustness and reproducibility. To address this, a 3D-printed microneedle biosensing platform was introduced for continuous subcutaneous glucose monitoring.<sup>382</sup> The patch comprises a microneedle array that penetrates the stratum corneum and uses capillary action to guide ISF toward embedded electrodes. The electrochemical sensing system consists of a PB-modified gold working electrode functionalized with glucose oxidase, and a silver/silver chloride reference/counter electrode. *In vivo* testing on mice demonstrated stable operation for up to seven days with consistent glucose readouts, significantly outperforming sweat-based alternatives (Fig. 11a(i–iv)). For infectious disease diagnostics, a biodegradable polylactic acid (PLA)-based microneedle immunosensor was designed for SARS-CoV-2 antibody detection.<sup>383</sup> The patch extracts ISF using porous microneedles and directs it to a paper-based immunoassay. Vertical and lateral fluid flow mechanisms facilitate IgM/IgG visualization *via* colloidal gold nanoparticle labeling. Rat studies confirmed rapid ISF sampling within five minutes, though further validation in human models is needed. Transdermal ISF extraction through reverse iontophoresis was employed in a fully integrated glucose-sensing smartwatch.<sup>384</sup> A flexible Nafion-coated electrochemical sensor patch adhered to the watchband enables real-time monitoring with on-board signal processing and wireless data transmission. On-body trials with 23 volunteers showed 84.34% accuracy, even during physical motion. The system includes a flexible polyimide-based electrode array with GOx membranes and Prussian blue transducers, integrated into the watch for continuous data visualization (Fig. 11b–e).

Despite these advances, current ISF biosensors predominantly rely on passive capillary forces, which may limit performance under variable skin conditions. Incorporating active microfluidic strategies such as electroosmotic or vacuum-assisted extraction could enhance fluid control. Furthermore, maintaining long-term sensor calibration and stability remains a critical barrier for clinical deployment. Future directions should include integrating flexible electronics, machine learning-based analytics, and closed-loop drug delivery to enable autonomous, real-time health monitoring in wearable formats. For instance, in one study, a closed-loop system was developed by integrating a microneedle-based electrochemical sensor for real-time methotrexate (MTX) monitoring with an iontophoretic microneedle patch for on-demand transdermal drug delivery, enabling continuous feedback-based therapeutic regulation. This approach was shown to ensure precise, minimally invasive drug dosing within the therapeutic range, significantly advancing personalized treatment for conditions such as cancer and rheumatoid arthritis.<sup>385</sup> In another example, a wearable closed-loop microneedle system was developed, in which interstitial glucose levels were continuously monitored and, upon exceeding the normal range, an ultrasonic pump was automatically activated to

deliver insulin, enabling effective glycemic control (Table 5).<sup>386</sup>

## 6. Clinical applications consideration and clinical evaluation studies

### 6.1 Clinical studies

Wearable biosensing devices are transforming healthcare by enabling continuous, non-invasive monitoring of physiological and biochemical parameters. To translate their promise into clinical reality, rigorous clinical trials are essential—not only to validate device accuracy and safety, but also to understand their impact on real-world health outcomes and support regulatory approvals approval.<sup>396,397</sup> Historically, initial evaluations of integrated wearable systems have relied on feasibility studies with fewer than 10 participants,<sup>398</sup> which serve as proof-of-concept demonstrations. However, broader clinical acceptance requires large-scale, statistically powered studies that meet regulatory standards and ethical frameworks.<sup>199,398–400</sup> These include validated performance metrics, safety and risk assessments, transparent informed consent processes, unbiased cohort selection, and robust data security protocols. Crucially, developers must consider whether the wearable is intended for medical-grade use or consumer wellness, as this distinction impacts the design, regulatory pathway, and required clinical evidence.

To gain approval for clinical use, wearable sensors must demonstrate analytical and clinical performance comparable to existing diagnostic methods. For example, glucose sensors require detection limits of 0.06–0.11 mM for non-diabetic patients and 0.01–1 mM for diabetic patients.<sup>22</sup> Such benchmarks necessitate both technical optimization and validation in diverse populations. A key component of clinical validation is establishing strong correlations between sweat or saliva biomarkers and reference fluids like blood or plasma, often requiring large study cohorts.<sup>358</sup> Minimally invasive designs improve user adherence. Innovations such as skin-like flexible electronics and microneedles under 200 µm reduce discomfort while enabling biofluid access.<sup>34,401</sup> These features are vital as biosensors are increasingly deployed on sensitive skin areas and used for extended durations.

Recent clinical studies underscore growing confidence in wearable biosensing. Baker *et al.*<sup>317</sup> demonstrated large-scale clinical deployment of a microfluidic colorimetric sweat patch in over 300 athletes, monitoring sweat chloride and rate. Choi *et al.*<sup>402</sup> evaluated sweat chloride dynamics in 50 individuals during physical activity, while Ray *et al.*<sup>403</sup> assessed a sweat-based diagnostic sticker for cystic fibrosis across 51 participants aged 2 months to 51 years. However, broader trials involving infants and children are still needed. Clinical trials often involve moderate physical exertion, with devices placed on sweat-prone regions such as the forearm or lower back. Environmental factors—including body temperature, evaporation rates under the patch, and user



movement—must be accounted for during design and interpretation.<sup>7</sup>

Beyond biomarker monitoring, wearable systems are gaining traction in neurological and chronic disease management. A smartwatch-based system for Parkinson's disease symptom tracking was evaluated in 343 participants, with a six-month longitudinal trial on 225 patients.<sup>404</sup> Such large cohorts provide critical evidence for digital therapeutics and behavioral phenotyping. From a regulatory standpoint, wearable sensors may be classified as *in vitro* diagnostic devices (IVDs), with classification determined by invasiveness and intended use. Clinical validation, scalability, reproducibility, and patient benefit must be demonstrated for regulatory clearance.<sup>396</sup> Several platforms, such as the Apple Watch and VitalPatch, have received FDA clearance for monitoring vital signs using embedded ECG sensors.<sup>405</sup> Interestingly, industries such as fitness, cosmetics, and sports have embraced wearable biosensors more rapidly, offering a streamlined pathway to mass production and broader public acceptance. Manufacturing costs for some devices have dropped to as low as \$0.50 per chip, enabling scalable production exceeding 10 million units. As more wearable platforms achieve regulatory clearance, the foundation is being laid for comprehensive clinical trials, long-term real-world evidence generation, and mainstream clinical adoption.

## 6.2 Regulatory requirements for wearable biosensors

To achieve clinical use, wearable biosensors must navigate structured regulatory pathways to ensure safety, performance, and reliability. In the United States, the Food and Drug Administration (FDA) classifies these devices under the Federal Food, Drug, and Cosmetic Act (FD&C Act), with most diagnostic wearables falling into Class II and requiring a 510(k) premarket notification that demonstrates substantial equivalence to an existing legally marketed device.

Several devices have successfully obtained FDA clearance through this pathway. Dexcom's G6 and G7 continuous glucose monitors (CGMs) were cleared under 510(k) submissions (K182041 and K193371), as was Abbott's FreeStyle Libre 2 flash glucose monitor.<sup>406</sup> VitalConnect's VitalPatch, which tracks ECG, heart rate, respiratory rate, and other metrics, was also cleared under 510(k) (K152139), reflecting regulatory acceptance of multi-analyte wearable biosensors.<sup>407</sup>

In contrast, novel sensing platforms often face greater regulatory hurdles. Bioliniq's intradermal microneedle-based glucose sensor, which represents a departure from conventional designs, has not yet received FDA clearance and remains in clinical trials. Without a clear predicate device, it is likely to require *de novo* classification or even premarket approval (PMA)—both more rigorous routes requiring extensive safety and efficacy data.<sup>408</sup>

Devices incorporating high-risk features (e.g., implantable biosensors) fall under class III and must go through the PMA process. This includes clinical trials, manufacturing audits, and FDA inspections, as seen with implantable cardiac pacemakers.<sup>409</sup>

Beyond classification, all medical biosensors must comply with FDA's Quality System Regulation (21 CFR Part 820), which sets standards for design controls, risk management, and manufacturing quality.<sup>410</sup> Biosensors containing software, wireless communication, or AI algorithms must also follow Software as a Medical Device (SaMD) guidelines. These include validation, cybersecurity safeguards (e.g., threat modeling, encryption), and compliance with HIPAA for data protection.<sup>410,411</sup>

In Europe, wearable biosensors must meet the Medical Device Regulation (MDR) and obtain CE marking for distribution in the European Economic Area. Most diagnostic devices are classified as class IIa or IIb, requiring technical documentation, risk assessments, and clinical evaluation reports (CERs).<sup>396</sup> These submissions are assessed by Notified Bodies, adding time and complexity to approval.

Globally, ISO standards play a central role in regulatory compliance. ISO 13485:2016 specifies quality management systems for medical devices,<sup>412</sup> while the ISO 10993 series outlines biocompatibility requirements for materials in contact with the body—covering cytotoxicity, irritation, and systemic toxicity. Devices with embedded software must follow ISO/IEC 62304, and electrical and usability standards are addressed by IEC 60601-1 and IEC 62366, respectively.

One of the primary challenges in wearable biosensor approval is demonstrating analytical and clinical validity. Devices must detect analytes accurately at physiological levels, particularly in alternative biofluids like sweat or tears where concentrations are lower and more variable than in blood. Rigorous validation is necessary to ensure consistent performance across populations and environmental conditions. Clinical trials are essential to support FDA or CE submissions. These must adhere to Good Clinical Practice (GCP), receive IRB approval, and—for significant-risk devices—comply with FDA Investigational Device Exemption (IDE) regulations (21 CFR Part 812).<sup>412</sup> Trials should include both clinical and at-home scenarios and address safety, usability (as guided by IEC 62366), statistical rigor, and adverse event reporting.

Overall, several wearable biosensors—such as Dexcom's CGMs, FreeStyle Libre, and VitalPatch—have successfully passed through established regulatory pathways.<sup>406,407</sup> However, next-generation platforms with novel sensing modalities face additional barriers, including lack of predicates, technical complexity, and demands for robust validation. Overcoming these challenges requires coordinated efforts across regulatory strategy, quality systems, cybersecurity, biocompatibility, and clinical design to bring safe, reliable biosensors to market.



### 6.3 AI and machine learning for wearable applications

Recent developments in AI and machine learning (ML) have significantly enhanced the utility of wearable biosensors, particularly in processing data from sweat, saliva, ISF, and other non-invasive fluids. AI algorithms such as support vector machines (SVM), artificial neural networks (ANN), and convolutional neural networks (CNN) have been employed to extract meaningful patterns, remove noise, and compensate for fluid variability and environmental interferences, thereby improving prediction accuracy and reliability in real-time biosensing.<sup>413–416</sup> For instance, Moon *et al.*<sup>417</sup> integrated ML into a meta-plasmonic DNA biosensor, achieving a 13-fold sensitivity enhancement through neural network-guided design. Similarly, CNNs trained on simulated data improved ultrasonic biosensor output by reducing noise 15 dB and achieving high signal-to-noise ratios in real-time protein detection.<sup>418</sup> Other fluidics-focused platforms have incorporated LS-SVM to resolve fluorescence signal overlap in dual-analyte sweat biosensors,<sup>418</sup> and ANN models to enhance multiplex detection of tyrosine and uric acid in sweat and saliva using molybdenum polysulfide electrodes.<sup>419</sup>

Capillary microfluidic systems have also benefited from ML-assisted design optimization. Using supervised models trained on large datasets mapping channel geometry to delivery profiles, researchers achieved sub-percent fluidic prediction errors—accelerating design cycles and enhancing biosensor functionality. In colorimetric biosensing, CNNs trained on over 4600 images of microarray outputs enabled precise analysis of glucose, lactate, and pH in sweat with >91% accuracy.<sup>420</sup> Smartphone-integrated ML platforms like “DeepLactate” further expanded accessibility, achieving >99% lactate classification accuracy in sweat using image-based deep learning.<sup>421</sup>

These examples underscore the transformative potential of ML in wearable diagnostics—especially in overcoming the unique challenges of fluid-derived biosensing such as low analyte levels, matrix complexity, and motion artifacts. Integration of ML with flexible substrates, neuromorphic edge processors, and multimodal sensing architectures is driving the next generation of autonomous, real-time, and personalized health monitoring systems.

## 7. Outlook and future directions

Wearable sensors and technologies hold immense potential to revolutionize health monitoring in both clinical trials and outpatient care by enabling continuous, non-invasive or minimally invasive tracking of physiological and pathological parameters. Despite advances in detecting a wide range of analytes including glucose, lactate, uric acid, tyrosine, cortisol, ethanol, pH, and electrolytes like potassium, chloride, and sodium further studies are needed to characterize their detection capabilities across both normal and disease states. While much of the existing research focuses on *in vitro* or early-stage validation, bridging the gap

between wearable data and standard blood chemistry is essential for clinical translation.

### 7.1 Sweat

Sweat-based biosensors are particularly attractive due to their non-invasive nature and rich biomarker content, offering a comprehensive window into an individual's health. However, several technical barriers must be overcome before these devices can be widely adopted. Current microfluidic platforms utilizing capillary circuits face challenges such as sweat contamination, poor fluid handling under variable evaporation rates, and limitations in sample transport. A key issue is the reliable, high-sensitivity detection of multiple analytes over time, particularly in low-volume and fluctuating sweat flows. A fundamental bottleneck in sweat biosensing is the need for continuous sweat production. Most current studies depend on exercise-induced sweating for 30–40 minutes, which limits usability outside of athletic contexts.<sup>19,313</sup> For commercialization, sweat generation must be achievable at rest and they must be able to generate enough to perform sensing several times. Strategies such as localized skin heating using Peltier elements<sup>422</sup> or iontophoresis with pilocarpine-containing hydrogels,<sup>423</sup> have been explored, but these methods may alter analyte concentrations due to artificial stimulation. Further investigation is required to validate these techniques for clinical use. Most existing wearable systems provide single-point or short-duration measurements. To be clinically impactful, wearable devices must deliver continuous, non-invasive analyte sensing over extended periods, enabling longitudinal monitoring and integration into personalized medicine frameworks. This shift requires significant improvements in microfluidic design. Current systems based on absorbent pads and cellulose fibers are limited in their ability to channel microliter sweat volumes into sensing zones with the precision needed for multiplexed real-time analysis. Next-generation wearable platforms should incorporate capillary microfluidic circuits optimized for passive flow control, burst valve regulation, and multi-analyte integration. Further, leveraging synthetic biology and molecular engineering could expand the biosensing repertoire to include nucleic acids, bacteria, and viral targets,<sup>12</sup> unlocking new applications in infectious disease surveillance and pandemic response. Scalability is another critical factor. Advancements in rapid prototyping such as laser cutting and roll-to-roll manufacturing combined with the use of low-cost, modular materials will be key to achieving the reproducibility and throughput needed for mass production. Fig. 12a highlights the significant challenges and solutions that must be addressed to realize the sweat based wearable biosensors as next generation health monitoring devices. By addressing these technical, biological, and manufacturing challenges, wearable biosensors can evolve from proof-of-concept tools to clinically



## Sweat based wearable biosensors



## Challenges

- Non continuous sweat production
- Artificial sweat stimulation technique
- Poor fluid handling
- Low sample volume
- Variable sweat composition

## Solutions

- Advanced microfluidic designs
- Multiplexed detection
- Integration of synthetic biology
- Scalable fabrication methods
- Artificial sweat generation techniques

## Saliva based wearable biosensors



## Challenges

- Low biomarker concentrations
- Lack of standard collection & sampling protocol
- Complex fluid properties
- Biofouling and signal interference

## Solutions

- Advanced sensing, signal processing
- Standard sampling protocols
- High specificity and selectivity sensors
- Microfluidics for saliva rheology
- Low cost

## Tear based wearable biosensors



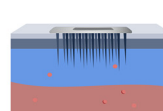
## Challenges

- Low Tear Volume & Collection Difficulty
- Stringent Ocular Requirements
- Dynamic Tear Composition
- Biofouling & Interferences

## Solutions

- Advanced Microfluidic Engineering
- Biocompatible and Transparent Materials
- Selective Sensing & Surface Modification
- AI-Enhanced Signal Processing
- Integrated Wearable Systems

## ISF based wearable biosensors



## Challenges

- Low ISF Volume and Slow Replenishment Rate
- Analyte Distortion Due to Invasiveness
- Inflammation and Local Tissue Response
- Signal Degradation Over Time

## Solutions

- Ultra-Sensitive, Low-Volume Sensors
- Passive or Low-Pressure Extraction Techniques
- Anti-Inflammatory Microneedle Materials
- Anti-Fouling and Self-Cleaning Sensor Coatings

**Fig. 12** Overview of key challenges and technological solutions in wearable biosensing across four major biofluids: sweat, saliva, tears, and ISF. The figure highlights biofluid-specific barriers—such as low secretion rates, biofouling, and signal degradation—and outlines engineering strategies including microfluidic design, advanced materials, and sensor integration to enable reliable, continuous, and non-invasive health monitoring.

robust systems capable of reshaping diagnostics, chronic disease management, and precision healthcare.

## 7.2 Saliva

One of the primary challenges in developing saliva-based wearable devices lies in the significantly lower concentration of biomarkers compared to blood. Several analytes are present in saliva at levels up to 1000-fold lower than in blood, necessitating highly sensitive detection methods to achieve clinically meaningful results.<sup>424</sup> This vast concentration disparity poses a substantial obstacle for accurate quantification, especially within the constrained form factors of wearable platforms. While modern analytical technologies can now detect biomolecules at picogram-per-milliliter concentrations, translating this sensitivity into compact, energy-efficient, and cost-effective wearable devices remains technically demanding.<sup>425</sup> Another key barrier is the lack of standardized saliva collection protocols, which compromises measurement reproducibility and inter-study comparability. Saliva sampling is influenced by numerous factors, including circadian rhythm, oral hygiene, hydration status, recent food

intake, and the method used to stimulate glandular secretion.<sup>424</sup> Even with commercial collection devices and predefined protocols, inconsistencies persist. Standard practices often involve mouth rinsing, absorbent pad placement, time-controlled collection, membrane filtration, and tube-based transfer.<sup>426</sup> Each step introduces variability and contamination risks, which can distort biomarker levels and affect downstream analysis. Consequently, there is a pressing need for unified, clinically validated collection procedures to support reliable salivary biomarker sensing in wearable applications.

Microfluidic integration further complicates saliva-based wearables due to the unique rheological characteristics of saliva. Its variable viscosity and heterogeneous molecular composition often result in microchannel clogging, erratic flow, and uneven delivery to detection zones.<sup>427</sup> Moreover, salivary mucins and proteins readily adsorb onto microchannel surfaces, altering fluid dynamics and compromising sensor performance.<sup>425</sup> These effects demand microfluidic designs that are resilient to biofouling, ensure steady flow, and deliver precise sample volumes to sensor interfaces.



Electrochemical biosensors, a common modality in wearables, face additional complications due to the presence of numerous electroactive species in saliva. These endogenous molecules can interfere with detection signals, necessitating the use of selective membranes or advanced filtering strategies.<sup>428</sup> However, even conventional filtration techniques such as using 0.22 µm or 0.45 µm filters have been shown to disrupt sample composition, particularly by removing extracellular vesicles that carry critical diagnostic information.<sup>429</sup> Transitioning from laboratory-scale prototypes to commercially viable saliva-based wearables are further hindered by operational complexity, cost, and regulatory challenges. Most current systems require supervised operation, involve multi-step protocols, and demand user training.<sup>428</sup> The absence of inter-laboratory standardization adds to the difficulty of clinical validation and regulatory approval.<sup>424</sup> Additionally, the high manufacturing costs of sensitive biosensors and microfluidic systems can make commercial pricing untenable. These barriers collectively explain why, despite significant scientific progress, only a limited number of saliva-based wearable platforms have reached the market. Fig. 12b highlights the significant challenges and solutions that must be addressed for saliva-based wearables. Overcoming these limitations will require innovations in ultra-sensitive detection, standardized sample handling, biofouling-resistant microfluidics, and scalable manufacturing processes.

### 7.3 Tears

Current tear collection strategies include flexible epidermal microfluidic patches placed beneath the eye and contact lens-based platforms that interface directly with the ocular surface.<sup>430</sup> While these approaches provide promising routes for tear-based biosensing, both face significant challenges in consistently collecting sufficient tear volumes without compromising ocular health or user comfort particularly in the context of continuous, long-term monitoring. Microfluidic channels for such applications must be precisely engineered at microscale dimensions to accommodate the inherently limited tear volume, minimize evaporation, and ensure accurate sample delivery to sensing regions.<sup>431</sup> The ocular environment imposes strict requirements for biocompatibility, mechanical compliance, and transparency. Contact lens-based sensors must simultaneously preserve essential characteristics such as oxygen permeability and optical clarity while incorporating functional microfluidic and sensing components.<sup>430</sup> These concurrent demands constrain material choices and complicate device design. Even slight deviations from baseline comfort can stimulate reflex tearing, diluting tear analytes and introducing variability that affects diagnostic reliability. Thus, sustained biocompatibility, particularly for devices intended for prolonged wear, remains a central concern.

Tear composition is inherently dynamic, subject to fluctuations driven by environmental exposure, emotional

responses, circadian rhythms, and other physiological variables. These factors introduce significant variability in biomarker levels, necessitating advanced signal processing methods to differentiate between pathophysiological signals and normal physiological noise.<sup>431</sup> Additionally, tear fluid contains proteins, lipids, and electrolytes that can interfere with sensor readouts, requiring selective sensing strategies and surface modifications to improve detection fidelity. To address these complexities, emerging tear biosensing systems are integrating machine learning and AI algorithms—such as deep neural networks—to correct for pH shifts, ambient light conditions, and colorimetric response variability.<sup>431</sup> Despite their considerable potential, tear-based wearable biosensors face significant commercialization hurdles, including regulatory, manufacturing, and end-user challenges. Ocular devices are subject to stringent oversight due to their proximity to sensitive tissues, lengthening development cycles and increasing compliance costs. On the manufacturing front, producing microscales, transparent, and biocompatible devices with integrated sensing and communication capabilities poses non-trivial fabrication challenges. Moreover, user adoption is heavily dependent on achieving contact lens-level comfort while delivering reliable, actionable health insights. Fig. 12c highlights the significant challenges and corresponding solutions that need to be addressed, which help explain the limited commercial availability of tear-based wearables, despite increasing research interest and technological progress in this field.

### 7.4 ISF

ISF offers a promising biofluid for continuous health monitoring; however, it presents intrinsic volume limitations that severely constrain its usability in wearable diagnostics. In even the most ISF-rich regions of the dermis, only about 120 µL of ISF is present per cm<sup>2</sup> of skin, and most current extraction methods can yield only 1–10 µL at a time.<sup>432</sup> Compounding the issue, ISF replenishment occurs at extremely low rates typically 5 to 50 nL min<sup>-1</sup> cm<sup>-2</sup> making continuous or high-frequency sampling particularly challenging.<sup>41</sup> These low volumes necessitate the development of ultra-sensitive detection technologies and impose strict limitations on sensor design, microfluidic handling, and device longevity. Extraction methods for ISF face a difficult trade-off between invasiveness and sample fidelity. Traditional approaches such as suction blisters, reverse iontophoresis, sonophoresis, micro dialysis, and thermal ablation often cause significant tissue disruption or inflammatory responses that can in turn alter the biomarker landscape of ISF itself.<sup>306</sup> Although microneedles are widely regarded as a minimally invasive alternative, they still penetrate the skin and may induce localized inflammation, which can distort analyte concentrations for hours post-insertion complicating longitudinal monitoring and undermining data reliability. Microfluidic integration with ISF extraction technologies introduces a distinct set of



engineering and physiological challenges. Channels must be optimized to accommodate nanoliter-scale flow rates while preventing analyte degradation from adsorption or evaporation, and avoiding blockage caused by biofouling or particulate matter.<sup>41,432</sup> Furthermore, fluidic interfaces between extraction sites and microchannels must minimize dead volume and transfer delays, while maintaining mechanical flexibility to withstand skin deformation and movement without compromising performance. One critical issue often overlooked is analyte distortion due to filtration effects during forced ISF extraction. When pressure-based techniques such as vacuum or iontophoresis are used, small molecules like water and electrolytes pass through tissue barriers more readily than larger biomarkers. This results in sample compositions that may no longer reflect true ISF physiology.<sup>41,432</sup> For example, vacuum methods can extract fluid at rates up to  $5 \mu\text{L min}^{-1} \text{cm}^{-2}$ , but the resulting samples exhibit significant deviations from serum composition, particularly for proteins and larger macromolecules. Such filtration artifacts necessitate complex calibration strategies or correction algorithms to restore measurement accuracy. Sensor integration in ISF platforms poses further hurdles. Devices must be capable of operating reliably with minimal sample volumes, all while compensating for variability in extraction efficiency and analyte distortion.

In long-term applications, biofouling and foreign body responses often degrade signal quality and sensor accuracy. Although surface coatings and anti-fouling strategies have shown short-term efficacy, ensuring stable performance over days or weeks remains an unresolved challenge in most ISF-based wearable systems.<sup>41,432</sup> From a commercialization standpoint, ISF-based wearables face high barriers. These include the manufacturing complexity of miniaturized extraction and sensing components, as well as stringent regulatory hurdles tied to their minimally invasive nature. Compared to non-invasive sweat or saliva-based systems, ISF wearables typically require more rigorous clinical validation and longer approval timelines. Fig. 12 outlines the key challenges and proposed solutions for ISF-based wearable devices. In addition to technical hurdles, issues related to user comfort, skin puncture, and the risk of irritation or visible marks significantly influence consumer acceptance. Together, these factors help explain the limited commercial adoption of ISF-based monitors, despite their strong potential in targeted applications such as continuous glucose monitoring.<sup>41</sup>

## 7.5 Commercial landscape and translation outlook: wearable biosensors

From needle-free glucose sensors to sweat-based hydration patches, a new generation of wearable biosensing technologies is reshaping personalized healthcare. This section highlights key innovators and commercially promising platforms across different biofluids. Bioliniq, a San

Diego-based startup, is advancing a next-generation intradermal biosensor platform for continuous metabolic monitoring, with a focus on non-invasive, needle-free glucose sensing.<sup>433</sup> Its skin-conformal patch contains microscale electrochemical sensors that continuously measure glucose beneath the skin, while also tracking metrics such as activity and sleep. The device uses a user-friendly, color-coded interface that eliminates the need for external readers. Currently undergoing pivotal clinical trials in the U.S., Bioliniq is preparing for FDA submission and commercial release. VitalConnect, based in San Jose, offers the VitalPatch RTM®, a single-lead, wearable biosensor patch that continuously monitors up to 11 vital signs, including ECG, heart rate, respiratory rate, skin temperature, posture, activity, and fall detection.<sup>405</sup> FDA 510(k)-cleared and deployed in both inpatient and outpatient settings, VitalPatch has demonstrated strong clinical utility and market adoption.

Profusa has developed a novel class of tissue-integrating biosensors composed of flexible hydrogel fibers implanted beneath the skin. These sensors monitor key analytes like oxygen and, in the future, aim to track glucose, lactate, and ions through a wearable optical reader linked to a smartphone.<sup>434</sup> Profusa's Lumee Oxygen Platform™ is already CE-marked in Europe and under FDA investigation in the U.S., with its minimally invasive, tissue-compatible design holding promise for long-term biochemical monitoring. Allez Health contributes to the CGM ecosystem with a next-generation wearable sensor designed for 15-day use.<sup>435</sup> Using a minimally invasive electrochemical filament, Allez's CGM system offers real-time glucose monitoring with medical-grade accuracy and smartphone connectivity. The system is currently under FDA investigation and backed by funding to support clinical trials and manufacturing scale-up, with a focus on affordability and access. Dexcom, a market leader in CGM, offers a robust suite of FDA-cleared systems including the G6, G7, and the recently launched Stelo—an over-the-counter CGM with a 15-day wear period.<sup>436</sup> Dexcom sensors use a subcutaneous electrochemical filament to measure interstitial glucose every minute, transmitting data wirelessly to mobile devices or receivers. With wide clinical adoption, Dexcom sets the benchmark for CGM performance and integration.

Epicore Biosystems is leading innovations in sweat-based biosensing, with several platforms tailored to athletic, industrial, and clinical use cases.<sup>437</sup> The Gx Sweat Patch, developed in partnership with Gatorade, leverages soft microfluidics to monitor fluid and electrolyte loss in athletes, offering real-time feedback *via* a connected app. The Discovery Patch is FDA-registered for remote sweat collection in clinical trials, while the Connected Hydration system targets industrial workers, tracking sweat rate, electrolyte loss, and skin temperature to mitigate heat stress. With over \$32m in funding and industry collaborations (*e.g.*, DuPont, Chevron), Epicore is a recognized leader in sweat biosensing. Nutromics offers a minimally invasive platform called the Lab on a Patch®, which uses DNA aptamer-functionalized



microneedles to continuously monitor biomarkers in interstitial fluid.<sup>438</sup> The coin-sized wearable has demonstrated real-time vancomycin tracking in clinical trials. Based on electrochemical aptamer sensing, the platform enables multiplex monitoring of drug levels, organ function, and inflammatory markers. Although regulatory approval is pending, Nutromics' approach holds significant promise for precision medicine applications such as therapeutic drug monitoring and sepsis detection.

These companies illustrate the diversity and momentum of the wearable biosensor ecosystem. Their platforms span multiple biofluids, sensing modalities, and clinical use cases—from metabolic tracking and hydration monitoring to drug dosing and remote patient care. Looking forward, the convergence of advanced microfluidics, stretchable electronics, and AI-driven analytics is expected to propel the next generation of smart biosensors. Future systems will likely integrate multimodal sensing, closed-loop feedback, and secure wireless transmission, enabling continuous, autonomous, and predictive health monitoring across both clinical and consumer domains.

## Conclusion

The integration of wearable biosensing technologies with microfluidic platforms is rapidly advancing the capabilities of non-invasive health monitoring. By enabling continuous, real-time analysis of biomarkers in sweat, saliva, tears, and ISF, these systems present a compelling alternative to conventional diagnostic modalities. Each biofluid offers specific advantages—such as the non-invasiveness of sweat and saliva or the close correlation of ISF with systemic biomarkers—yet poses distinct challenges in terms of sampling volume, analyte stability, and device integration. Recent innovations in soft materials, microfabrication techniques, capillary and active microfluidics, and biochemical sensing have collectively improved the feasibility of chrono-sampling and multiplexed analysis in wearable formats. Nevertheless, widespread clinical translation is impeded by several critical limitations, including insufficient fluid volumes (particularly in ISF and tears), variability in biofluid composition, limited long-term sensor stability, and lack of standardized sampling protocols. Furthermore, achieving continuous sampling at rest, addressing signal drift over time, and ensuring compatibility with dynamic skin movements remain non-trivial. To advance the field, future efforts should prioritize the integration of adaptive microfluidic interfaces, robust anti-fouling sensor chemistries, and machine learning-enabled data processing to enhance sensitivity, specificity, and interpretability. Rigorous clinical validation through well-designed cohort studies and alignment with regulatory standards will also be essential to facilitate real-world implementation. Overall, wearable microfluidic biosensors represent a transformative class of analytical platforms that may redefine point-of-care diagnostics, personalized medicine, and digital health.

Continued interdisciplinary collaboration will be key to overcoming current limitations and unlocking their full diagnostic and therapeutic potential.

## Data availability

Data sharing is not applicable to this article as no new data were created or analyzed in this study.

## Conflicts of interest

There are no conflicts to declare.

## Acknowledgements

The authors thank Mitacs Canada and Canada Research Chairs for funding this work and the University of Calgary for their support.

## References

- 1 H. C. Ates, P. Q. Nguyen, L. Gonzalez-Macia, E. Morales-Narváez, F. Güder, J. J. Collins and C. Dincer, *Nat. Rev. Mater.*, 2022, **7**, 887–907.
- 2 J. Kim, A. S. Campbell, B. E.-F. De Ávila and J. Wang, *Nat. Biotechnol.*, 2019, **37**, 389–406.
- 3 S. M. Mugo, W. Lu, M. Wood and S. Lemieux, *Electrochem. Sci. Adv.*, 2022, **2**, e2100039.
- 4 M. Smuck, C. A. Odonkor, J. K. Wilt, N. Schmidt and M. A. Swiernik, *npj Digit. Med.*, 2021, **4**, 45.
- 5 J. Choi, D. Kang, S. Han, S. B. Kim and J. A. Rogers, *Adv. Healthcare Mater.*, 2017, **6**, 1601355.
- 6 R. Ghaffari, J. Choi, M. S. Raj, S. Chen, S. P. Lee, J. T. Reeder, A. J. Aranyosi, A. Leech, W. Li, S. Schon, J. B. Model and J. A. Rogers, *Adv. Funct. Mater.*, 2020, **30**, 1907269.
- 7 A. Koh, D. Kang, Y. Xue, S. Lee, R. M. Pielak, J. Kim, T. Hwang, S. Min, A. Banks, P. Bastien, M. C. Manco, L. Wang, K. R. Ammann, K.-I. Jang, P. Won, S. Han, R. Ghaffari, U. Paik, M. J. Slepian, G. Balooch, Y. Huang and J. A. Rogers, *Sci. Transl. Med.*, 2016, **8**(366), 366ra165.
- 8 L. Tai, W. Gao, M. Chao, M. Bariya, Q. P. Ngo, Z. Shahpar, H. Y. Y. Nyein, H. Park, J. Sun, Y. Jung, E. Wu, H. M. Fahad, D. Lien, H. Ota, G. Cho and A. Javey, *Adv. Mater.*, 2018, **30**, 1707442.
- 9 M. Wang, Y. Yang, J. Min, Y. Song, J. Tu, D. Mukasa, C. Ye, C. Xu, N. Heflin, J. S. McCune, T. K. Hsiai, Z. Li and W. Gao, *Nat. Biomed. Eng.*, 2022, **6**, 1225–1235.
- 10 S. Imani, A. J. Bandodkar, A. M. V. Mohan, R. Kumar, S. Yu, J. Wang and P. P. Mercier, *Nat. Commun.*, 2016, **7**, 11650.
- 11 Y. Yang, Y. Song, X. Bo, J. Min, O. S. Pak, L. Zhu, M. Wang, J. Tu, A. Kogan, H. Zhang, T. K. Hsiai, Z. Li and W. Gao, *Nat. Biotechnol.*, 2020, **38**, 217–224.
- 12 P. Q. Nguyen, L. R. Soenksen, N. M. Donghia, N. M. Angenent-Mari, H. De Puig, A. Huang, R. Lee, S. Slomovic, T. Galbersanini, G. Lansberry, H. M. Sallum, E. M. Zhao, J. B. Niemi and J. J. Collins, *Nat. Biotechnol.*, 2021, **39**, 1366–1374.



13 A. Olanrewaju, M. Beaugrand, M. Yafia and D. Juncker, *Lab Chip*, 2018, **18**, 2323–2347.

14 R. Safavieh and D. Juncker, *Lab Chip*, 2013, **13**, 4180.

15 T. Shay, T. Saha, M. D. Dickey and O. D. Velev, *Biomicrofluidics*, 2020, **14**, 034112.

16 J. Guerrero, Y. Chang, A. A. Fragkopoulos and A. Fernandez-Nieves, *Small*, 2020, **16**, 1904344.

17 J. Songok, M. Tuominen, H. Teisala, J. Haapanen, J. Mäkelä, J. Kuusipalo and M. Toivakka, *ACS Appl. Mater. Interfaces*, 2014, **6**, 20060–20066.

18 S. Hassan, A. Tariq, Z. Noreen, A. Donia, S. Z. J. Zaidi, H. Bokhari and X. Zhang, *Diagnostics*, 2020, **10**, 509.

19 S. Shajari, R. Salahandish, A. Zare, M. Hassani, S. Moossavi, E. Munro, R. Rashid, D. Rosenegger, J. S. Bains and A. Sanati Nezhad, *Adv. Sci.*, 2023, **10**, 2204171.

20 T. Abbasiasl, F. Mirlou, E. Istif, H. Ceylan Koydemir and L. Beker, *Sens. Diagn.*, 2022, **1**, 775–786.

21 Q. Cao, B. Liang, T. Tu, J. Wei, L. Fang and X. Ye, *RSC Adv.*, 2019, **9**, 5674–5681.

22 L. Zheng, Y. Liu and C. Zhang, *Sens. Actuators, B*, 2021, **343**, 130131.

23 E. VanArsdale, J. Pitzer, G. F. Payne and W. E. Bentley, *iScience*, 2020, **23**, 101545.

24 K. Manibalan, P. Arul, H.-J. Wu, S.-T. Huang and V. Mani, *ACS Meas. Sci. Au*, 2024, **4**, 163–183.

25 G. Wu, E. T. Zhang, Y. Qiang, C. Esmonde, X. Chen, Z. Wei, Y. Song, X. Zhang, M. J. Schneider, H. Li, H. Sun, Z. Weng, S. Santaniello, J. He, R. Y. Lai, Y. Li, M. R. Bruchas and Y. Zhang, *bioRxiv*, 2023, preprint, DOI: [10.1101/2023.10.18.562080](https://doi.org/10.1101/2023.10.18.562080).

26 J. Kim, R. Kumar, A. J. Bandodkar and J. Wang, *Adv. Electron. Mater.*, 2017, **3**, 1600260.

27 FDA extends use of implantable CGM sensor to 6 months, <https://www.healio.com/news/endocrinology/20220211/fda-extends-use-of-implantable-cgm-sensor-to-6-months>, (accessed March 25, 2025).

28 Q. Zhang, D. Jiang, C. Xu, Y. Ge, X. Liu, Q. Wei, L. Huang, X. Ren, C. Wang and Y. Wang, *Sens. Actuators, B*, 2020, **320**, 128325.

29 K. Spychaliska, D. Zajac, S. Baluta, K. Halicka and J. Cabaj, *Polymers*, 2020, **12**, 1154.

30 B. Babamiri, M. Farrokhnia, M. Mohammadi and A. Sanati Nezhad, *Sci. Rep.*, 2025, **15**, 8859.

31 F. Lopes, J. G. Pacheco, P. Rebelo and C. Delerue-Matos, *Sens. Actuators, B*, 2017, **243**, 745–752.

32 O. S. Ahmad, T. S. Bedwell, C. Esen, A. Garcia-Cruz and S. A. Piletsky, *Trends Biotechnol.*, 2019, **37**, 294–309.

33 Y. Li, L. Zhang, Y. Dang, Z. Chen, R. Zhang, Y. Li and B.-C. Ye, *Biosens. Bioelectron.*, 2019, **127**, 207–214.

34 H. Park, W. Park and C. H. Lee, *NPG Asia Mater.*, 2021, **13**, 23.

35 M. Padash, C. Enz and S. Carrara, *Sensors*, 2020, **20**, 4236.

36 N. Brasier, J. Wang, W. Gao, J. R. Sempionatto, C. Dincer, H. C. Ates, F. Güder, S. Olenik, I. Schauwecker, D. Schaffarczyk, E. Vayena, N. Ritz, M. Weisser, S. Mtenga, R. Ghaffari, J. A. Rogers and J. Goldhahn, *Nature*, 2024, **636**, 57–68.

37 A. Childs, B. Mayol, J. A. Lasalde-Ramírez, Y. Song, J. R. Sempionatto and W. Gao, *ACS Nano*, 2024, **18**, 24605–24616.

38 N. Davis, J. Heikenfeld, C. Milla and A. Javey, *Nat. Biotechnol.*, 2024, **42**, 860–871.

39 R. F. R. Ursem, A. Steijlen, M. Parrilla, J. Bastemeijer, A. Bossche and K. De Wael, *Lab Chip*, 2025, **25**, 1296–1315.

40 A. A. Smith, R. Li and Z. T. H. Tse, *Sci. Rep.*, 2023, **13**, 4998.

41 J. Heikenfeld, A. Jajack, J. Rogers, P. Gutruf, L. Tian, T. Pan, R. Li, M. Khine, J. Kim, J. Wang and J. Kim, *Lab Chip*, 2018, **18**, 217–248.

42 J. Min, J. Tu, C. Xu, H. Lukas, S. Shin, Y. Yang, S. A. Solomon, D. Mukasa and W. Gao, *Chem. Rev.*, 2023, **123**, 5049–5138.

43 F. Gao, C. Liu, L. Zhang, T. Liu, Z. Wang, Z. Song, H. Cai, Z. Fang, J. Chen, J. Wang, M. Han, J. Wang, K. Lin, R. Wang, M. Li, Q. Mei, X. Ma, S. Liang, G. Gou and N. Xue, *Microsyst. Nanoeng.*, 2023, **9**, 1.

44 B. Lindsay, D. M. Engel and A. S. Wolfe, Gatorade Sports Science Institute, 2022.

45 B. A. Katchman, M. Zhu, J. Blain Christen and K. S. Anderson, *Proteomics: Clin. Appl.*, 2018, **12**(6), 1800010.

46 L. Lyzwinski, M. Elgendi, A. V. Shokurov, T. J. Cuthbert, C. Ahmadizadeh and C. Menon, *Commun. Eng.*, 2023, **2**, 48.

47 N. Brasier and J. Eckstein, *Digit. Biomark.*, 2019, **3**, 155–165.

48 P. Pandit, B. Crewther, C. Cook, C. Punyadeera and A. K. Pandey, *Mater. Adv.*, 2024, **5**, 5339–5350.

49 M. Song, H. Bai, P. Zhang, X. Zhou and B. Ying, *Int. J. Oral Sci.*, 2023, **15**, 2.

50 A. K. Ghosh, A. Nath, E. Elangovan, A. Banerjee, K. Ramalingam and S. Sethuraman, *Cureus*, 2024, **16**, e65725.

51 S. Williamson, C. Munro, R. Pickler, M. J. Grap and R. K. Elswick, *Nurs. Res. Pract.*, 2012, **2012**, 246178.

52 M. Elgendi, L. Lyzwinski, E. Kübler, A. V. Shokurov, N. Howard and C. Menon, *npj Biosensing*, 2024, **1**, 1–10.

53 L. Anchidin-Noroce, W. K. Savage, A. Nemțoi and C. Cobuz, *Chemosensors*, 2024, **12**(12), 269.

54 F. J. Ascaso and V. Huerva, *Optom. Vis. Sci.*, 2016, **93**, 426–434.

55 W. Park, H. Seo, J. Kim, Y.-M. Hong, H. Song, B. J. Joo, S. Kim, E. Kim, C.-G. Yae, J. Kim, J. Jin, J. Kim, Y. Lee, J. Kim, H. K. Kim and J.-U. Park, *Nat. Commun.*, 2024, **15**, 2828.

56 A. Rajan, J. Vishnu and B. Shankar, *Biosensors*, 2024, **14**, 483.

57 N. L. Kazanskiy, S. N. Khonina and M. A. Butt, *Biosensors*, 2023, **13**, 933.

58 H. Haslene-Hox, E. Oveland, K. C. Berg, O. Kolmannskog, K. Woie, H. B. Salvesen, O. Tenstad and H. Wiig, *PLoS One*, 2011, **6**, e19217.

59 P. P. Samant, M. M. Niedzwiecki, N. Raviele, V. Tran, J. Mena-Lapaix, D. I. Walker, E. I. Felner, D. P. Jones, G. W. Miller and M. R. Prausnitz, *Sci. Transl. Med.*, 2020, **12**, eaaw0285.

60 A. Oharazawa, G. Maimaituxun, K. Watanabe, T. Nishiyasu and N. Fujii, *J. Dermatol. Sci.*, 2024, **114**, 141–147.

61 Y. Kim and M. R. Prausnitz, *Nat. Biomed. Eng.*, 2021, **5**, 3–5.



62 Z. Wu, Z. Qiao, S. Chen, S. Fan, Y. Liu, J. Qi and C. T. Lim, *Commun. Mater.*, 2024, **5**, 1–15.

63 P. A. Kusov, Y. V. Kotelevtsev and V. P. Drachev, *Molecules*, 2023, **28**, 2353.

64 C.-E. Karachaliou, G. Koukouvinos, D. Goustouridis, I. Raptis, S. Kakabakos, P. Petrou and E. Livaniou, *Biosensors*, 2023, **13**, 285.

65 M. Jia, W. M. Chew, Y. Feinstein, P. Skeath and E. M. Sternberg, *Analyst*, 2016, **141**, 2053–2060.

66 V. Vignesh, B. Castro-Dominguez, T. D. James, J. M. Gamble-Turner, S. Lightman and N. M. Reis, *ACS Sens.*, 2024, **9**, 1666–1681.

67 M. Imamovic, N. Bäcklund, S. Lundstedt, G. Brattsand, E. Aardal, T. Olsson and P. Dahlqvist, *Endocr. Connect.*, 2022, **12**(1), e220324.

68 L. Johnston, G. Wang, K. Hu, C. Qian and G. Liu, *Front. Bioeng. Biotechnol.*, 2021, **9**, 733810.

69 J. Giaretta, R. Zulli, T. Prabhakar, R. J. Rath, S. Naficy, S. Spilimbergo, P. S. Weiss, S. Farajikhah and F. Dehghani, *Adv. Sens. Res.*, 2024, **3**, 2400065.

70 T. I. L. Chan, Y. W. Y. Yip, T. T. C. Man, C. P. Pang and M. E. Brelén, *Transl. Vis. Sci. Technol.*, 2022, **11**, 3.

71 S. Dobashi, D. Funabashi, K. Sameshima, N. Tsuruoka and T. Matsui, *bioRxiv*, 2023, preprint, DOI: [10.1101/2023.10.23.563585](https://doi.org/10.1101/2023.10.23.563585).

72 T.-T. Luo, Z.-H. Sun, C.-X. Li, J.-L. Feng, Z.-X. Xiao and W.-D. Li, *J. Physiol. Sci.*, 2021, **71**, 26.

73 X. Xuan, C. Pérez-Rafols, C. Chen, M. Cuartero and G. A. Crespo, *ACS Sens.*, 2021, **6**, 2763–2771.

74 A.-M. Spehar-Délèze, S. Anastasova and P. Vadgama, *Chemosensors*, 2021, **9**, 195.

75 L. B. Baker, *Sports Med.*, 2017, **47**, 111–128.

76 L. B. Baker, P. J. D. De Chavez, R. P. Nuccio, S. D. Brown, M. A. King, B. C. Sopeña and K. A. Barnes, *J. Appl. Physiol.*, 2022, **133**, 1250–1259.

77 P. Pampani, S. Shenoy, R. V. Anegundi, M. K. Shekar, K. Dharani and L. Fathima, *J. Indian Soc. Periodontol.*, 2024, **28**, 569–574.

78 I. M. Thowsen, T. V. Karlsen, E. Nikpey, H. Haslene-Hox, T. Skogstrand, G. J. Randolph, B. H. Zinselmeyer, O. Tenstad and H. Wiig, *J. Physiol.*, 2022, **600**, 2293–2309.

79 N. I. Dmitrieva, D. Liu, C. O. Wu and M. Boehm, *Eur. Heart J.*, 2022, **43**, 3335–3348.

80 D. Vairo, L. Bruzzese, M. Marlinge, L. Fuster, N. Adjriou, N. Kipson, P. Brunet, J. Cautela, Y. Jammes, G. Mottola, S. Burtey, J. Ruf, R. Guieu and E. Fenouillet, *Sci. Rep.*, 2017, **7**, 11801.

81 B. Kallapur, K. Ramalingam, Bastian, A. Mujib, A. Sarkar and S. Sethuraman, *J. Nat. Sci. Biol. Med.*, 2013, **4**, 341–345.

82 Body Fluids and Fluid Compartments | Anatomy and Physiology II, <https://courses.lumenlearning.com/suny-ap2/chapter/body-fluids-and-fluid-compartments-no-content/>, (accessed June 30, 2025).

83 Office of Dietary Supplements - Potassium, <https://ods.od.nih.gov/factsheets/Potassium-HealthProfessional/>, (accessed June 30, 2025).

84 A. G. Faria, F. A. L. Marson, C. C. S. Gomez, M. de F. Servidoni, A. F. Ribeiro and J. D. Ribeiro, *Front. Pediatr.*, 2017, **5**, 222.

85 A. C. Gonçalves, F. A. de L. Marson, R. M. de H. Mendonça, J. D. Ribeiro, A. F. Ribeiro, I. A. Paschoal and C. E. Levy, *Diagn. Pathol.*, 2013, **8**, 46.

86 A. C. Gonçalves, F. A. L. Marson, R. M. H. Mendonça, C. S. Bertuzzo, I. A. Paschoal, J. D. Ribeiro, A. F. Ribeiro and C. E. Levy, *J. Pediatr.*, 2019, **95**, 443–450.

87 S. K. Raut, K. Singh, S. Sanghvi, V. Loyo-Celis, L. Varghese, E. R. Singh, S. Gururaja Rao and H. Singh, *Biosci. Rep.*, 2024, **44**, BSR20240029.

88 N. Sagar and S. Lohiya, *Cureus*, 2024, **16**, e55625.

89 C.-T. Huang, M.-L. Chen, L.-L. Huang and I.-F. Mao, *Chin. J. Physiol.*, 2002, **45**, 109–115.

90 A. Jaiswal, S. Madaan, N. Acharya, S. Kumar, D. Talwar and D. Dewani, *Cureus*, 2021, **13**, e19649.

91 L. Du, Y. Zong, H. Li, Q. Wang, L. Xie, B. Yang, Y. Pang, C. Zhang, Z. Zhong and J. Gao, *Signal Transduction Targeted Ther.*, 2024, **9**, 212.

92 J. Maiuolo, F. Oppedisano, S. Gratteri, C. Muscoli and V. Mollace, *Int. J. Cardiol.*, 2016, **213**, 8–14.

93 C. O. Page and J. S. Remington, *J. Lab. Clin. Med.*, 1967, **69**, 634–650.

94 T. Okada, H. Konishi, M. Ito, H. Nagura and J. Asai, *J. Invest. Dermatol.*, 1988, **90**, 648–651.

95 K. Matsuzaki, N. Sugimoto, R. Islam, M. E. Hossain, E. Sumiyoshi, M. Katakura and O. Shido, *Int. J. Mol. Sci.*, 2020, **21**, 815.

96 P. Patel, Z. Jamal and K. Ramphul, in *StatPearls*, StatPearls Publishing, Treasure Island (FL), 2025.

97 W. P. Nikolaejek and H. M. Emrich, *Eur. J. Pediatr.*, 1976, **122**, 289–291.

98 A. L. Mandel, C. Peyrot des Gachons, K. L. Plank, S. Alarcon and P. A. S. Breslin, *PLoS One*, 2010, **5**, e13352.

99 K. Pierzynowska, P. Wychowański, K. Zaworski, J. Wolinski, J. Donaldson, D. Szkopek, K. Roszkowicz-Ostrowska, A. Kondej and S. G. Pierzynowski, *World J. Exp. Med.*, 2024, **14**, 92589.

100 Amylase - blood Information | Mount Sinai - New York, <https://www.mountsinai.org/health-library/tests/amylase-blood>, (accessed June 30, 2025).

101 Chromogranin A Test, <https://www.quironsalud.com/en/diagnostic-tests/chromogranin-test>, (accessed June 30, 2025).

102 E. C. Wyatt, E. L. Wyatt and R. L. Graham, *JAAD Case Rep.*, 2025, **60**, 41–43.

103 Y. Kanamaru, A. Kikukawa and K. Shimamura, *Stress*, 2006, **9**, 127–131.

104 M. Tammayan, N. Jantaratnotai and P. Pachimsawat, *PLoS One*, 2021, **16**, e0256172.

105 A. Corti, *Cell. Mol. Neurobiol.*, 2010, **30**, 1163–1170.

106 A. J. Steckl and P. Ray, *ACS Sens.*, 2018, **3**, 2025–2044.

107 F. Akutsu, S. Sugino, M. Watanabe, Y.-A. Barde and M. Kojima, *F1000Research*, 2025, **14**, 161.

108 Y. K. Yoo, J. Lee, J. Kim, G. Kim, S. Kim, J. Kim, H. Chun, J. H. Lee, C. J. Lee and K. S. Hwang, *Sci. Rep.*, 2016, **6**, 33694.



109 K. Wójtowicz, K. Czarzasta, L. Przepiorka, S. Kujawski, A. Cudnoch-Jedrzejewska, A. Marchel and P. Kunert, *Cureus*, 2023, **15**, e48237.

110 É. Csósz, G. Emri, G. Kalló, G. Tsaprailis and J. Tőzsér, *J. Eur. Acad. Dermatol. Venereol.*, 2015, **29**, 2024–2031.

111 M. K. Mahmood, H. A. Kurda, B. H. Qadir, H. Tassery, R. Lan, D. Tardivo and M. A. Abdulghafor, *Saudi Dent. J.*, 2024, **36**, 698–707.

112 M. Ellmerer, L. Schaupp, G. A. Brunner, G. Sendlhofer, A. Wutte, P. Wach and T. R. Pieber, *Am. J. Physiol.*, 2000, **278**, E352–E356.

113 H. L. Poulsen, *Scand. J. Clin. Lab. Invest.*, 1974, **34**(2), 119–122.

114 Albumin Blood Test, <https://medlineplus.gov/lab-tests/albumin-blood-test/>, (accessed June 30, 2025).

115 S. Adelaars, C. S. M. Lapré, P. Raaijmakers, C. J. A. M. Konings, M. Mischi, R. A. Bouwman and D. van de Kerkhof, *J. Chromatogr. B*, 2025, **1252**, 124444.

116 Y. Zhang, H. Guo, S. B. Kim, Y. Wu, D. Ostojich, S. H. Park, X. Wang, Z. Weng, R. Li, A. J. Bandodkar, Y. Sekine, J. Choi, S. Xu, S. Quaggin, R. Ghaffari and J. A. Rogers, *Lab Chip*, 2019, **19**, 1545–1555.

117 Comparing creatinine levels in blood and interstitial fluid, <https://www.hra.nhs.uk/planning-and-improving-research/application-summaries/research-summaries/comparing-creatinine-levels-in-blood-and-interstitial-fluid/>, (accessed June 30, 2025).

118 A. Córdova and F. J. Navas, *Ann. Nutr. Metab.*, 1998, **42**, 274–282.

119 J. L. Stauber and T. M. Florence, *Sci. Total Environ.*, 1988, **74**, 235–247.

120 A. Mathur, K. Wallenius and M. Abdulla, *Scand. J. Clin. Lab. Invest.*, 1977, **37**, 469–472.

121 J. L. Stauber and T. M. Florence, *Sci. Total Environ.*, 1987, **60**, 263–271.

122 M. Schaefer, M. Schellenberg, U. Merle, K. H. Weiss and W. Stremmel, *BMC Gastroenterol.*, 2008, **8**, 29.

123 V. R. Reddy, S. Devakar, N. Chowdhary, S. M. Chaitan, R. Peddi and P. S. Kumar, *Int. J. Clin. Pediatr. Dent.*, 2021, **14**, 235–237.

124 E. W. Rice and N. P. Goldstein, *Metabolism*, 1966, **15**, 1050–1053.

125 C. Muñoz-Bravo, E. Soler-Iborte, M. Lozano-Lorca, M. Kouiti, C. González-Palacios Torres, R. Barrios-Rodríguez and J. J. Jiménez-Moleón, *Front. Cardiovasc. Med.*, 2023, **10**, DOI: [10.3389/fcvm.2023.1217748](https://doi.org/10.3389/fcvm.2023.1217748).

126 C. A. Coltman and N. J. Rowe, *Am. J. Clin. Nutr.*, 1966, **18**, 270–274.

127 A. M. Gawaly, A. A. Y. El-Naby and G. M. Alghazaly, *Egypt. J. Haematol.*, 2020, **45**, 156.

128 Anemia - Iron-Deficiency Anemia | NHLBI, NIH, <https://www.nhlbi.nih.gov/health/anemia/iron-deficiency-anemia>, (accessed June 30, 2025).

129 A. Bardow, J. Madsen and B. Nauntofte, *Clin. Oral Investig.*, 2000, **4**, 245–253.

130 Serum Bicarbonate - Range, levels, testing | National Kidney Foundation, <https://www.kidney.org/kidney-failure-risk-factor-serum-bicarbonate>, (accessed June 30, 2025).

131 C. A. Prompt, P. M. Quinton and C. R. Kleeman, *Nephron*, 1978, **20**, 4–9.

132 M. S. Razzaque, *FASEB BioAdv.*, 2022, **4**, 102–108.

133 What Is Hypophosphatemia?, <https://my.clevelandclinic.org/health/diseases/24040-hypophosphatemia>, (accessed June 30, 2025).

134 S. Itoh and T. Nakayama, *Jpn. J. Physiol.*, 1951, **2**, 248–253.

135 Y. Nakamura, H. Kodama, T. Satoh, K. Adachi, S. Watanabe, Y. Yokote and H. Sakagami, *In Vivo*, 2010, **24**, 837–842.

136 Gutierrez, Anderstam and Alvestrand, *Eur. J. Clin. Invest.*, 1999, **29**, 947–952.

137 J. A. Schmidt, S. Rinaldi, A. Scalbert, P. Ferrari, D. Achaintre, M. J. Gunter, P. N. Appleby, T. J. Key and R. C. Travis, *Eur. J. Clin. Nutr.*, 2016, **70**, 306–312.

138 R. W. Keller, J. L. Bailey, Y. Wang, J. D. Klein and J. M. Sands, *Physiol. Rep.*, 2016, **4**, e12825.

139 A. G. Kovalčíková, K. Pavlov, R. Lipták, M. Hladová, E. Renczés, P. Boor, L. Podracká, K. Šebeková, J. Hodosy, L. Tóthová and P. Celec, *Sci. Rep.*, 2020, **10**, 21260.

140 T. J. Lasisi, Y. R. Raji and B. L. Salako, *BMC Nephrol.*, 2016, **17**, 10.

141 T. Takemura, P. W. Wertz and K. Sato, *Br. J. Dermatol.*, 1989, **120**, 43–47.

142 S. Karjalainen, L. Sewón, E. Söderling, B. Larsson, I. Johansson, O. Simell, H. Lapinleimu and R. Seppänen, *J. Dent. Res.*, 1997, **76**, 1637–1643.

143 What Should My Cholesterol Levels Be?, <https://my.clevelandclinic.org/health/articles/11920-cholesterol-numbers-what-do-they-mean>, (accessed June 30, 2025).

144 K. Agrawal, R. K. Sivamani and J. W. Newman, *Sking Res. Technol.*, 2019, **25**, 3–11.

145 V. Singh, R. Patil, S. Singh, A. Tripathi, V. Khanna and W. Ali, *Natl. J. Maxillofac. Surg.*, 2021, **12**, 188–192.

146 B. Larsson, G. Olivecrona and T. Ericsen, *Arch. Oral Biol.*, 1996, **41**, 105–110.

147 O. Zagoory-Sharon, A. Levine and R. Feldman, *Psychoneuroendocrinology*, 2023, **158**, 106407.

148 B. Keevil, P. MacDonald, W. Macdowall, D. Lee and F. Wu, *Ann. Clin. Biochem.*, 2014, **51**, 368–378.

149 I.-S. Huang, L.-H. Li, W.-J. Chen, E. Y.-H. Huang, C.-C. Juan and W. J. Huang, *Eur. Urol. Open Sci.*, 2023, **54**, 88–96.

150 M. Diver, *Front. Horm. Res.*, 2009, **37**, 21–31.

151 C. Ye, M. Wang, J. Min, R. Y. Tay, H. Lukas, J. R. Sempionatto, J. Li, C. Xu and W. Gao, *Nat. Nanotechnol.*, 2024, 330–337.

152 B. K. Gandara, L. Leresche and L. Mancl, *Ann. N. Y. Acad. Sci.*, 2007, **1098**, 446–450.

153 H. T. Depypere, S. Bolca, M. Bracke, J. Delanghe, F. Comhaire and Ph. Blondeel, *Maturitas*, 2015, **81**, 42–45.

154 S. Glynne, D. Reisel, A. Kamal, A. Neville, L. McColl, R. Lewis and L. Newson, *Menopause*, 2025, **32**, 103.

155 J. Brunmair, M. Gotsmy, L. Niederstaetter, B. Neuditschko, A. Bileck, A. Slany, M. L. Feuerstein, C. Langbauer, L. Janker, J. Zanghellini, S. M. Meier-Menches and C. Gerner, *Nat. Commun.*, 2021, **12**, 5993.

156 C. C. Muir, K. Treasurywala, S. McAllister, J. Sutherland, L. Dukas, R. G. Berger, A. Khan and D. deCatanzaro, *Horm. Metab. Res.*, 2008, **40**, 819–826.



157 E. Ferrer, G. Rodas, G. Casals, A. Trilla, L. Balagué-Dobon, J. R. González, K. Ridley, R. White and R. J. Burden, *Front. Sports Act. Living*, 2024, **6**, DOI: [10.3389/fspor.2024.1430158](https://doi.org/10.3389/fspor.2024.1430158).

158 Y. Lu, G. R. Bentley, P. H. Gann, K. R. Hodges and R. T. Chatterton, *Fertil. Steril.*, 1999, **71**, 863–868.

159 J. Tu, J. Min, Y. Song, C. Xu, J. Li, J. Moore, J. Hanson, E. Hu, T. Parimon, T.-Y. Wang, E. Davoodi, T.-F. Chou, P. Chen, J. J. Hsu, H. B. Rossiter and W. Gao, *Nat. Biomed. Eng.*, 2023, **7**, 1293–1306.

160 J. B. Pay and A. M. Shaw, *Clin. Biochem.*, 2019, **68**, 1–8.

161 A. Grammoustianou, A. Saeidi, J. Longo, F. Risch and A. M. Ionescu, *arXiv*, 2024, preprint, arXiv:2407.16734, DOI: [10.48550/arXiv.2407.16734](https://doi.org/10.48550/arXiv.2407.16734).

162 L. E. McCrae, W.-T. Ting and M. M. R. Howlader, *Biosens. Bioelectron.: X*, 2023, **13**, 100288.

163 M. Hladek, S. L. Szanton, Y.-E. Cho, C. Lai, C. Sacko, L. Roberts and J. Gill, *J. Immunol. Methods*, 2018, **454**, 1–5.

164 M. M. Grisius, D. K. Bermudez and P. C. Fox, *J. Rheumatol.*, 1997, **24**, 1089–1091.

165 E. A. Said, I. Al-Reesi, N. Al-Shizawi, S. Jaju, M. S. Al-Balushi, C. Y. Koh, A. A. Al-Jabri and L. Jeyaseelan, *J. Med. Virol.*, 2021, **93**, 3915–3924.

166 R. P. Hirten, K.-C. Lin, J. Whang, S. Shahub, D. Helmus, S. Muthukumar, B. E. Sands and S. Prasad, *Sci. Rep.*, 2024, **14**, 2833.

167 H. R. Mozaffari, M. Ramezani, M. Mahmoudiahmadabadi, N. Omidpanah and M. Sadeghi, *Oral Surg. Oral Med. Oral Pathol.*, 2017, **124**, e183–e189.

168 Y. Nakai, S. Hamagaki, R. Takagi, A. Taniguchi and F. Kurimoto, *J. Clin. Endocrinol. Metab.*, 1999, **84**, 1226–1228.

169 B. Zinman, A. J. Hanley, S. B. Harris, J. Kwan and I. G. Fantus, *J. Clin. Endocrinol. Metab.*, 1999, **84**, 272–278.

170 C. Alexander, C. J. Cochran, L. Gallicchio, S. R. Miller, J. A. Flaws and H. Zaccur, *Fertil. Steril.*, 2010, **94**, 1037–1043.

171 T. L. Laursen, R. B. Zak, R. J. Shute, M. W. S. Heesch, N. E. Dinan, M. P. Bubak, D. T. La Salle and D. R. Slivka, *Temp. Multidiscip. Biomed. J.*, 2017, **4**, 166–175.

172 A. Khorsand, M. Bayani, S. Yaghobee, S. Torabi, M. J. Kharrazifard and F. Mohammadnejhad, *J. Dent.*, 2016, **13**, 1–9.

173 G. Sendlhofer, G. Brunner, L. Schaupp, A. Wutte, M. Ellmerer and T. R. Pieber, *Eur. J. Clin. Invest.*, 2015, **45**, 445–451.

174 M. Toda, R. Tsukinoki and K. Morimoto, *Acta Diabetol.*, 2007, **44**, 20–22.

175 F.-Y. Lin, H. C. Wu, K. C. Cheng, C. L. Tung, C. P. Chang and Y. H. Feng, *Int. J. Hematol.*, 2015, **102**, 312–317.

176 K. Hotta, T. Funahashi, Y. Arita, M. Takahashi, M. Matsuda, Y. Okamoto, H. Iwahashi, H. Kuriyama, N. Ouchi, K. Maeda, M. Nishida, S. Kihara, N. Sakai, T. Nakajima, K. Hasegawa, M. Muraguchi, Y. Ohmoto, T. Nakamura, S. Yamashita, T. Hanafusa and Y. Matsuzawa, *Arterioscler. Thromb., Vasc. Biol.*, 2000, **20**, 1595–1599.

177 R. Dall, J. Kanaley, T. K. Hansen, N. Møller, J. S. Christiansen, H. Hosoda, K. Kangawa and J. O. L. Jørgensen, *Eur. J. Endocrinol.*, 2002, **147**, 65–70.

178 C. Stylianou, A. Galli-Tsinopoulou, G. Koliakos, M. Fotoulaki and S. Nousia-Arvanitakis, *J. Cystic Fibrosis*, 2007, **6**, 293–296.

179 T. Shiiya, M. Nakazato, M. Mizuta, Y. Date, M. S. Mondal, M. Tanaka, S.-I. Nozoe, H. Hosoda, K. Kangawa and S. Matsukura, *J. Clin. Endocrinol. Metab.*, 2002, **87**, 240–244.

180 I. Salarić, I. Karmelić, J. Lovrić, K. Baždarić, M. Rožman, I. Čvrlejvić, I. Zajc, D. Brajdić and D. Macan, *Sci. Rep.*, 2021, **11**, 13201.

181 D. J. Kennaway, *J. Pineal Res.*, 2019, **67**, e12572.

182 A. W. Hsing, T. E. Meyer, S. Niwa, S. M. Quraishi and L. W. Chu, *Cancer Epidemiol. Biomarkers Prev.*, 2010, **19**, 932–937.

183 M. J. Nunes, J. J. G. Moura, J. P. Noronha, L. C. Branco, A. Samhan-Arias, J. P. Sousa, C. Rouco and C. M. Cordas, *Analytica*, 2022, **3**, 178–194.

184 M. S. Karbownik and S. D. Hicks, *Front. Psychiatry*, 2022, **13**, 788153.

185 N. M. Kushnir-Sukhov, E. Brittain, L. Scott and D. D. Metcalfe, *Eur. J. Clin. Invest.*, 2008, **38**, 953–958.

186 Serotonin | University Hospitals, <https://www.uhhospitals.org/health-information/health-and-wellness-library/article/lab-tests-v1/serotonin>, (accessed June 30, 2025).

187 G. R. Van Loon, *Fed. Proc.*, 1983, **42**, 3012–3018.

188 X. Zeng, Y. Zhang, X. Li, C. Wang, X. Xia, C. Jin, D. Huo and C. Hou, *Anal. Chem.*, 2025, **97**, 12090–12099.

189 D. Tomassoni, E. Traini, M. Mancini, V. Bramanti, S. S. Mahdi and F. Amenta, *Am. J. Physiol.*, 2015, **309**, R585–R593.

190 N. Blohm, *Theses Diss. Proj.*, Smith College, 2017.

191 M. R. Keerthanaa, L. R. Panicker, R. Narayan and Y. G. Kotagiri, *RSC Adv.*, 2024, **14**, 7131–7141.

192 Y. Ding, K. Tan, S. Zhang, S. Wang, X. Zhang and P. Hu, *Chem. Eng. J.*, 2023, **477**, 146844.

193 H. J. Hurley and J. A. Witkowski, *J. Appl. Physiol.*, 1961, **16**, 652–654.

194 K. O. Schwab, G. Heubel and H. Bartels, *Eur. J. Clin. Chem. Clin. Biochem.*, 1992, **30**, 541–544.

195 B. Kennedy, E. Dillon, P. J. Mills and M. G. Ziegler, *Life Sci.*, 2001, **69**, 87–99.

196 O. Rachid, M. M. Rawas-Qalaji, F. E. R. Simons and K. J. Simons, *J. Allergy Clin. Immunol.*, 2013, **131**, 236–238.

197 Catecholamine blood test Information | Mount Sinai - New York, <https://www.mountsinai.org/health-library/tests/catecholamine-blood-test>, (accessed June 30, 2025).

198 L. Wang, L. Pan, X. Han, M. N. Ha, K. Li, H. Yu, Q. Zhang, Y. Li, C. Hou and H. Wang, *J. Colloid Interface Sci.*, 2022, **616**, 326–337.

199 J. Zhao, H. Y. Y. Nyein, L. Hou, Y. Lin, M. Bariya, C. H. Ahn, W. Ji, Z. Fan and A. Javey, *Adv. Mater.*, 2021, **33**, 2006444.

200 E. Mäkilä and P. Kirveskari, *Arch. Oral Biol.*, 1969, **14**, 1285–1292.

201 L. W. Evans and S. T. Omaye, *Antioxidants*, 2017, **6**, 5.

202 A. F. Hagel, H. Albrecht, W. Dauth, W. Hagel, F. Vitali, I. Ganzleben, H. W. Schultis, P. C. Konturek, J. Stein, M. F. Neurath and M. Raithel, *J. Int. Med. Res.*, 2018, **46**, 168–174.



203 Q. Chen, M. G. Espey, A. Y. Sun, J.-H. Lee, M. C. Krishna, E. Shacter, P. L. Choyke, C. Pooput, K. L. Kirk, G. R. Buettner and M. Levine, *Proc. Natl. Acad. Sci. U. S. A.*, 2007, **104**, 8749–8754.

204 Folic acid - test Information | Mount Sinai - New York, <https://www.mountsinai.org/health-library/tests/folic-acid-test>, (accessed June 30, 2025).

205 E. Mäkilä, *Arch. Oral Biol.*, 1966, **11**, 839–844.

206 B. C. Johnson, T. S. Hamilton and H. H. Mitchell, *J. Biol. Chem.*, 1945, **159**, 425–429.

207 TSH test, <https://medlineplus.gov/ency/article/003684.htm>, (accessed June 30, 2025).

208 N. Brasier, C. Niederberger and G. A. Salvatore, *Soft Sci.*, 2024, **4**, 6.

209 N. Sawicka-Gutaj, P. Glinicki, K. Nijakowski, B. Bromińska, M. Ostrowska, A. Szatko, Z. Sobol, K. Kowalski, P. Wilk, W. Zgliczyński and M. Ruchala, in *Endocrine Abstracts*, Bioscientifica, 2023, p. 90.

210 F. M. Matschinsky and D. F. Wilson, *Front. Physiol.*, 2019, **10**, DOI: [10.3389/fphys.2019.00148](https://doi.org/10.3389/fphys.2019.00148).

211 M. N. Nakrani, R. H. Wineland and F. Anjum, in *StatPearls*, StatPearls Publishing, Treasure Island (FL), 2025.

212 P. Wu, T. Zhu, Y. Huang, Z. Fang and F. Luo, *Front. Endocrinol.*, 2023, **14**, 1205442.

213 X. Li, Y. Yang, B. Zhang, X. Lin, X. Fu, Y. An, Y. Zou, J. Wang, Z. Wang and T. Yu, *Signal Transduction Targeted Ther.*, 2022, **7**, 305.

214 P. Strazzullo and C. Leclercq, *Adv. Nutr.*, 2014, **5**, 188–190.

215 A. J. Viera and N. Wouk, *Am. Fam. Physician*, 2015, **92**, 487–495.

216 T. J. Jentsch, V. Stein, F. Weinreich and A. A. Zdebik, *Physiol. Rev.*, 2002, **82**, 503–568.

217 R. El Ridi and H. Tallima, *J. Adv. Res.*, 2017, **8**, 487–493.

218 A. Breedveld and M. van Egmond, *Front. Immunol.*, 2019, **10**, 553.

219 B. Tota, T. Angelone and M. C. Cerra, *Front. Chem.*, 2014, **14**(2), 64.

220 M. A. D'amico, B. Ghinassi, P. Izzicupo, L. Manzoli and A. Di Baldassarre, *Endocr. Connect.*, 2014, **3**, R45–R54.

221 L. Colucci-D'Amato, L. Speranza and F. Volpicelli, *Int. J. Mol. Sci.*, 2020, **21**, 7777.

222 S.-H. Dou, Y. Cui, S.-M. Huang and B. Zhang, *Front. Hum. Neurosci.*, 2022, **16**, 1–11.

223 V. Gounden, R. Vashisht and I. Jialal, in *StatPearls*, StatPearls Publishing, Treasure Island (FL), 2025.

224 Calcium disorders | Medical Council of Canada, <https://mcc.ca/objectives/medical-expert/calcium-disorders/>, (accessed February 24, 2025).

225 Magnesium in diet, <https://medlineplus.gov/ency/article/002423.htm>, (accessed February 24, 2025).

226 R. Swaminathan, *Clin. Biochem. Rev.*, 2003, **24**, 47–66.

227 A. Hussain, W. Jiang, X. Wang, S. Shahid, N. Saba, M. Ahmad, A. Dar, S. U. Masood, M. Imran and A. Mustafa, *Front. Nutr.*, 2022, **9**, 717064.

228 M. Maywald and L. Rink, *Biomolecules*, 2022, **12**, 1748.

229 J. Gale and E. Aizenman, *Eur. J. Neurosci.*, 2024, **60**, 3505–3543.

230 K. Alka and J. R. Casey, *IUBMB Life*, 2014, **66**, 596–615.

231 C. A. Wagner, *Nephrol., Dial., Transplant.*, 2024, **39**, 190–201.

232 I. Portales-Castillo, T. Rieg, S. B. Khalid, S. U. Nigwekar and J. A. Neyra, *Adv. Kidney Dis. Health*, 2023, **30**, 177–188.

233 Z.-N. Ling, Y.-F. Jiang, J.-N. Ru, J.-H. Lu, B. Ding and J. Wu, *Signal Transduction Targeted Ther.*, 2023, **8**, 1–32.

234 O. I. Adeyomoye, C. O. Akintayo, K. P. Omotuyi and A. N. Adewumi, *Indian J. Nephrol.*, 2022, **32**, 539–545.

235 T. Huff, B. Boyd and I. Jialal, in *StatPearls*, StatPearls Publishing, Treasure Island (FL), 2025.

236 B. J. Delgado and W. Lopez-Ojeda, in *StatPearls*, StatPearls Publishing, Treasure Island (FL), 2025.

237 P. M. Wise, S. Suzuki and C. M. Brown, *Dialogues Clin. Neurosci.*, 2009, **11**, 297–303.

238 J. A. MacLean and K. Hayashi, *Cells*, 2022, **11**, 647.

239 T. W. Du Clos, *Ann. Med.*, 2000, **32**, 274–278.

240 Y. Luan and Y. Yao, *Front. Immunol.*, 2018, **7**(9), 1302.

241 E. Grebenciucova and S. VanHaerents, *Front. Immunol.*, 2023, **4**, 1255533.

242 K. You, H. Gu, Z. Yuan and X. Xu, *Front. Cell Dev. Biol.*, 2021, **9**, 8–13.

243 D. Jang, A.-H. Lee, H.-Y. Shin, H.-R. Song, J.-H. Park, T.-B. Kang, S.-R. Lee and S.-H. Yang, *Int. J. Mol. Sci.*, 2021, **22**, 2719.

244 R. Maurya, P. Bhattacharya, R. Dey and H. L. Nakhasi, *Front. Immunol.*, 2018, **9**, 2741.

245 R. Hardeland, *Sci. World J.*, 2012, **2012**, 640389.

246 A. Mishra, S. Singh and S. Shukla, *J. Exp. Neurosci.*, 2018, **12**, 1179069518779829.

247 L. Fiore, V. Mazzaracchio, A. Serani, G. Fabiani, L. Fabiani, G. Volpe, D. Moscone, G. M. Bianco, C. Occhiuzzi, G. Marrocco and F. Arduini, *Sens. Actuators, B*, 2023, **379**, 133258.

248 A. K. Yetisen, M. S. Akram and C. R. Lowe, *Lab Chip*, 2013, **13**, 2210.

249 J. Liu, X. Kong, H. Wang, Y. Zhang and Y. Fan, *Microfluid. Nanofluid.*, 2020, **24**, 6.

250 S. Nishat, A. T. Jafry, A. W. Martinez and F. R. Awan, *Sens. Actuators, B*, 2021, **336**, 129681.

251 A.-G. Niculescu, C. Chircov, A. C. Bîrcă and A. M. Grumezescu, *Int. J. Mol. Sci.*, 2021, **22**, 2011.

252 U. Mogera, H. Guo, M. Namkoong, M. S. Rahman, T. Nguyen and L. Tian, *Sci. Adv.*, 2022, **8**, eabn1736.

253 *Microfluidics and Bio-MEMS: devices and applications*, ed. T. S. Santra, Jenny Stanford Publishing, Singapore, 2021.

254 A. N. Nordin and A. Abd Manaf, in *Microfluidic Biosensors*, Elsevier, 2023, pp. 41–85.

255 L. DeFrancesco and I. Jarchum, *Nat. Biotechnol.*, 2019, **37**, 329–329.

256 J. C. Yeo, K. Kenry and C. T. Lim, *Lab Chip*, 2016, **16**, 4082–4090.

257 G. Chen, J. Zheng, L. Liu and L. Xu, *Small Methods*, 2019, **3**, 1900688.

258 L. Meng, I. Jeerapan and W. C. Mak, in *Microfluidic Biosensors*, Elsevier, 2023, pp. 107–157.



259 C. B. Goy, R. E. Chaile and R. E. Madrid, *React. Funct. Polym.*, 2019, **145**, 104314.

260 L. Gervais and E. Delamarche, *Lab Chip*, 2009, **9**, 3330.

261 C. W. Bae, P. T. Toi, B. Y. Kim, W. I. Lee, H. B. Lee, A. Hanif, E. H. Lee and N.-E. Lee, *ACS Appl. Mater. Interfaces*, 2019, **11**, 14567–14575.

262 S. Jo, D. Sung, S. Kim and J. Koo, *Biomed. Eng. Lett.*, 2021, **11**, 117–129.

263 M. Sekar, R. Sriramprabha, P. K. Sekhar, S. Bhansali, N. Ponpandian, M. Pandiaraj and C. Viswanathan, *J. Electrochem. Soc.*, 2020, **167**, 067508.

264 J. G. Turner, L. R. White, P. Estrela and H. S. Leese, *Macromol. Biosci.*, 2021, **21**, 2000307.

265 X. Zhang, L. Li and C. Luo, *Lab Chip*, 2016, **16**, 1757–1776.

266 T. Shay, M. D. Dickey and O. D. Velev, *Lab Chip*, 2017, **17**, 710–716.

267 Y. K. Jung, J. Kim and R. A. Mathies, *Biosens. Bioelectron.*, 2016, **79**, 371–378.

268 T. Biswal, S. K. Badjena and D. Pradhan, *Mater. Today: Proc.*, 2020, **30**, 305–315.

269 K. Markandan and C. Q. Lai, *Composites, Part B*, 2023, **256**, 110661.

270 Y. Fu, J. Dai, Y. Ge, Y. Zhang, H. Ke and W. Zhang, *Molecules*, 2018, **23**, 2552.

271 S. Peng, Y. Yu, S. Wu and C.-H. Wang, *ACS Appl. Mater. Interfaces*, 2021, **13**, 43831–43854.

272 Md. A. Ali, S. Srivastava, P. R. Solanki, V. Reddy, V. V. Agrawal, C. Kim, R. John and B. D. Malhotra, *Sci. Rep.*, 2013, **3**, 2661.

273 H. Tavakoli, S. Mohammadi, X. Li, G. Fu and X. Li, *TrAC, Trends Anal. Chem.*, 2022, **157**, 116806.

274 S. Wang, X. Zhang, C. Ma, S. Yan, D. Inglis and S. Feng, *Biosensors*, 2021, **11**, 405.

275 Y. Yu, L. Shang, J. Guo, J. Wang and Y. Zhao, *Nat. Protoc.*, 2018, **13**, 2557–2579.

276 C. Nie, A. Frijns, M. Zevenbergen and J. D. Toonder, *Sens. Actuators, B*, 2016, **227**, 427–437.

277 M. Rovira, C. Fernández-Sánchez and C. Jiménez-Jorquera, *Biosensors*, 2021, **11**, 303.

278 M. Naeimirad, R. Abuzade, V. Babaahmadi and F. Dabirian, *Mater. Des. Process. Commun.*, 2019, **1**, e78.

279 C. Zhang, Y. Su, Y. Liang and W. Lai, *Biosens. Bioelectron.*, 2020, **168**, 112391.

280 M. S. Maria, P. E. Rakesh, T. S. Chandra and A. K. Sen, *Sci. Rep.*, 2017, **7**, 43457.

281 Z. He, X. Yang, N. Wang, L. Mu, J. Pan, X. Lan, H. Li and F. Deng, *Front. Bioeng. Biotechnol.*, 2021, **9**, 807357.

282 C. Chen, P. Duru, P. Joseph, S. Geoffroy and M. Prat, *Sci. Rep.*, 2017, **7**, 15110.

283 M. I. Mohammed, E. Abraham and M. P. Y. Desmulliez, *J. Micromech. Microeng.*, 2013, **23**, 035034.

284 A. Sena-Torralba, M. Parrilla, A. Hernanz-Grimalt, A. Steijlen, E. Ortiz-Zapater, C. Cabaleiro-Otero, N. López-Riquelme, S. Cerveró-Ferragut, Á. Maquieira, K. De Wael and S. Morais, *Anal. Chem.*, 2024, **96**, 20684–20692.

285 M. Parrilla, A. Steijlen, R. Kerremans, J. Jacobs, L. den Haan, J. De Vreese, Y. Van Noten Géron, P. Clerx, R. Watts and K. De Wael, *Chem. Eng. J.*, 2024, **500**, 157254.

286 A. O. Olanrewaju, A. Robillard, M. Dagher and D. Juncker, *Lab Chip*, 2016, **16**, 3804–3814.

287 A. O. Olanrewaju, A. Ng, P. DeCorwin-Martin, A. Robillard and D. Juncker, *Anal. Chem.*, 2017, **89**, 6846–6853.

288 H. Zhang, Y. Qiu, S. Yu, C. Ding, J. Hu, H. Qi, Y. Tian, Z. Zhang, A. Liu and H. Wu, *Biomicrofluidics*, 2022, **16**, 044104.

289 A. S. M. Steijlen, J. Bastemeijer, P. Groen, K. M. B. Jansen, P. J. French and A. Bossche, *Anal. Methods*, 2020, **12**, 5885–5892.

290 N. Uemura, R. P. Nath, M. R. Harkey, G. L. Henderson, J. Mendelson and R. T. Jones, *J. Anal. Toxicol.*, 2004, **28**, 253–259.

291 I. PharmChem, The Comprehensive Guide to Sweat Patches, <https://www.pharmchek.com/resources/blog/the-comprehensive-guide-to-sweat-patches-how-the-patch-works-and-how-to-use-it>, (accessed March 25, 2025).

292 H. Shi, Y. Cao, Y. Zeng, Y. Zhou, W. Wen, C. Zhang, Y. Zhao and Z. Chen, *Talanta*, 2022, **240**, 123208.

293 C. A. Porucznik, K. J. Cox, D. G. Wilkins, D. J. Anderson, N. M. Bailey, K. M. Szczotka and J. B. Stanford, *J. Anal. Toxicol.*, 2015, **39**, 562–566.

294 A. R. Naik, B. Warren, A. Burns, R. Lenigk, J. Morse, A. Alizadeh and J. J. Watkins, *Microfluid. Nanofluid.*, 2021, **25**, 2.

295 A. S. M. Steijlen, K. M. B. Jansen, J. Bastemeijer, P. J. French and A. Bossche, *Anal. Chem.*, 2022, **94**, 6893–6901.

296 J. Pieczyński, U. Szulc, J. Harazna, A. Szulc and J. Kiewisz, *Eur. J. Ophthalmol.*, 2021, **31**, 2245–2251.

297 A. Posa, L. Bräuer, M. Schicht, F. Garreis, S. Beileke and F. Paulsen, *Ann. Anat.*, 2013, **195**, 137–142.

298 A. K. Yetisen, B. Soylemezoglu, J. Dong, Y. Montelongo, H. Butt, M. Jakobi and A. W. Koch, *RSC Adv.*, 2019, **9**, 11186–11193.

299 E. Lindner, D. Bordelon, M. D. Kim, S. A. Dergunov, E. Pinkhassik and E. Chaum, *Electroanalysis*, 2012, **24**, 42–52.

300 E. Ponzini, C. Santambrogio, A. De Palma, P. Mauri, S. Tavazzi and R. Grandori, *Mass Spectrom. Rev.*, 2022, **41**, 842–860.

301 A. Barmada and S. A. Shippy, *Anal. Bioanal. Chem.*, 2019, **411**, 329–338.

302 B.-H. Kang, M. Park and K.-H. Jeong, *BioChip J.*, 2017, **11**, 294–299.

303 F. Bachhuber, A. Huss, M. Senel and H. Tumani, *Sci. Rep.*, 2021, **11**, 10064.

304 E. V. Mukerjee, S. D. Collins, R. R. Isseroff and R. L. Smith, *Sens. Actuators, A*, 2004, **114**, 267–275.

305 D. D. Zhu, L. W. Zheng, P. K. Duong, R. H. Cheah, X. Y. Liu, J. R. Wong, W. J. Wang, S. T. Tien Guan, X. T. Zheng and P. Chen, *Biosens. Bioelectron.*, 2022, **212**, 114412.

306 K. M. Saifullah and Z. Faraji Rad, *Adv. Mater. Interfaces*, 2023, **10**, 2201763.



307 D. J. O'Brien, D. Mills, J. Farina and M. Paranjape, *IEEE Trans. Biomed. Eng.*, 2023, **70**, 2573–2580.

308 K. Takeuchi, N. Takama, K. Sharma, O. Paul, P. Ruther, T. Suga and B. Kim, *Drug Delivery Transl. Res.*, 2022, **12**, 435–443.

309 X. Jiang and P. B. Lillehoj, *Microsyst. Nanoeng.*, 2020, **6**, 96.

310 T. A. Hakala, A. García Pérez, M. Wardale, I. A. Ruuth, R. T. Vänskä, T. A. Nurminen, E. Kemp, Z. A. Boeva, J.-M. Alakoskela, K. Pettersson-Fernholm, E. Hæggström and J. Bobacka, *Sci. Rep.*, 2021, **11**, 7609.

311 R. Raman, E. B. Rousseau, M. Wade, A. Tong, M. J. Cotler, J. Kuang, A. A. Lugo, E. Zhang, A. M. Graybiel, F. M. White, R. Langer and M. J. Cima, *Sci. Adv.*, 2020, **6**, eabb0657.

312 M. Akkurt Arslan, G. Rabut, S. Chardonnet, C. Pionneau, A. Kobal, M. Gratas Pelletier, N. Harfouche, A. Réaux La Goazigo, C. Baudouin, F. Brignole-Baudouin and K. Kessal, *Exp. Eye Res.*, 2023, **237**, 109679.

313 H. Y. Y. Nyein, L.-C. Tai, Q. P. Ngo, M. Chao, G. B. Zhang, W. Gao, M. Bariya, J. Bullock, H. Kim, H. M. Fahad and A. Javey, *ACS Sens.*, 2018, **3**, 944–952.

314 Q. Zeng, M. Xu, W. Hu, W. Cao, Y. Zhan, Y. Zhang, Q. Wang and T. Ma, *Biosensors*, 2023, **13**, 537.

315 Y. Qiao, J. Du, R. Ge, H. Lu, C. Wu, J. Li, S. Yang, S. Zada, H. Dong and X. Zhang, *Anal. Chem.*, 2022, **94**, 5538–5545.

316 A. He, X. Wang, L. Zhang, H. Zhang, X. Xu, C. Yu, Y. Ma, W. Wei and P. Niu, *Nanotechnol. Precis. Eng.*, 2024, **8**, 013006.

317 L. B. Baker, J. B. Model, K. A. Barnes, M. L. Anderson, S. P. Lee, K. A. Lee, S. D. Brown, A. J. Reimel, T. J. Roberts, R. P. Nuccio, J. L. Bonsignore, C. T. Ungaro, J. M. Carter, W. Li, M. S. Seib, J. T. Reeder, A. J. Aranyosi, J. A. Rogers and R. Ghaffari, *Sci. Adv.*, 2020, **6**, eabe3929.

318 T. Kim, Q. Yi, E. Hoang and R. Esfandyarpour, *Adv. Mater. Technol.*, 2021, **6**, 2001021.

319 P. Pirovano, M. Dorrian, A. Shinde, A. Donohoe, A. J. Brady, N. M. Moyna, G. Wallace, D. Diamond and M. McCaul, *Talanta*, 2020, **219**, 121145.

320 X. Mei, J. Yang, X. Yu, Z. Peng, G. Zhang and Y. Li, *Sens. Actuators, B*, 2023, **381**, 133451.

321 J. Kim, Y. Wu, H. Luan, D. S. Yang, D. Cho, S. S. Kwak, S. Liu, H. Ryu, R. Ghaffari and J. A. Rogers, *Adv. Sci.*, 2022, **9**, 2103331.

322 S. Liu, D. S. Yang, S. Wang, H. Luan, Y. Sekine, J. B. Model, A. J. Aranyosi, R. Ghaffari and J. A. Rogers, *EcoMat*, 2023, **5**, e12270.

323 D. S. Yang, Y. Wu, E. E. Kanatzidis, R. Avila, M. Zhou, Y. Bai, S. Chen, Y. Sekine, J. Kim, Y. Deng, H. Guo, Y. Zhang, R. Ghaffari, Y. Huang and J. A. Rogers, *Mater. Horiz.*, 2023, **10**, 4992–5003.

324 Y. Wu, X. Li, K. E. Madsen, H. Zhang, S. Cho, R. Song, R. F. Nuxoll, Y. Xiong, J. Liu, J. Feng, T. Yang, K. Zhang, A. J. Aranyosi, D. E. Wright, R. Ghaffari, Y. Huang, R. G. Nuzzo and J. A. Rogers, *Lab Chip*, 2024, **24**, 4288–4295.

325 A. Martín, J. Kim, J. F. Kurniawan, J. R. Sempionatto, J. R. Moreto, G. Tang, A. S. Campbell, A. Shin, M. Y. Lee, X. Liu and J. Wang, *ACS Sens.*, 2017, **2**, 1860–1868.

326 M. Parrilla, I. Ortiz-Gómez, R. Cánovas, A. Salinas-Castillo, M. Cuartero and G. A. Crespo, *Anal. Chem.*, 2019, **91**, 8644–8651.

327 S. B. Kim, J. Koo, J. Yoon, A. Hourlier-Fargette, B. Lee, S. Chen, S. Jo, J. Choi, Y. S. Oh, G. Lee, S. M. Won, A. J. Aranyosi, S. P. Lee, J. B. Model, P. V. Braun, R. Ghaffari, C. Park and J. A. Rogers, *Lab Chip*, 2020, **20**, 84–92.

328 A. R. Naik, Y. Zhou, A. A. Dey, D. L. G. Arellano, U. Okoroanyanwu, E. B. Secor, M. C. Hersam, J. Morse, J. P. Rothstein, K. R. Carter and J. J. Watkins, *Lab Chip*, 2022, **22**, 156–169.

329 J. Kim, I. Jeerapan, S. Imani, T. N. Cho, A. Bandodkar, S. Cinti, P. P. Mercier and J. Wang, *ACS Sens.*, 2016, **1**, 1011–1019.

330 J. Kim, G. Valdés-Ramírez, A. J. Bandodkar, W. Jia, A. G. Martinez, J. Ramírez, P. Mercier and J. Wang, *Analyst*, 2014, **139**, 1632–1636.

331 J. Kim, S. Imani, W. R. De Araujo, J. Warchall, G. Valdés-Ramírez, T. R. L. C. Paixão, P. P. Mercier and J. Wang, *Biosens. Bioelectron.*, 2015, **74**, 1061–1068.

332 T. Arakawa, Y. Kuroki, H. Nitta, P. Chouhan, K. Toma, S. Sawada, S. Takeuchi, T. Sekita, K. Akiyoshi, S. Minakuchi and K. Mitsubayashi, *Biosens. Bioelectron.*, 2016, **84**, 106–111.

333 T. Arakawa, K. Tomoto, H. Nitta, K. Toma, S. Takeuchi, T. Sekita, S. Minakuchi and K. Mitsubayashi, *Anal. Chem.*, 2020, **92**, 12201–12207.

334 R. Moreddu, J. S. Wolffsohn, D. Vigolo and A. K. Yetisen, *Sens. Actuators, B*, 2020, **317**, 128183.

335 Z. Li, J. Yun, X. Li, M. Kim, J. Li, D. Lee, A. Wu and S. W. Lee, *Adv. Funct. Mater.*, 2023, **33**, 2304647.

336 J. Park, J. Kim, S.-Y. Kim, W. H. Cheong, J. Jang, Y.-G. Park, K. Na, Y.-T. Kim, J. H. Heo, C. Y. Lee, J. H. Lee, F. Bien and J.-U. Park, *Sci. Adv.*, 2018, **4**, eaap9841.

337 D. Hee, J. Won, B. Ho, K. Jae, S. Hyun and S. Kwang, *Sci. Adv.*, 2020, **6**(17), eaba3252.

338 M. Ku, J. Kim, J.-E. Won, W. Kang, Y.-G. Park, J. Park, J.-H. Lee, J. Cheon, H. H. Lee and J.-U. Park, *Sci. Adv.*, 2020, **6**, eabb2891.

339 E. De La Paz, T. Saha, R. Del Caño, S. Seker, N. Kshirsagar and J. Wang, *Talanta*, 2023, **254**, 124122.

340 K. Y. Goud, K. Mahato, H. Teymourian, K. Longardner, I. Litvan and J. Wang, *Sens. Actuators, B*, 2022, **354**, 131234.

341 M. Dervisevic, E. Dervisevic, L. Esser, C. D. Easton, V. J. Cadarso and N. H. Voelcker, *Biosens. Bioelectron.*, 2023, **222**, 114955.

342 B. Yang, X. Fang and J. Kong, *Adv. Funct. Mater.*, 2020, **30**, 2000591.

343 J. Kim, J. R. Sempionatto, S. Imani, M. C. Hartel, A. Barfidokht, G. Tang, A. S. Campbell, P. P. Mercier and J. Wang, *Adv. Sci.*, 2018, **5**, 1800880.

344 M. Razzaghi, A. Seyfoori, E. Pagan, E. Askari, A. Hassani Najafabadi and M. Akbari, *Polymers*, 2023, **15**, 1389.

345 B. Yang, J. Kong and X. Fang, *Nat. Commun.*, 2022, **13**, 3999.



346 J. R. Sempionatto, M. Lin, L. Yin, E. De La Paz, K. Pei, T. Sonsa-ard, A. N. De Loyola Silva, A. A. Khorshed, F. Zhang, N. Tostado, S. Xu and J. Wang, *Nat. Biomed. Eng.*, 2021, **5**, 737–748.

347 F. Tehrani, H. Teymourian, B. Wuerstle, J. Kavner, R. Patel, A. Furmidge, R. Aghavali, H. Hosseini-Toudeshki, C. Brown, F. Zhang, K. Mahato, Z. Li, A. Barfidokht, L. Yin, P. Warren, N. Huang, Z. Patel, P. P. Mercier and J. Wang, *Nat. Biomed. Eng.*, 2022, **6**, 1214–1224.

348 X. Weng, Z. Fu, C. Zhang, W. Jiang and H. Jiang, *Anal. Chem.*, 2022, **94**, 3526–3534.

349 A. Panneer Selvam, S. Muthukumar, V. Kamakoti and S. Prasad, *Sci. Rep.*, 2016, **6**, 23111.

350 A. Alizadeh, A. Burns, R. Lenigk, R. Gettings, J. Ashe, A. Porter, M. McCaul, R. Barrett, D. Diamond, P. White, P. Skeath and M. Tomeczak, *Lab Chip*, 2018, **18**, 2632–2641.

351 Y. Cheng, S. Feng, Q. Ning, T. Li, H. Xu, Q. Sun, D. Cui and K. Wang, *Microsyst. Nanoeng.*, 2023, **9**, 36.

352 A. Wiorek, M. Parrilla, M. Cuartero and G. A. Crespo, *Anal. Chem.*, 2020, **92**, 10153–10161.

353 M. Bariya, L. Li, R. Ghattamaneni, C. H. Ahn, H. Y. Y. Nyein, L.-C. Tai and A. Javey, *Sci. Adv.*, 2020, **6**, eabb8308.

354 W. He, C. Wang, H. Wang, M. Jian, W. Lu, X. Liang, X. Zhang, F. Yang and Y. Zhang, *Sci. Adv.*, 2019, **5**, eaax0649.

355 D.-H. Choi, G. B. Kitchen, M. T. Jennings, G. R. Cutting and P. C. Searson, *npj Digit. Med.*, 2020, **3**, 49.

356 T. Terse-Thakoor, M. Punjiya, Z. Matharu, B. Lyu, M. Ahmad, G. E. Giles, R. Owyitung, F. Alaimo, M. Shojaei Baghini, T. T. Brunyé and S. Sonkusale, *npj Flexible Electron.*, 2020, **4**, 18.

357 J. T. Reeder, J. Choi, Y. Xue, P. Gutruf, J. Hanson, M. Liu, T. Ray, A. J. Bandodkar, R. Avila, W. Xia, S. Krishnan, S. Xu, K. Barnes, M. Pahnke, R. Ghaffari, Y. Huang and J. A. Rogers, *Sci. Adv.*, 2019, **5**, eaau6356.

358 B. Wang, C. Zhao, Z. Wang, K.-A. Yang, X. Cheng, W. Liu, W. Yu, S. Lin, Y. Zhao, K. M. Cheung, H. Lin, H. Hojaiji, P. S. Weiss, M. N. Stojanović, A. J. Tomiyama, A. M. Andrews and S. Emaminejad, *Sci. Adv.*, 2022, **8**, eabk0967.

359 I. Shitanda, N. Muramatsu, R. Kimura, N. Takahashi, K. Watanabe, H. Matsui, N. Loew, M. Motosuke, T. Mukaimoto, M. Kobayashi, T. Mitsuhashi, Y. Sugita, K. Matsuo, S. Yanagita, T. Suzuki, H. Watanabe and M. Itagaki, *ACS Sens.*, 2023, **8**, 2889–2895.

360 D. Liu, Z. Liu, S. Feng, Z. Gao, R. Chen, G. Cai and S. Bian, *Biosensors*, 2023, **13**, 157.

361 E. Scarpa, V. M. Mastronardi, F. Guido, L. Algieri, A. Qualtieri, R. Fiammengo, F. Rizzi and M. De Vittorio, *Sci. Rep.*, 2020, **10**, 10854.

362 G. Bolat, E. De La Paz, N. F. Azeredo, M. Kartolo, J. Kim, A. N. De Loyola, E. Silva, R. Rueda, C. Brown, L. Angnes, J. Wang and J. R. Sempionatto, *Anal. Bioanal. Chem.*, 2022, **414**, 5411–5421.

363 Y. Zheng, R. Omar, R. Zhang, N. Tang, M. Khatib, Q. Xu, Y. Milyutin, W. Saliba, Y. Y. Broza, W. Wu, M. Yuan and H. Haick, *Adv. Mater.*, 2022, **34**, 2108607.

364 S. Sharma, H. Byrne and R. J. O'Kennedy, *Essays Biochem.*, 2016, **60**, 9–18.

365 Y. Wu, F. Tehrani, H. Teymourian, J. Mack, A. Shaver, M. Reynoso, J. Kavner, N. Huang, A. Furmidge, A. Duvvuri, Y. Nie, L. M. Laffel, F. J. Doyle, M.-E. Patti, E. Dassau, J. Wang and N. Arroyo-Currás, *Anal. Chem.*, 2022, **94**, 8335–8345.

366 N. K. Singh, S. Chung, A.-Y. Chang, J. Wang and D. A. Hall, *Biosens. Bioelectron.*, 2023, **227**, 115097.

367 S. Mross, S. Pierrat, T. Zimmermann and M. Kraft, *Biosens. Bioelectron.*, 2015, **70**, 376–391.

368 K. Sadani, P. Nag, X. Y. Thian and S. Mukherji, *Biosens. Bioelectron.: X*, 2022, **12**, 100278.

369 T. Saha, J. Fang, S. Mukherjee, M. D. Dickey and O. D. Velev, *ACS Appl. Mater. Interfaces*, 2021, **13**, 8071–8081.

370 A. M. Nightingale, C. L. Leong, R. A. Burnish, S. Hassan, Y. Zhang, G. F. Clough, M. G. Boutelle, D. Voegeli and X. Niu, *Nat. Commun.*, 2019, **10**, 2741.

371 H. Zhao, X. Zhang, Y. Qin, Y. Xia, X. Xu, X. Sun, D. Yu, S. M. Mugo, D. Wang and Q. Zhang, *Adv. Funct. Mater.*, 2023, **33**, 2212083.

372 M. Dautta, L. Fernando Ayala-Cardona, N. Davis, A. Aggarwal, J. Park, S. Wang, L. Gillan, E. Jansson, M. Hietala, H. Ko, J. Hiltunen and A. Javey, *Adv. Mater. Technol.*, 2023, **8**(6), 2201187.

373 Q.-F. Li, X. Chen, H. Wang, M. Liu and H.-L. Peng, *ACS Appl. Mater. Interfaces*, 2023, **15**, 13290–13298.

374 Y. Hashimoto, T. Ishihara, K. Kuwabara, T. Amano and H. Togo, *Micromachines*, 2022, **13**, 575.

375 M. Dautta, L. F. Ayala-Cardona, N. Davis, A. Aggarwal, J. Park, S. Wang, L. Gillan, E. Jansson, M. Hietala, H. Ko, J. Hiltunen and A. Javey, *Adv. Mater. Technol.*, 2023, **8**, 2201187.

376 H. Y. Y. Nyein, M. Bariya, B. Tran, C. H. Ahn, B. J. Brown, W. Ji, N. Davis and A. Javey, *Nat. Commun.*, 2021, **12**, 1823.

377 M. A. Zahed, D. K. Kim, S. H. Jeong, M. Selim Reza, M. Sharifuzzaman, G. B. Pradhan, H. Song, M. Asaduzzaman and J. Y. Park, *ACS Sens.*, 2023, **8**, 2960–2974.

378 R. Badugu, E. A. Reece and J. R. Lakowicz, *J. Biomed. Opt.*, 2018, **23**, 1.

379 A. Barmada and S. A. Shippy, *Eye*, 2020, **34**, 1731–1733.

380 J. Zhang, K. Kim, H. J. Kim, D. Meyer, W. Park, S. A. Lee, Y. Dai, B. Kim, H. Moon, J. V. Shah, K. E. Harris, B. Collar, K. Liu, P. Irazoqui, H. Lee, S. A. Park, P. S. Kollbaum, B. W. Boudouris and C. H. Lee, *Nat. Commun.*, 2022, **13**, 5518.

381 H. Lee, T. K. Choi, Y. B. Lee, H. R. Cho, R. Ghaffari, L. Wang, H. J. Choi, T. D. Chung, N. Lu, T. Hyeon, S. H. Choi and D.-H. Kim, *Nat. Nanotechnol.*, 2016, **11**, 566–572.

382 Y. Liu, Q. Yu, X. Luo, L. Yang and Y. Cui, *Microsyst. Nanoeng.*, 2021, **7**, 75.

383 L. Bao, J. Park, B. Qin and B. Kim, *Sci. Rep.*, 2022, **12**, 10693.

384 T. Chang, H. Li, N. Zhang, X. Jiang, X. Yu, Q. Yang, Z. Jin, H. Meng and L. Chang, *Microsyst. Nanoeng.*, 2022, **8**, 25.

385 M. Parrilla, U. Detamornrat, J. Domínguez-Robles, S. Tunca, R. F. Donnelly and K. De Wael, *ACS Sens.*, 2023, **8**, 4161–4170.



386 X. Luo, Q. Yu, L. Yang and Y. Cui, *ACS Sens.*, 2023, **8**, 1710–1722.

387 S. Kim, S. Park, J. Choi, W. Hwang, S. Kim, I.-S. Choi, H. Yi and R. Kwak, *Nat. Commun.*, 2022, **13**, 6705.

388 Y. Xu, E. De La Paz, A. Paul, K. Mahato, J. R. Sempionatto, N. Tostado, M. Lee, G. Hota, M. Lin, A. Uppal, W. Chen, S. Dua, L. Yin, B. L. Wuerstle, S. Deiss, P. Mercier, S. Xu, J. Wang and G. Cauwenberghs, *Nat. Biomed. Eng.*, 2023, **7**, 1307–1320.

389 E. Volkova, A. Perchik, K. Pavlov, E. Nikolaev, A. Ayuev, J. Park, N. Chang, W. Lee, J. Y. Kim, A. Doronin and M. Vilenskii, *Sci. Rep.*, 2023, **13**, 13371.

390 Z. Wang, Y. Huang, K. Xu, Y. Zhong, C. He, L. Jiang, J. Sun, Z. Rao, J. Zhu, J. Huang, F. Xiao, H. Liu and B. Y. Xia, *Nat. Commun.*, 2023, **14**, 69.

391 J. Kim, J. Park, Y.-G. Park, E. Cha, M. Ku, H. S. An, K.-P. Lee, M.-I. Huh, J. Kim, T.-S. Kim, D. W. Kim, H. K. Kim and J.-U. Park, *Nat. Biomed. Eng.*, 2021, **5**, 772–782.

392 L. Bao, J. Park, B. Qin and B. Kim, *Sci. Rep.*, 2022, **12**, 10693.

393 R. Moreddu, M. Elsherif, H. Butt, D. Vigolo and A. K. Yetisen, *RSC Adv.*, 2019, **9**, 11433–11442.

394 S. Kim, H.-J. Jeon, S. Park, D. Y. Lee and E. Chung, *Sci. Rep.*, 2020, **10**, 8254.

395 M. Elsherif, M. U. Hassan, A. K. Yetisen and H. Butt, *ACS Nano*, 2018, **12**, 5452–5462.

396 A. Ravizza, C. De Maria, L. Di Pietro, F. Sternini, A. L. Audenino and C. Bignardi, *Front. Bioeng. Biotechnol.*, 2019, **7**, 313.

397 J. B. Brönneke, J. Müller, K. Mouratis, J. Hagen and A. D. Stern, *Sensors*, 2021, **21**, 4937.

398 W. Gao, S. Emaminejad, H. Y. Y. Nyein, S. Challa, K. Chen, A. Peck, H. M. Fahad, H. Ota, H. Shiraki, D. Kiriya, D.-H. Lien, G. A. Brooks, R. W. Davis and A. Javey, *Nature*, 2016, **529**, 509–514.

399 J. Zhao, Y. Lin, J. Wu, H. Y. Y. Nyein, M. Bariya, L.-C. Tai, M. Chao, W. Ji, G. Zhang, Z. Fan and A. Javey, *ACS Sens.*, 2019, **4**, 1925–1933.

400 J. Tu and W. Gao, *Adv. Healthcare Mater.*, 2021, **10**, 2100127.

401 Y. Chen, S. Lu, S. Zhang, Y. Li, Z. Qu, Y. Chen, B. Lu, X. Wang and X. Feng, *Sci. Adv.*, 2017, **3**, e1701629.

402 D.-H. Choi, G. Kitchen, J. S. Kim, Y. Li, K. Kim, I. C. Jeong, J. Nguyen, K. J. Stewart, S. L. Zeger and P. C. Searson, *Sci. Rep.*, 2019, **9**, 17877.

403 T. R. Ray, M. Ivanovic, P. M. Curtis, D. Franklin, K. Guventurk, W. J. Jeang, J. Chafetz, H. Gaertner, G. Young, S. Rebollo, J. B. Model, S. P. Lee, J. Ciraldo, J. T. Reeder, A. Hourlier-Fargette, A. J. Bandodkar, J. Choi, A. J. Aranyosi, R. Ghaffari, S. A. McColley, S. Haymond and J. A. Rogers, *Sci. Transl. Med.*, 2021, **13**, eabd8109.

404 F. Lipsmeier, K. I. Taylor, T. Kilchenmann, D. Wolf, A. Scotland, J. Schjødt-Eriksen, W.-Y. Cheng, I. Fernandez-Garcia, J. Siebourg-Polster, L. Jin, J. Soto, L. Verselis, F. Boess, M. Koller, M. Grundman, A. U. Monsch, R. B. Postuma, A. Ghosh, T. Kremer, C. Czech, C. Gossens and M. Lindemann, *Mov. Disord.*, 2018, **33**(8), 1287–1297.

405 Home, <https://vitalconnect.com/>, (accessed March 25, 2025), 406 510(k) Premarket Notification.

406 <https://www.accessdata.fda.gov/scripts/cdrh/cfdocs/cfpmn/pmn.cfm?ID=k182041>, (accessed June 29, 2025).

407 CDRH Medical Device Databases, <https://www.fda.gov/medical-devices/device-advice-comprehensive-regulatory-assistance/medical-device-databases>, (accessed June 29, 2025).

408 U.S. Food and Drug Administration (FDA), (2020), Classify Your Medical Device, Retrieved from <https://www.fda.gov/medical-devices/overview-device-regulation/classify-your-medical-device>.

409 O. of the Commissioner, FDA.

410 C. for D. and R. Health, Quality System (QS) Regulation/ Medical Device Current Good Manufacturing Practices (CGMP), <https://www.fda.gov/medical-devices/postmarket-requirements-devices/quality-system-qs-regulationmedical-device-current-good-manufacturing-practices-cgmp>, (accessed June 29, 2025).

411 C. for D. and R. Health, Cybersecurity in Medical Devices, <https://www.fda.gov/regulatory-information/search-fda-guidance-documents/cybersecurity-medical-devices-quality-system-considerations-and-content-premarket-submissions>, (accessed June 29, 2025).

412 ISO 13485, <https://www.iso.org/standard/59752.html>, (accessed June 29, 2025).

413 S. S. Arya, S. B. Dias, H. F. Jelinek, L. J. Hadjileontiadis and A.-M. Pappa, *Biosens. Bioelectron.*, 2023, **235**, 115387.

414 S. Hamed, H. D. Jahromi and A. Lotfiani, *Eng. Appl. Artif. Intell.*, 2023, **118**, 105646.

415 S. Shahari, K. Kuruvinashetti, A. Komeili and U. Sundararaj, *Sensors*, 2023, **23**, 9498.

416 S. Kadian, P. Kumari, S. Shukla and R. Narayan, *Talanta Open*, 2023, **8**, 100267.

417 G. Moon, J. Choi, C. Lee, Y. Oh, K. H. Kim and D. Kim, *Biosens. Bioelectron.*, 2020, **164**, 112335.

418 D. Pelenis, D. Barauskas, G. Vanagas, M. Dzikaras and D. Viržonis, *Ultrasonics*, 2019, **99**, 105956.

419 V. Kammarchedu, D. Butler and A. Ebrahimi, *Anal. Chim. Acta*, 2022, **1232**, 340447.

420 S. Wang, C. Lafaye, M. Saubade, C. Besson, J. M. Margarit-Taulé, V. Gremeaux and S.-C. Liu, *IEEE J. Biomed. Health Inform.*, 2022, **26**, 4725–4732.

421 E. Yüzer, V. Doğan, V. Kılıç and M. Şen, *Sens. Actuators, B*, 2022, **371**, 132489.

422 S. Hong, Y. Gu, J. K. Seo, J. Wang, P. Liu, Y. S. Meng, S. Xu and R. Chen, *Sci. Adv.*, 2019, **5**, eaaw0536.

423 S. Li, K. Hart, N. Norton, C. A. Ryan, L. Guglani and M. R. Prausnitz, *Bioeng. Transl. Med.*, 2021, **6**, e10222.

424 Y. Li, Y. Ou, K. Fan and G. Liu, *Theranostics*, 2024, **14**, 6969–6990.

425 T. W. Pittman, D. B. Decsi, C. Punyadeera and C. S. Henry, *Theranostics*, 2023, **13**, 1091–1108.

426 N. Farsaeivahid, C. Grenier and M. L. Wang, *Diagnostics*, 2024, **14**, 1088.



427 S. Apoorva, N.-T. Nguyen and K. R. Sreejith, *Lab Chip*, 2024, **24**, 1833–1866.

428 R. S. P. Malon, S. Sadir, M. Balakrishnan and E. P. Córcoles, *BioMed Res. Int.*, 2014, **2014**, 962903.

429 J. Boulestreau, L. Molina, A. Ouedraogo, L. Laramy, I. Grich, T. N. N. Van, F. Molina and M. Kahli, *Sci. Rep.*, 2024, **14**, 31233.

430 A. Rajan, J. Vishnu and B. Shankar, *Biosensors*, 2024, **14**, 483.

431 Z. Wang, Y. Dong, X. Sui, X. Shao, K. Li, H. Zhang, Z. Xu and D. Zhang, *npj Flexible Electron.*, 2024, **8**, 1–11.

432 M. Friedel, I. A. P. Thompson, G. Kasting, R. Polsky, D. Cunningham, H. T. Soh and J. Heikenfeld, *Nat. Biomed. Eng.*, 2023, **7**, 1541–1555.

433 Bioliniq | Sensing your path to better health, <https://www.bioliniq.com/>, (accessed June 29, 2025).

434 Profusa, Inc. | Join The Conversation With Your Body, <https://profusa.com/>, (accessed June 29, 2025).

435 Allez Health, <https://www.allezhealth.com/>, (accessed June 29, 2025).

436 Dexcom Continuous Glucose Monitoring - The most accurate CGM system1, <https://www.dexcom.com>, (accessed June 29, 2025).

437 Epicore Biosystems | Wearable Hydration & Heat Stress Monitor, <https://www.epicorebiosystems.com>, (accessed June 29, 2025).

438 Nutromics – Solving some of the biggest healthcare challenges, <https://www.nutromics.com>, (accessed June 29, 2025).

